

Silesian University of Technology  
Faculty of Mechanical Engineering  
Department of Fundamentals of Machinery Design

## Doctoral Dissertation

# The Method of Increasing the Flight Endurance of Vertical Take-Off and Landing Unmanned Aerial Vehicle

MSc, Eng. Krzysztof Mateja

Supervisor:

PhD, DSc, Eng. Wojciech Skarka, Prof. SUT

Gliwice, 2023

# Contents

- Contents ..... 2**
- List of Used Acronyms and Symbols ..... 5**
- 1. Introduction..... 7**
  - 1.1 Aim and Thesis..... 8
  - 1.2 Scope ..... 8
  - 1.3 Scientific Problem..... 9
  - 1.4 Author's Publications..... 10
  - 1.5 Acknowledgments ..... 10
- 2. Literature Review..... 11**
  - 2.1 Solar Power Management System ..... 12
  - 2.2 Energy Storage System ..... 12
  - 2.3 Energy Harvesting System ..... 14
    - 2.3.1 Solar Cells ..... 14
    - 2.3.2 MPPT ..... 16
    - 2.3.3 Solar Cell Lamination ..... 17
    - 2.3.4 Installation of PV Panels on the UAV Structure..... 18
  - 2.4 Energy Demand System..... 18
  - 2.5 Summary..... 18
- 3. Methods ..... 20**
  - 3.1 Functional Principle of the Simulation Model ..... 23
  - 3.2 Irradiance Model ..... 25
    - 3.2.1 Solar Energy Limitations ..... 29
  - 3.3 PV System Model..... 30
  - 3.4 Battery Model..... 31
  - 3.5 Model Simplifications ..... 32
    - 3.5.1 Irradiance Model Simplification ..... 32
    - 3.5.2 PV Model Simplification ..... 33
    - 3.5.3 Battery Model Simplification..... 33
- 4. Preliminary Verification Results..... 34**

4.1	Irradiance Model .....	34
4.2	PV System Model.....	37
4.3	Battery Model.....	39
4.4	Summary.....	40
<b>5.</b>	<b>Case Study .....</b>	<b>42</b>
5.1	Energy Consumption .....	44
5.1.1	Twin Stratos 17 .....	44
5.1.2	Twin Stratos 12 .....	46
5.1.3	VTOL Tail-Sitter .....	48
5.2	Photovoltaic Energy.....	50
5.3	Batteries .....	52
5.4	Summary.....	52
<b>6.</b>	<b>Fine-Tuning of Simulation Models .....</b>	<b>54</b>
6.1	Planned Scenarios .....	54
6.1.1	Twin Stratos 17 .....	54
6.1.2	Twin Stratos 12 .....	55
6.1.3	VTOL .....	56
6.1.4	Summary.....	57
6.2	Photovoltaic Cell.....	58
6.2.1	Laminating Film .....	59
6.2.2	Research of Laminated Photovoltaic Cells .....	60
6.2.3	Observations of a Solar Cell on a Microscopic Scale .....	63
6.3	Batteries .....	64
6.4	Summary.....	75
<b>7.</b>	<b>Results.....</b>	<b>77</b>
7.1	Twin Stratos UAVs .....	77
7.1.1	Twin Stratos 17 .....	77
7.1.2	Twin Stratos 12 .....	82
7.2	VTOL .....	89
7.3	Summary.....	92
7.3.1	Cloudiness.....	93
<b>8.</b>	<b>Verification .....</b>	<b>97</b>
8.1	Twin Stratos 17 Prototype.....	97
8.1.1	Batteries and Battery Management System .....	98
8.1.2	MPPT .....	98
8.1.3	Photovoltaic Cells .....	100

8.2	System Check Before First Flight .....	103
<b>9.</b>	<b>Summary .....</b>	<b>106</b>
9.1	Conclusions.....	106
9.2	Future Works.....	110
<b>References</b> .....	<b>112</b>	
<b>Abstract</b> .....	<b>121</b>	
<b>Streszczenie</b> .....	<b>122</b>	

# List of Used Acronyms and Symbols

$\beta$	Inclination Angle
$\gamma_s$	Solar Azimuth Angle
$\delta$	Declination Angle
$\theta_z$	Zenith Angle
$\lambda$	Coefficient of Thermal Conductivity
$\varphi$	Latitude Angle
$\tau_b$	Ratio of the Transmitted Direct Radiation to the Total Radiation Incident at the Top of The Atmosphere
$\tau_d$	Ratio of the Transmitted Diffuse Radiation to the Total Radiation Incident at the Top of The Atmosphere
$\omega$	Hour Angle
A	Altitude of the Site Above Sea Level
AGV	Automated Guided Vehicle
AM	Air Mass
AoA	Angle of Attack
BMS	Battery Management System
CSV	Comma Separated Values
DSSC	Dye-Sensitized Solar Cell
FCM	Flight Control Module
$G_c$	Total Radiation
$G_{cb}$	Beam Radiation
$G_{cd}$	Diffuse Radiation
$G_{on}$	Irradiation on Surface
$G_{sc}$	Solar Constant
GaAs	Gallium Arsenide
HALE	High-Altitude Long-Endurance
HAPS	High-Altitude Pseudo-Satellite
$H_o$	Daily Radiation
$H_R$	Relative Height of the Flight,
$I_c$	Hourly Radiation on a Horizontal Surface
$I_{mp}$	Optimum Operating Current
$I_o$	Hourly Radiation
$I_{sc}$	Short Circuit Current
I-V	Current-Voltage
JSON	JavaScript Object Notation
LALE	Low-Altitude Long-Endurance
MBD	Model-Based Design
MBE	Model-Based Enterprise
MBSE	Model-Based System Engineering
MPPT	Maximum Power Point Tracking
n	Day of the Year

N	Day Length
PCE	Power-Conversion Efficiency
$P_{mpp}$	Nominal Maximum Power
P-V	Power-Voltage
PSC	Perovskite Solar Cell
PV	Photovoltaics
PVC	Polyvinyl Chloride
PWM	Pulse Width Modulation
$r_0, r_1, r_k$	Coefficients for Climate Type
ROC	Rate of Climb
ROD	Rate of Descent
SOC	State of Charge
SPMS	Solar Power Management System
SysML	Systems Modeling Language
$T_c$	Current Temperature at the Height of the Flight
$T_D$	Temperature Drop
$T_i$	Temperature on the Ground
TS	Twin Stratos
TS12	Twin Stratos 1:2
TS17	Twin Stratos 1:7
TS18	Twin Stratos 1:8
TS110	Twin Stratos 1:10
UAV	Unmanned Aerial Vehicle
UML	Unified Modeling Language
$V_{oc}$	Open Circuit Voltage
$V_{mp}$	Optimum Operating Voltage
$V_{mpp}$	Maximum Power Point Voltage
VTOL	Vertical Take-Off and Landing
WCA	Worst-Case Analysis
XML	Extensible Markup Language

# 1. Introduction

Aircraft for over 100 years, i.e., since the first successful flight of the Wright brothers in 1903 [1,2], have been developed in terms of aerodynamics, propulsion, lightweight material structures, range, and flight time. In recent decades, special attention has been focused on Unmanned Aerial Vehicles (UAVs) [3]. This direction results primarily from the fact that there is no need for the presence of a pilot on board the aircraft. This has both financial benefits — no need to pay pilots and crew — and in the case of military applications, the possibility of saving lives during shelling, because there are no soldiers, crew, or reporters on board the UAV [4]. UAVs can be divided into many categories [5], thanks to which some of them are able to fly at very high altitudes [6], perform operations with high maneuverability and mobility [4], which are not possible for massive vehicles with a pilot on board, e.g. in highly urbanized areas.

The implementation of artificial intelligence, algorithms, and machine learning allows UAVs not only to be remotely controlled from the ground by the user, but more and more often these vehicles have the option of autonomous flight or perform some part of the flight in this way [7]. Such a refined control system allows for internal integration of flight path planning systems [8], control the flight conditions, limitations, and implement the necessary changes during the planned mission.

UAVs equipped with cameras [9] allow for filming and shooting scenes from a bird's eye view. Such use makes Unmanned Aerial Vehicles gain more and more popularity in recent years not only in the commercial industry, but also among hobbyists who use them for fun, filming and taking photos.

The army can use them to control borders and monitor events that are dangerous from the point of view of the state's interests [10]. UAV applications are very wide. They can also include distribution of shipments [11], crop control [4], monitoring of threats, e.g., fires, mapping of areas, search and rescue works [12,13]. Depending on their design, geometry, power transmission method, endurance of the flight, the final UAV destination may change.

The issue that most restricts UAVs and other flying vehicles is the time and range of flight. The limited flight time of the UAV causes the need to land and the associated loss of time in terms of aborting the mission, charging, or replacing the batteries. In order to extend the flight mission, engineers are looking for possibilities to obtain energy from the outside [14,15]. The goal is to achieve full energy autonomy enabling continuous flight without the need for unnecessary landings. Energy autonomy of UAVs is an important direction in the field of cosmonautics, because in addition to the possibility of continuous operation, an additional advantage of UAVs is the lower cost of this type of application than using a satellite [16].

One of the most frequently used sources of energy is a solar cell [12,14]. The solar-powered UAV is not a new aircraft concept. We can distinguish many types of solar-powered aircraft: Atlantic Solar [14,17], Solar Impulse 2 [18], Airbus zephyr [19], PHASA-35 [20], Odysseus [21], pathfinder plus, Helios, centurion, pathfinder, global observer [22], Solong UAV [23]. Each of the above aircraft is based on a lightweight composite

structure, energy-saving propulsion system, and it is equipped with photovoltaic (PV) panels that enable the production of energy during the flight. Energy is then used by propulsion systems and avionics or stored in batteries.

Most solar-powered UAVs are classified as High-Altitude Pseudo-Satellite (HAPS) flying objects, also called “stratosphere drone” [24] or High-Altitude Long-Endurance (HALE). High-Altitude Long-Endurance unmanned aerial vehicle generally refers to UAVs flying at an altitude of 15–20 km with a low speed [25].

In contrast to HAPS and HALE, smaller-scale solar-powered UAVs are mostly designed for Low-Altitude Long-Endurance (LALE) applications [17]. LALE class objects, due to their lower flight ceilings, are more exposed to weather conditions and the impact of weather conditions on the mission accomplishment [15].

Both HALE and LALE class flying vehicles are mostly Fixed-wing UAVs [17,19,23]. The reason is the advantage of using this type of UAV design. The wings provide surfaces on which photovoltaic panels can be placed. In addition, in some constructions there is also an empennage on which additional solar cells can also be placed [17,23]. Other designs that do not have sufficient wing area are rarely considered for flight extension with photovoltaics.

One of such types of Unmanned Aerial Vehicles are Vertical Take-off and Landing (VTOL). The possibility of vertical take-off allows to launch anywhere without the runway [26]. The advantage of VTOL is also good maneuverability in heavily urbanized areas, access to remote areas, and observation in difficult weather conditions. These UAVs are more failproof, making them more reliable than other configurations [27,28]. A few examples of VTOL UAVs are: SkyX [29], E-flite Convergence [30], VALAQ Patrol [31], WingtraOne [32], and SkyEye Sierra [33].

We can include multirotor drones, tilt-wing UAVs, tail-sitter UAVs, and other hybrid structures in this group. Hybrid VTOLs combine the features of fixed-wing vehicles (wings and fuselage) and multirotor drones (horizontal propellers). After reaching the set ceiling, the UAV is able to “transform” into a horizontal position to continue the flight with the help of its wings. This design allows us to extend the UAV’s endurance and obtain better performance during flight [27,34].

## 1.1 Aim and Thesis

The aim of the doctoral dissertation is to develop a method which allow to extend the flight time of an Unmanned Aerial Vehicle, in particular Vertical Take-off and Landing. Due to its universality, the method should be applicable to various types of UAVs, including, e.g. fixed-wing UAVs of the HALE, LALE class and in other types of UAVs.

The thesis of this doctoral dissertation is:

**The method based on Model-Based Design (MBD) modeling allows to design a VTOL UAV with a significantly increased flight endurance.**

## 1.2 Scope

The thesis focuses on a simulation model based on the Model-Based Design (MBD) methodology. Depending on the weather conditions (irradiation, cloud cover), the model is able to calculate the operating time of the system for a given flight scenario. The doctoral dissertation deals with issues in the fields of astronomy, geography, mechanical engineering, and electrical engineering.

The first chapter contains an introduction to the scientific problem presented in the doctoral dissertation, the current state of art, and the author's publications on which the doctoral dissertation is based.

The second chapter focuses on the literature review related to the general construction of the solar-powered UAV, including energy storage systems, external energy harvesting, and methods of connecting PV panels with UAV surface.

The third chapter deals with the issue of modeling the simulation environment, taking into account the models of irradiation, the limitation of solar energy reaching the PV panels, the model of the solar cell, the model of energy storage, and the model of the device controlling the operation of the PV system.

The fourth chapter presents preliminary results verifying the correct operation of the models.

The fifth chapter presents a case study on which the calculations will be based. Three types of UAVs were taken into account. Two fixed-wing UAVs — of the LALE and HALE classes — as well as tail-sitter VTOL. The data in this chapter has been developed partially by aviation engineers. The chapter deals with the issue of UAV energy demand, the estimated value of energy produced by UAVs, and the energy balance in a specific period.

The sixth chapter presents the fine-tuning of the models that occurred on the test stands. Solar cells, battery cells, foil used for lamination of solar cells, and the microscopic scale of the solar cell were tested. The data obtained during the tests were implemented in a simulation model, thanks to which the final configuration of the solar power system was selected for each case study. The chapter also presents proposed flight scenarios.

The seventh chapter presents the results of the work. The most important from the point of view of the thesis was to obtain information about the extension of flight time and the possibility of obtaining full energy autonomy. The finalization of the chapter is the elaboration of conclusions from the conducted analyses.

The eighth chapter concerns the verification work. One of the case studies — a LALE UAV — was manufactured during the work on the thesis. The tests carried out on the target UAV allowed to verify the correct operation of the simulation model on a real object.

The last, the ninth chapter summarizes the work carried out, draws conclusions, and considers further stages of work with future research plans.

### **1.3 Scientific Problem**

The necessity of landings due to exhausted energy storage causes time loss, additional financial outlays, lack of continuity of missions, research, and measurements. The use of renewable energy sources, which can include solar cells, is intended to ensure partial or full battery charging during a given flight operation. Obtaining a positive energy balance means that the energy consumed by the entire UAV is lower than the energy produced by the PV panels. Obtaining a positive energy balance is correlated with the flight path planning, the date and time of the flight operation, weather conditions, and other factors. Depending on the purpose of the UAV, the payload and weight of the measuring and control devices should also be taken into account. The weight of the UAV should be as low as possible. Then the load-bearing structure enables a greater payload or an increase in the capacity of the batteries, which allows the UAV to fly longer [11,14]. The goal is to maximize the flight endurance of the UAV as much as possible.

The research gap consists in limiting the flight endurance only for fixed-wing UAVs. Due to the specific nature of VTOL UAV (in particular take-off and landing stage) this kind of UAV is not taken into account in this type of research. In order to verify the increase in the flight endurance, simulation models should be developed that will be able to manage the energy balance of the UAV, taking into account various phases of flight, atmospheric phenomena, and flight scenarios performed.

Continuous development of technology requires constant verification of products and developed prototypes. New types of battery cells, solar cells, electric motors, and controllers allow to discover new possibilities and configurations of UAVs. While in the case of manned aircraft it is a certain finite configuration of vehicles, in the case of drones, new concepts and configurations of UAVs are constantly being introduced. Designers take their cue from, for example, birds, insects, etc. This type of development of UAVs means that continuous design improvements also require methods to check the energy capabilities of UAVs.

## **1.4 Author's Publications**

In this doctoral dissertation, the author relies mainly on three of his publications in scientific journals with a global range, which are a series of works related to the development of the solar-powered UAV power supply system. These publications take into account the research carried out on solar cells and the decrease in their efficiency after the lamination process, which extends the life of the solar cells, increases their mechanical resistance and allows them to be placed on the UAV structure [35].

The developed method of increasing UAV flight endurance is much more popular and used in fixed-wing UAVs. The publication [15] took into account this type of UAV to carry out a numerical simulation examining the energy balance and the possibility of achieving full energy autonomy of the HALE class fixed-wing UAV.

The latest publication is an article that aimed to study the effect of solar cells on the tail-sitter drone [27]. The aim was to check whether the PV panels placed on the VTOL structure would extend the UAV's flight time.

## **1.5 Acknowledgments**

The research described in the doctoral dissertation was partially carried out and financed by the Norwegian Funds for 2014-2021 as part of project no. 10/60/ZZB/153 entitled "Long-endurance UAV for collecting air quality data with high spatial and temporal resolutions (LEADER)" and as part of the grants of the Silesian University of Technology No. 10/060/BKM20/01 and 10/060/BKM22/2025.

The developed method was elaborated by me for SkyTech eLab LLC and is its property. The work also presents the technical solutions of Twin Stratos UAVs owned by SkyTech eLab. SkyTech eLab LLC consented to publication of presented content.

## 2. Literature Review

The principle of operation of the UAV, which should be able to increase the endurance of the flight, may include several options for performing this task:

1. Reducing the weight of the UAV through the use of lightweight materials and composite structures, thanks to which the energy demand of the UAV will be reduced;
2. The mass of the payload may be an earmark for additional energy storage. It will increase the capacity of using battery;
3. The use of components that enable obtaining energy from the outside, e.g., photovoltaic cells.

The increase in flight endurance can be short-term or long-term. The first and second points allow for a short-term extension of the flight time. It is more about optimizing or maximizing performance. The third point allows to extend the flight time for a long time, i.e., in favorable conditions (external conditions, such as time of day, weather conditions; internal, such as UAV construction), the UAV may even be able to achieve full energy autonomy, which will reduce the number of landings caused by a discharged battery, while ensuring the continuity of the mission [15]. From the point of view of energy autonomy, the first two points exclude the possibility of obtaining it.

The sun is the largest source of free energy on Earth [36]. Solar energy is a renewable, pollution-free, sustainable, and inexhaustible resource [35]. The scheme of using such an energy source consists in obtaining energy during the day [15,17]. The produced energy is used on an ongoing basis to meet the energy requirements of the air mission and its surplus is stored in batteries [37]. The energy surplus can also be used in the form of potential energy as flight altitude. Climbing the UAV to the highest possible altitude enables for a longer time gliding, which additionally extends the flight time [15,35].

The surplus of energy accumulated in the energy storage and altitude can be used during periods of lack of solar energy, e.g., at night or when it is completely cloudy.

The electrical and mechanical connection requires optimization of the entire structure by minimizing the weight, providing space for placing PV panels, space inside the UAV for batteries, energy-efficient electric motors, and on-board equipment. In addition to changes in the UAV design and UAV systems, limitations for the planned air mission should also be taken into account.

Solar radiation depends on many variables such as geographical location, date and time, flight position, weather conditions, and ground and air reflectance [38,39,40,41]. In the energy balance calculation, due to the characteristics of the solar vehicle, the calculation process is simplified accordingly [41]. In the case of UAVs powered by solar energy, the power supply system is subject to many dependencies and limitations. It can be divided into two groups. The first is related to factors that are beyond human control, i.e., weather conditions, temperature, cloud cover, and air pollution. The second is related to the variable parameters that can be changed in the UAV, e.g., electric motor power, mass, payload, flight path planning [15].

Obtaining a negative energy balance makes it necessary to change the flight conditions or the construction of the drone, reduce energy consumption, and reduce the weight of the UAV [42]. Energy harvesting in the case of solar-powered UAVs mainly depends on the irradiation level, which depends on the date and time of flight [15].

## 2.1 Solar Power Management System

The general structure of the solar-powered UAV power supply system has been presented using a block diagram illustrating the principle of operation of the system (Figure 2.1).

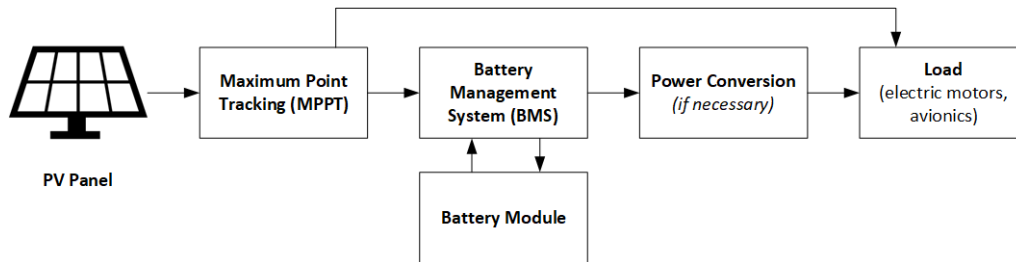


**Figure 2.1.** General diagram of the Solar Power Management System (SPMS).

The diagram above shows the features of a flow diagram. The data flow between successive blocks are both power lines and information buses.

The principle of operation of the system consists in generating solar energy by a photovoltaic system. Then, depending on the value of the energy produced, it is sent to the load (electric motors, on-board devices) and/or batteries in order to recharge the state of charge (SOC) of the battery. Energy is transmitted through the use of energy converters that monitor the correct energy management — Maximum Power Point Tracking (MPPT), Battery Management System (BMS), and DC-to-DC (Direct Current) converters.

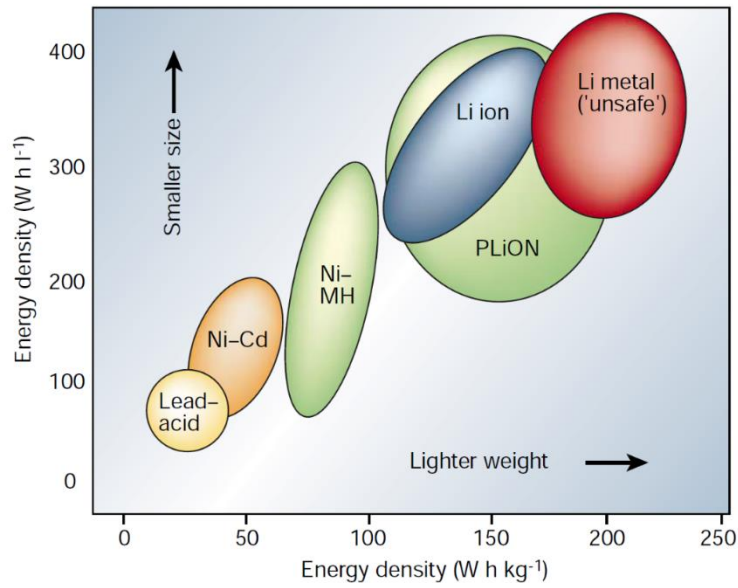
By assumption, the power supply system should be built in a universal way. By modifying the settings and changing the components, the developed power supply system can be used in various types of UAVs characterized by, e.g., other missions to be performed.

The general scheme of powering UAVs powered by solar cells was divided into 3 parts, on which further work was undertaken:

1. Energy storage system — described in subchapter 2.2;
2. Energy harvesting system — described in subchapter 2.3;
3. UAV energy demand system — described in subchapter 2.4.

## 2.2 Energy Storage System

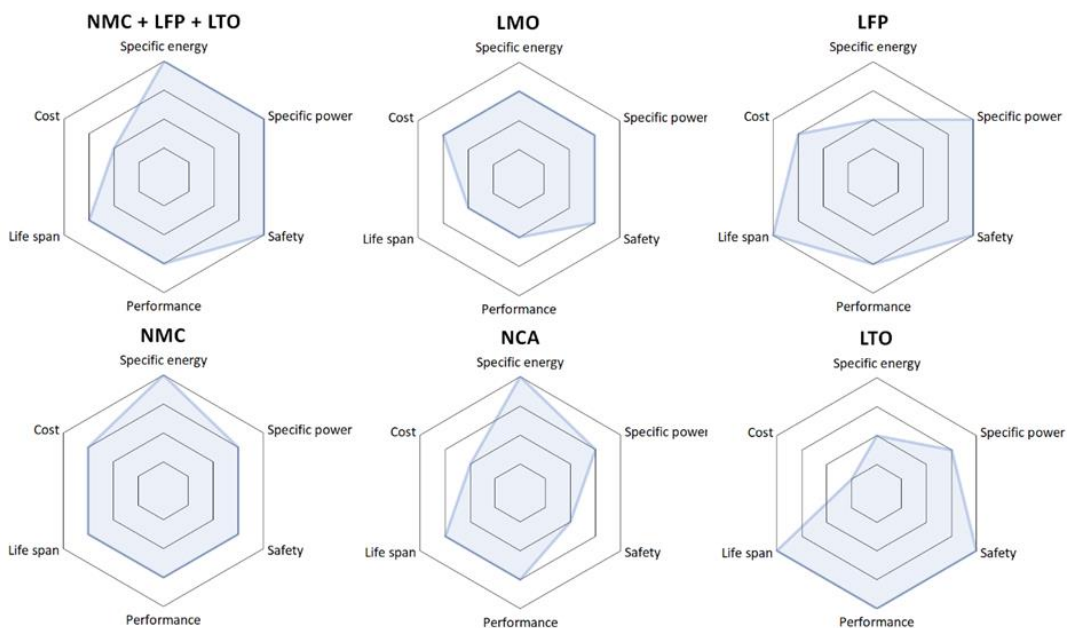
Batteries are the energy store of almost every electric vehicle. Lithium-ion (Li-ion) batteries are the most widely used in electromobility [43,44]. Batteries are basically a storage medium consisting of two electrodes in an electrolyte. This electrolyte is an ion exchange medium that generates electricity [45,46]. Figure 2.2 shows the relationship of different types of batteries depending on their specific energy (energy per unit mass) and energy density.



**Figure 2.2.** Comparison of different battery technologies in terms of volumetric and gravimetric energy density [47].

The advantage of Li-ion battery cells is their high energy density, number of charging cycles, and high efficiency [45,46,47,48]. The disadvantage, however, is the high cost, need to use battery cells operation monitoring systems, and safety systems [45,46,47,48].

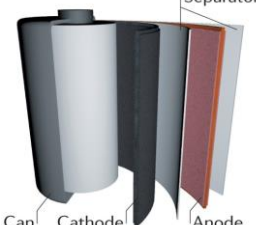
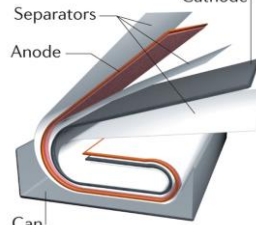
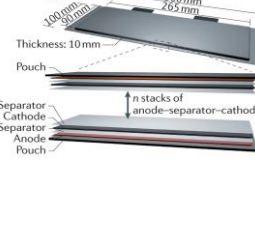
There are many types of Li-ion battery cells. Each of them has its own properties, thanks to which it will work in one specific application, but not necessarily in the other. Figure 2.3 presents the most popular Li-ion battery cells used in electromobility and the assessment of their parameters for specific energy, specific power, safety, performance, lifespan, and cost.



**Figure 2.3.** Comparison of different types of Li-ion batteries used in EVs from the following perspectives: specific energy, specific power, safety, performance, life span, and cost [46,49,50].

In addition to the internal parameters of Li-ion battery cells, external parameters can be distinguished, which are the dimensions and shape of the battery cell. We can distinguish three shapes of battery cells: cylindrical, prismatic, and pouch. Table 2.1 shows how the mechanical and electrical parameters change for different battery cell shapes.

**Table 2.1.** Cell designs and Relative Strengths and Weaknesses [51,52].

Shape	Cylindrical	Prismatic	Pouch
Diagram			
Electrode arrangement	Wound	Wound	Stacked
Mechanical Strength	++	+	-
Heat Management	-	+	+
Specific Energy	+	+	++
Energy Density	+	++	+
Cost	++	+	+

In the case of UAVs, the battery cell used should primarily be characterized by the lowest possible mass — high specific energy — and occupying the smallest possible space — energy density. Depending on the maximum ceiling at which the UAV will fly, the temperature range should also enable operation in subzero temperatures. Lifespan or safety are less important.

## 2.3 Energy Harvesting System

### 2.3.1 Solar Cells

The base of the energy harvesting and production system are photovoltaic cells. Solar cells are semiconductor electrical devices that convert light energy directly into electricity through the photovoltaic effect [53,54].

There are several types of solar cells, which are used to convert sunlight into electrical energy: monocrystalline silicon solar cells, polycrystalline silicon solar cells, thin-film solar cells, organic solar cells and hybrid solar cells [55]. Among them, crystalline silicon (c-Si) solar cell has more than 90% market share [56,57].

Standard silicon solar cells are brittle and breakable [58,59]. Under the influence of mechanical forces, they are easily damaged, losing their efficiency and electrical parameters. The disadvantage of the delicate structure and the inability to bend. It causes that this type of solar cell will not be able to effectively obtain energy for UAVs. In aviation and astronautics, flexible solar cells are used [14,35,60], which allow for bending, deformation, and adaptation to the surface of the aircraft, e.g., for wings, fuselage, empennage. The possibility of deformation of the solar cells allows them to be used in places where stress will act. Under their influence, the photovoltaic cell and the entire PV

panel will not break, but only deform. Flexible photovoltaic cells can be divided into several types [61,62,63,64]:

1. Gallium Arsenide (GaAs) solar cell ensures high efficiency, which even exceeds 30% [12,63,65,66]. It is used primarily in the space industry, in probes and in the defense industry [12]. The disadvantage of GaAs is the high price [67] and toxicity [68]. The high cost of these PV panels causes that constructors and designers, when building prototypes, cannot use them in the solutions they research and develop. In addition to high efficiency, the advantage of these cells is high resistance to heat damage [69].
2. Dye-Sensitized Solar Cell (DSSC) solar cell has lower efficiency compared to standard silicon photovoltaic cells. Their efficiency currently reaches a maximum of 15% [70]. Compared to other solar cells, they have become very competitive due to a number of advantages [62,71]:
  - Good price-performance ratio;
  - Ability to choose the color and change the degree of transparency (transparency allows the use of the solar cell, e.g., on roofs as a photovoltaic windowpane replacing traditional glass);
  - Flexibility and lightness;
  - A smaller decrease in efficiency at a large angle of incidence of sunlight;
  - Possibility to produce photovoltaic cells of various shapes;
  - Short payback time of the energy used to produce the photovoltaic module compared to other types of photovoltaic cells.
3. Perovskite solar cells (PSC) are one of the latest technologies in photovoltaic cells. The advantages of PSC are high efficiency in various lighting conditions, negligible thickness and weight, easy and cheap method of production using inkjet printing [72], which allows to significantly reduce production costs. Compared to standard polycrystalline and monocrystalline silicon cells, their efficiency is higher and currently amounts to approx. 25.7% [73]. Another advantage is the lower temperature coefficient of the perovskite, which is -0.13%/°C. For monocrystalline panels it is about -0.39%/°C, and for polycrystalline panels it is about -0.38%/°C [74,75].

The disadvantage of PSC cells is the initial development phase, which means that the real commercialization of these solar cells have not yet started. The material generates toxic lead. The lifetime of PSC cells is short and can last only about 2.5 years, which is 10 times less than in the case of standard silicon solar cells [75].
4. Amorphous silicon (a-Si) solar cells using amorphous silicon, a non-crystalline form of silicon. Silicon is used as a semiconductor material for a-Si solar cells or thin-film silicon solar cells. It is placed in thin layers on a variety of flexible substrates such as glass, metal, and plastic. Amorphous solar cells are thin-film cells of the second generation [69] and they are characterized by low efficiency [76]. They require much less silicon than conventional solar panels. Amorphous solar panels are also flexible and have significant durability, making them less prone to breakage than traditional panels constructed from solid silicon wafers. They are insensitive to high temperatures. Most types of amorphous solar panels have a conversion efficiency of around seven percent [77].
5. Crystalline silicon (c-Si) solar cells have been commercialized due to their low production cost, long lifetime of more than 20 years, and high power

conversion efficiency (PCE)  $\leq 26.7\%$  [78]. Crystalline silicon cells are divided into monocrystalline and polycrystalline cells [79]. Monocrystalline PV modules are the commercially most commonly used PV modules [80]. Monocrystalline photovoltaic cells are made of a single crystal of silicon, and therefore work with higher efficiency than polycrystalline cells, which are made of many fragments fused together [81]. Monocrystalline panels are more expensive than polycrystalline panels due to better electrical parameters. Crystalline silicon photovoltaic cells can become pliable and flexible when the silicon wafers are thin enough [79]. The advantages of flexible crystalline silicon solar cells are: high flexibility, lightness, and low price in relation to the generated efficiency.

### 2.3.2 MPPT

Photovoltaic cells have non-linear current-voltage (I-V) and power-voltage (P-V) characteristics. This non-linear nature of the photovoltaic panel reduces the energy conversion capacity and increases the system installation cost [82]. In order to ensure the proper operation of photovoltaic cells and the power generated by them, the power supply system should be equipped with a solar regulator of solar cells. There are two types of controllers in solar systems – PWM (Pulse-Width Modulation) and MPPT. MPPT controllers ensure a continuous supply of maximum power generated by the solar system [83] by continuously tracking the maximum power point. For this reason, this type of regulator is the most commonly used. PWM controllers have a number of limitations compared to MPPT controllers. The advantages of using MPPT charge controllers are [84]:

- Better efficiency than PWM (10 to 40%);
- Better performance during partial PV panel shading;
- Better performance in low light conditions;
- Any photovoltaic panel can be used;
- Less voltage drop in installation.

Each I-V and P-V characteristic has only one maximum power point  $P_{mpp}$ . The maximum power point is continuously tracked by the MPPT controller. It changes depending on the irradiation of the solar cell, temperature, shading, cloudiness. An example graph containing I-V and P-V characteristics is shown in Figure 2.4.

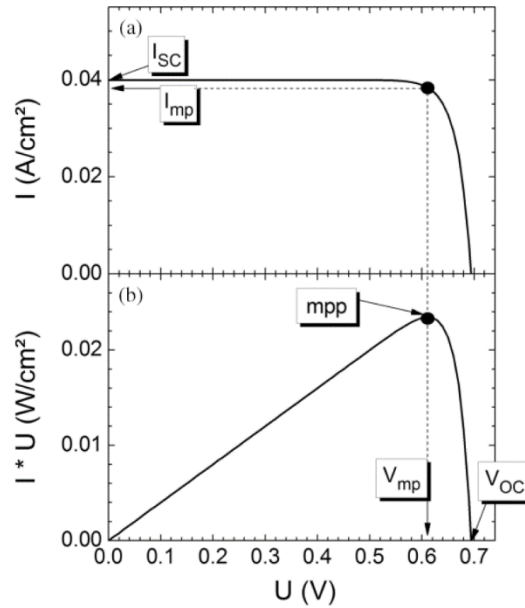


**Figure 2.4.** Example I-V and P-V characteristics [85].

### 2.3.3 Solar Cell Lamination

Solar cells, regardless of the type, cannot be directly attached to the surface of the wings of aircraft. Photovoltaic cells must be protected against external conditions. Thin films that are resistant to mechanical damage are used to protect solar cells [60,86]. Lamination of solar cells is one of the key processes to ensure the long life and durability of PV panels. The lamination process affects the amount of light entering the device. Each protective layer on the surface of the solar cell, together with the influence of ambient temperature and radiation intensity fluctuations, changes the parameters of photovoltaic panels [87,88,89,90].

In the case of using solar cells on the UAV surface, various protective coatings are used to protect and strengthen their structure: foils, resins, and composite materials [35]. This process is also aimed at improving UAV aerodynamics, facilitating the cleaning of solar cells from dirt, and preventing moisture and dust from entering the installation [35].

There are a few types of foils with different thicknesses that can be used as protective surfaces for solar cells. In aerospace, one of the most widely used encapsulating materials is EVA (Ethylene-vinyl acetate) [35]. The advantage of this material are high transmission [91]. The disadvantage in the case of EVA is the low aging resistance to UV radiation [91]. EVA also requires a vacuum method in the lamination process. To provide a smooth connection between the foil and the solar cell, it is necessary to use a vacuum ensuring that no air or humidity will be in contact with the solar cells. This requires advanced equipment that increases the cost of making the prototype of the UAV [35].

Another kind of film that can be used for solar cell lamination is PVC (Polyvinyl Chloride) film. PVC and EVA are similar materials. EVA is more flexible, lighter, and stronger than PVC, but the advantage of PVC is its ease of application to the solar cell. In this case, the use of vacuum is not necessary. The time needed to prepare PVC laminated solar cells is shorter than in the case of EVA [35].

### 2.3.4 Installation of PV Panels on the UAV Structure

The process of mounting solar cells on the wing can be divided into several types of technologies with PV modules [35,60]:

1. Adhering to an existing wing — this method is good for retrofitting an existing UAV. Aerodynamics are normally not affected as the modules are extremely thin. The biggest advantage of this solution is it allows the possibility to replace PV cells in the event of damage. Wiring between modules is time-consuming with large wings as strings of solar cells run from the root to tip. The biggest disadvantage of this solution is getting the gap between 2 modules sealed [60,92,93].
2. Placed into a mold. The challenge is to fix the modules in their exact position and to ensure no resin gets onto the front of the module. The advantage of this solution is the wiring which is easy to arrange. The effects of PV modules on aerodynamics are largely eliminated, but modules cannot be swapped in case of damage. One variation of this method is to place solar cells inside the wing structure with a transparent coating, e.g., transparent film. This technology is mainly practiced within hobby modeling circles and the production process can be seen on models that are often developed by enthusiasts, e.g., on YouTube channels. Due to the labor-intensive nature of this method and the impossibility of replacing damaged elements, it is rarely used in commercial UAVs.
3. As the wing surface — lightweight solar modules need more ribs, more sturdy solar modules need fewer ribs but have more weight. The wiring arrangements are easy in this solution [94,95,96,97].

## 2.4 Energy Demand System

UAV energy demand can be divided into several components. The most important from the energy point of view is the consumption generated by electric motors [98]. They consume most of the energy stored in the batteries and produced by the PV panels. The electric motors generate the greatest power during take-off and ascent to a given altitude [99]. During cruise flight, the value of the power needed to maintain flight at a certain altitude decreases. During gliding, it is assumed that the electric motors are not working, which means that then the energy from the batteries is consumed only by the on-board devices.

Devices on board the UAV include: flight controller, devices for telemetry, measurement, lighting, etc. Their energy consumption may be negligible, however, for accurate verification, a list of all electronic components that will be on board the UAV should be developed. This will allow to calculate the energy that will be consumed by these devices during the flight. For different types of UAVs, the number and type of devices on board will change. It is necessary to take into account the necessary equipment, e.g., lighting, GPS, and additional equipment, e.g., used to perform measurements.

## 2.5 Summary

At the stage of developing the general method of the solar-powered UAV power supply system, it was possible to come to preliminary conclusions that had to be taken into account in the next stages of thesis. One of them was the choice of the type of solar cell which can be used in the UAV.

The selection of the appropriate photovoltaic cell was carried out in a way that was to allow not only for theoretical testing of the used photovoltaic cells, but also for practical tests. Tests will consist in the possibility of conducting research on the ultimately selected solar cell, as well as developing a process for the target application of the selected cell, i.e., placing it on the UAV structure.

Due to the low efficiency of amorphous cells and DSSC, these solar cells were omitted. In the case of a limited area of the UAV structure, it is important to achieve the highest possible efficiency of the photovoltaic cells, because the available area can be rigidly defined, e.g. in the case of modernization of an existing UAV.

In the early stage of development of perovskites, the lack of commercialization of the product also resulted in the rejection of these solar cells. GaAs solar cells seem to be the best of the available solutions, especially due to their high efficiency. However, due to the large cost, these solar cells were rejected.

It was decided that crystalline flexible silicon solar cells, due to their high efficiency and much lower price than GaAs, will be chosen as the final solar cells for the UAV cases considered in this doctoral dissertation.

### 3. Methods

Currently, there are many tools on the market for modeling processes carried out by enterprises. One of them are graphical and textual modeling languages. They are intended to ensure consistency and improve communication. The aim is to accelerate development, ensure better quality of products, reduce the production time, and implement the solution on the market [100].

XML (Extensible Markup Language) is a text-based language for conveying content. Its advantage is the ease of transferring information between programs and numerous tools for content processing. The downside is that the readability gets worse as the size and detail of the XML files increase. Other text formats used to exchange information include, e.g., CSV (Comma Separated Values), JSON (JavaScript Object Notation).

The graphical way of describing the assumptions and requirements of the device is clearer than the text form. The Unified Modeling Language (UML) is a graphical language used to describe the structure and behavior of a system. UML distinguishes 14 types of diagrams, e.g., diagrams of classes, objects, and communication. This allows the mapping of the modeled problem. However, many types of diagrams make the language complex and difficult to learn.

Systems Modeling Language (SysML) is a language that aims to support design, analyze, and verify complex systems [101], and explain complex ideas in an easier way. The aim is to describe the device in the form of a system of cooperating components and the relationships between them. Thanks to it, engineers are able to create diagrams that take into account a wide range of systems, including hardware, software, information, processes, and staff [100]. SysML is an extension of UML. SysML contains seven UML diagrams, but adds two more: requirements diagram and parametric diagram [102]. Thanks to this, it is able to model a wider range of systems and is easier to use.

The developed methodology, which will be used to build the simulation model, should take into account many internal aspects of the UAV, such as size, available space, weight, payload, and external ones, such as the mission scenario, flight mechanics. More and more interesting and popular from the point of view of implementation complex engineering problems is the MB method — Model-Based [103].

The MB methodology can be divided into many different components. Mainly, they can be divided into two categories, which are gradually detailed: Model-Based System Engineering (MBSE) and Model-Based Enterprise (Figure 3.1).

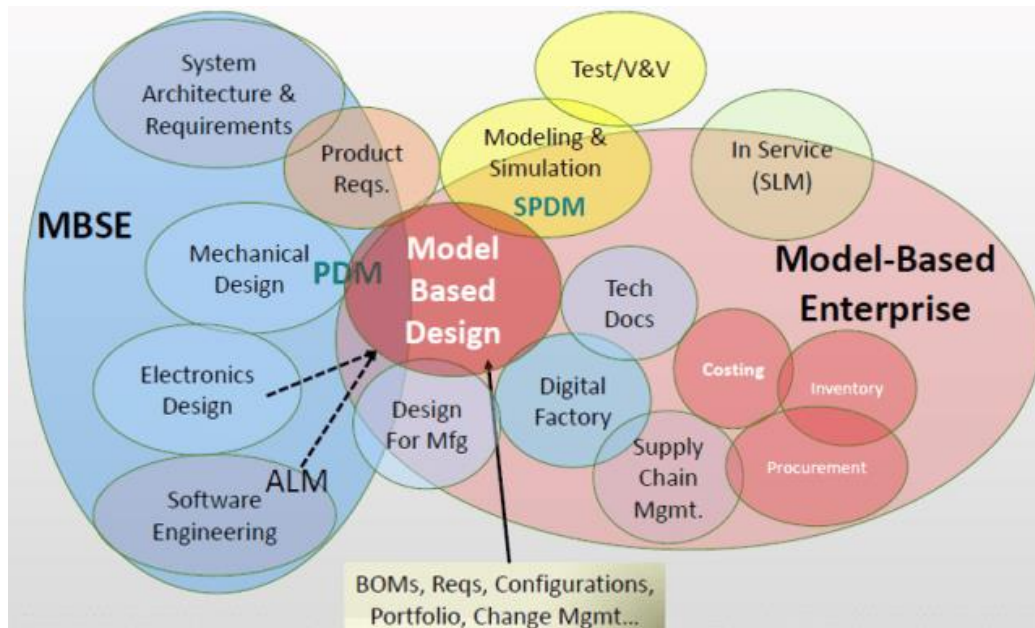


**Figure 3.1.** Division of the Model-Based methodologies [103].

The advantage of using the MB method is the smooth flow of information between different departments of the company. The exchange of information thanks to the use of MB methods is simplified and accelerated. Better connectivity makes the available information more visible, so it can be used at many stages of the production process.

Model-Based Enterprise (MBE) refers to the enterprise organizational environment. MBE deals with life cycle information management, supply chain development, cost control, and documentation.

Model-Based Systems Engineering (MBSE) is a methodology that supports engineering activities related to system requirements, analysis, verification, and validation from conceptual design, through development, to later phases of the life cycle. MBSE is basing the entire engineering life cycle on an approach based on the MB method.

Engineers use the MBSE method to gain knowledge (e.g., process efficiency, optimization, and cost reduction) and serve as a guide when implementing SysML and UML systems. SysML has become the de facto model-based language in the MBSE project [104]. MSBE consists of many components, including: software, mechanical design, electronics design. Individual systems can be modeled in the Model-Based Design (MBD) environment.

Model-Based Design is a method that combines both MBSE and MBE elements. MBD is a way to create a virtual representation of a real system [105]. Models are software representations of any component of the examined physical system and can cover a number of disciplines such as mechanics, hydraulics, pneumatics, electrical engineering, and their combination [106]. MBD reflects the operation of a physical object affected by physical laws and engineering principles. These can be single objects, components or systems.

Model-Based Design reflects the design flow described in V-Diagram (Figure 3.2). Each stage is a kind of project development phase.

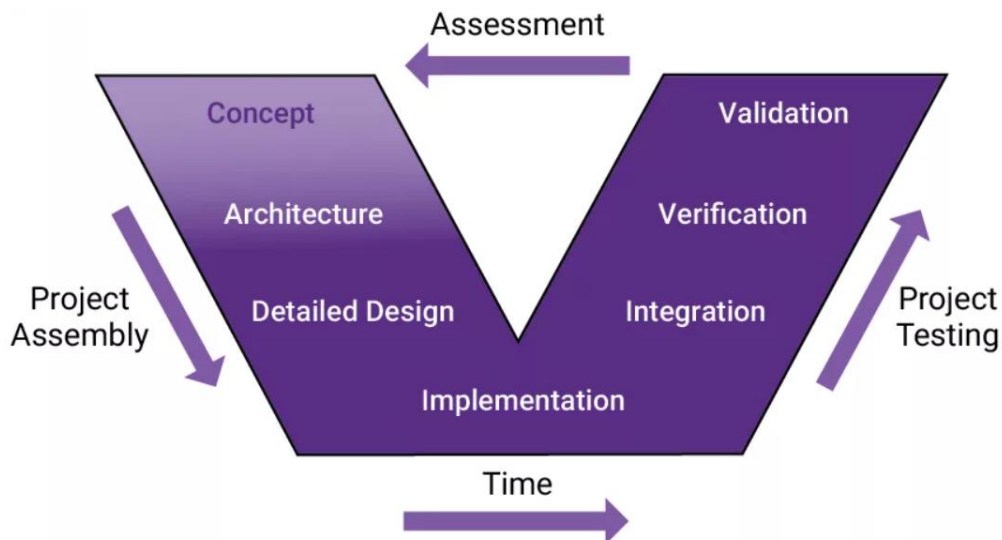


Figure 3.2. V-diagram of MBD flow [106].

Each model is individually developed, verified, and validated before being introduced to more complex systems. It can be relied on a general statement from particular to general.

The advantages of using MBD include: [106]:

- cost reduction — the ability to check the functionality of the system without the need to purchase the necessary components in advance;
- greater security — models are able to detect potential causes of software failures, unstable dynamic states;
- efficiency — shortened time to introduce new projects to the market;
- reduction of warranty-related costs — the ability to perform numerous statistical analyses, performance assessment — the worst-case analysis (WCA); ability to carry out production capacity, quality control.

In the case of creating simulation systems, the changes made to the systems and subsystems allow for their quick implementation and configuration. In order to precisely select the configuration and parts of the power supply system, taking into account many other factors and parts, such as the drive system, it was decided to use the MBD methodology.

This method has been used by many other teams, e.g., for solar-powered UAVs, both for testing propulsion systems [107], power supply system, and others [40,94]. Depending on the needs, it can be used both to optimize the structure, the flight planning path [8], and the power supply system [41].

By using the Model-Based Design (MBD) method, it will be possible to analyze the power supply system in terms of energy demand, reduce the system weight to a minimum, and provide an energy surplus that will allow continuing operations at night [108,109,110,111].

In the method of increasing the flight endurance of UAVs in particular in VTOLs, this method intends to be based on a simulation environment using the MATLAB/Simulink system. The simulation model concept includes both source code and ready-made block libraries which represent equations and modeling components. The extensive capabilities of this tool allow to gradually refine the idea and combine individual subsystems into one integrated system. Dependencies between the individual subsystems of the simulation model and the real system are shown in Figure 3.3.

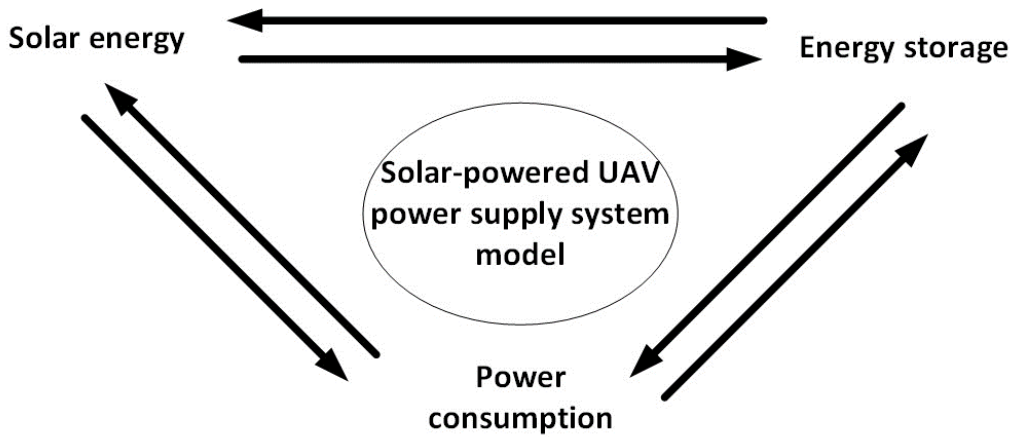


Figure 3.3. Dependencies between main subsystems in the power supply system.

### 3.1 Functional Principle of the Simulation Model

The build of the simulation models was aimed at developing a tool that would enable the calculation of the results related to the state of charge (SOC) of the battery, energy balance, and estimated flight time. A general diagram of the power supply system is shown in Figure 3.4.

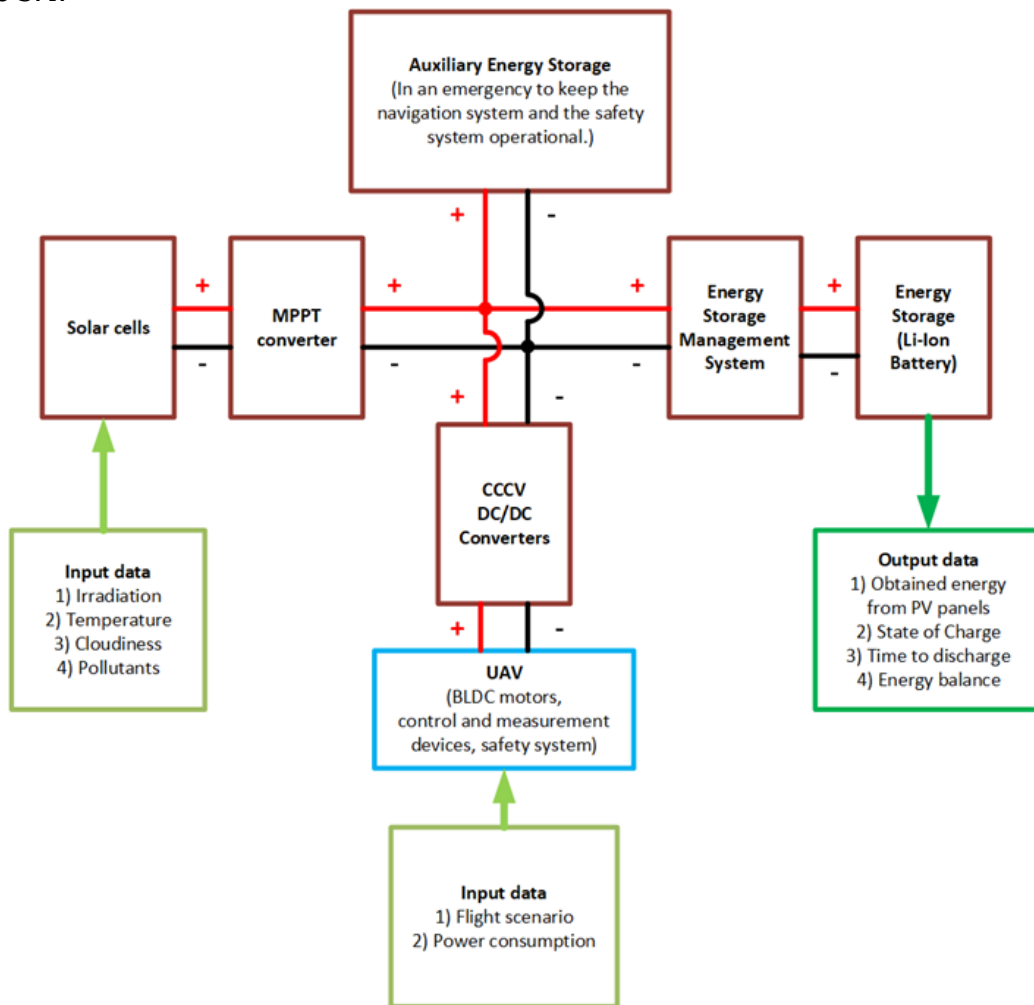


Figure 3.4. General solar-powered power supply system for UAV [15].

The first part of the input data concerns the energy produced by the photovoltaic system — irradiation, weather conditions, and pollution. These data are described in detail in subchapters 3.2 and 3.3. The second part of the input data is directly related to the flight scenario, and thus also with the energy demand. Accurate energy consumption data by electric motors require the development of a flight scenario along with accurate flight data — speed, angle of attack, sink rate, as well as taking into account external conditions — wind [112], its speed and direction.

The combination of variable inputs, solar cell parameters, and MPPT converters is the first part of the Solar Power Management System. The second element is the energy storage. Li-ion batteries, which have been chosen as the basis for the UAV power supply system, have been integrated with the photovoltaic system and with the load, which is made up of electric motors, avionics, and other peripheral systems. This part will be described in chapter 5 and 6.

The power supply system also includes elements that are not taken into account when modeling the simulation system. An example is an auxiliary battery used only in emergencies. The purpose of using such a solution is to be able to maintain the operation of critical systems in the event that the battery is drain, there is a short circuit or a failure of the power supply system.

Another element omitted from the simulation model is the Battery Management System (BMS). The battery model is supposed to provide feedback, e.g., SOC. The BMS, which balances the voltage between the battery cells, ensures optimal working conditions and does not change the charging and discharging characteristics of the battery cells and their parameters. It is an essential element in the case of building a power supply system consisting of at least several battery cells, but in the case of a simulation model based on general electrical parameters, this element can be omitted.

The last part that has been omitted is DC-to-DC converter. As in the case of the BMS, these are the elements necessary for the proper functioning of the power supply system, in which the devices on board the UAV have equal operating voltage values. Due to the lack of knowledge about the final UAV equipment and the parameters of these devices, the converters were omitted in the model. In addition, the converters are characterized by high efficiency, so the loss in these systems is negligible.

The main purpose of the simulation model is the ability to obtain results regarding the SOC of the battery, information on how long the UAV will be able to fly for a specific flight scenario. The whole thing is based on a constant comparison of the energy balance, which depends on external conditions — independent of constructors, UAV operators, as well as internal conditions that must be defined during the work. These include battery capacity taking into account the available space inside the UAV, flight path planning. Relationships regarding the UAV solar energy balance are shown in Figure 3.5.

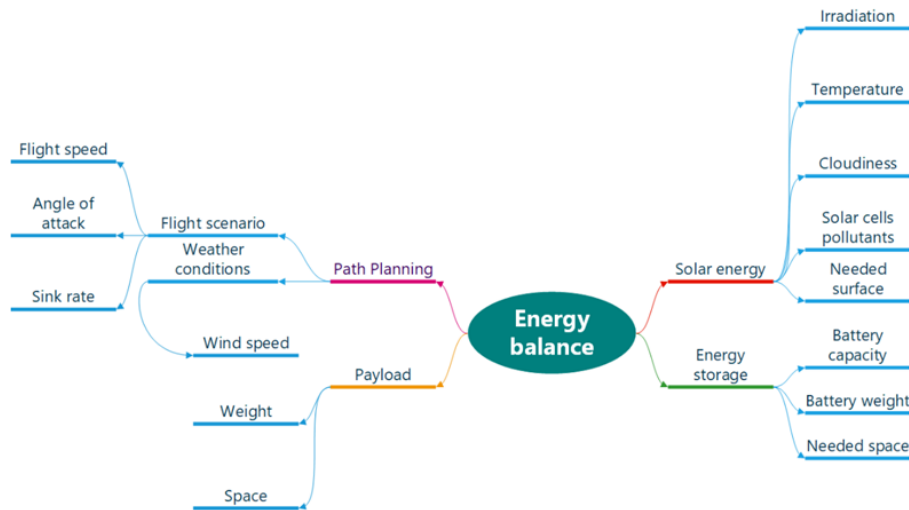


Figure 3.5. Energy balance general diagram [15].

### 3.2 Irradiance Model

Irradiation is the most important parameter in the case of obtaining solar energy. Photovoltaic cells produce energy when solar radiation hits their surface. The value of irradiation depends on several factors, where the most important are location and date. [39,113,114]. The value of solar energy is constant, but the rotation and revolution of the earth cause that it is not possible to receive this same value in one place for 24 hours. In order to calculate the irradiation value, certain equations should be used that allow to calculate the value of energy that is transferred to the photovoltaic cells. Solar constant  $G_{sc}$  is equal  $1367 \text{ W/m}^2$ . To calculate the energy at a specific location and time, it should be used the equations related to the position of the earth relative to the sun. All equations were based on publications [39,115].

The declination ( $\delta$ ) is the angle between the line to the sun and the plane of the equator.

$$\delta = 23.45 \times \sin\left(360 \times \frac{284 + n}{365}\right) \quad (3.1)$$

Where:

$n$  – day of the year.

The declination range is  $-23.45^\circ \ll \delta \ll 23.45^\circ$ . The maximum value occurs at the summer solstice (June 21) and the minimum at the winter solstice (December 22). The angle of declination is the same in the world for every location.

The hour angle ( $\omega$ ) changes all the time —  $15^\circ$  per hour. The hour angle equation  $\omega$  can be written as:

$$\omega = 15^\circ \times (\text{hour} - 12) \quad (3.2)$$

The hour angle range is  $-180^\circ \ll \omega \ll 180^\circ$ . A negative angle value occurs before noon, a positive one in the afternoon.

The zenith angle ( $\theta_z$ ) is the angle between the vertical and the line to the sun. It can be written as:

$$\theta_z = \cos(\varphi) \times \cos(\delta) \times \cos(\omega) + \sin(\varphi) \times \sin(\delta) \quad (3.3)$$

Where:

$\varphi$  = latitude  $\times \pi/180$ .

The zenith angle range is  $0^\circ \ll \theta_z \ll 90^\circ$ . The value reaches  $0^\circ$  when it is overhead and  $90^\circ$  when the Sun's disk bisects the horizon.

The length of the day (N) is calculated using the formula:

$$N = \frac{2}{15} \times \text{Arccos}(-\tan \varphi \times \tan \delta) \quad (3.4)$$

The irradiation of the surface  $G_{on}$ , when  $\theta_z = 0^\circ$  just outside the atmosphere can be calculated from the  $G_{sc}$  constant and the day of the year (n) by the formula:

$$G_{on} = G_{sc} \times \left[ 1 + 0.033 \times \cos \frac{360 \times n}{365} \right] \quad (3.5)$$

The solar constant  $G_{sc}$  is an averaged value. The earth's orbit, due to the shape of an ellipse (not a sphere), causes the distance between the sun and the earth to change by about 3.3% [39]. The hourly radiation  $I_o$  and the daily radiation  $H_o$  can be calculated using the following formulas:

$$\begin{aligned} I_o = & \frac{12 \times 3600}{\pi} \times G_{sc} \times \left[ 1 + 0.033 \times \cos \frac{360 \times n}{365} \right] \\ & \times \left[ \cos(\varphi) \times \cos(\delta) \times (\sin \omega_2 - \sin \omega_1) \right. \\ & \left. + \frac{\pi \times (\omega_2 - \omega_1)}{180} \times \sin \varphi \times \sin \delta \right] \end{aligned} \quad (3.6)$$

Where:

$\omega_1$  and  $\omega_2$  are the hour angles between the considered hours.

$$\begin{aligned} H_o = & \frac{24 \times 3600}{\pi} \times G_{sc} \times \left[ 1 + 0.033 \times \cos \frac{360 \times n}{365} \right] \\ & \times \cos(\varphi) \times \cos(\delta) \times \sin \omega_s + \frac{\pi \times \omega_s}{180} \times \sin \varphi \times \sin \delta \end{aligned} \quad (3.7)$$

The unit of hourly irradiation is  $J/m^2$  and daily irradiation  $J/day \times m^2$ . It is necessary to convert the obtained irradiation values to watt-hours (Wh) for consistency of the units in subsequent equations.

Air Mass (AM) Factor is the distance traveled by the sun's rays to reach the earth's surface. The value of the AM factor can be calculated using the formula:

$$AM = \frac{\text{path length travelled}}{\text{vertical depth of the atmosphere}} = \frac{1}{\cos \theta_z} \quad (3.8)$$

An explanation of the air mass factor is shown in Figure 3.6.

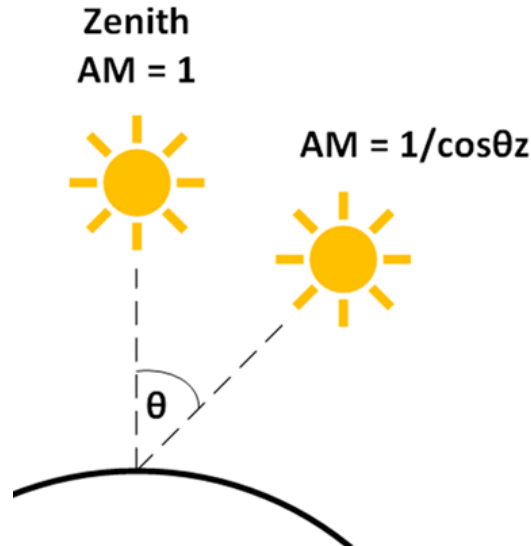


Figure 3.6. Air Mass [15].

The above formulas presented in this chapter allow to calculate the general value of irradiation that is able to reach the ground. Solar radiation can be divided into direct, diffused, and reflected radiation. In the case of PV panels, the first two are the most important. Reflected radiation is difficult to define numerically, as it depends on the environment and the location of the solar cells. In the case of UAVs, this radiation type can be completely omitted.

Direct radiation falls directly from the sun onto the surface of the photovoltaic panel. This type of radiation is not dispersed in any way. Diffuse radiation is scattered by the atmosphere in every direction, and only a fraction of this radiation reaches the earth's surface.

In 1976, Hoyt C. Hottel [116] presented an approximate method for calculating the value of direct and diffuse radiation. This method took into account the zenith angle and the height above sea level. It also took into account the use of different coefficients for different climates (tropical, midlatitude summer, subarctic summer, midlatitude winter).

Direct radiation  $G_{cb}$  can be written using the formula:

$$G_{cb} = \tau_b \times G_{on} \times [\cos(\varphi) \times \cos(\delta) \times \cos(\omega) + \sin(\varphi) \times \sin(\delta)] \quad (3.9)$$

Where:

$\tau_b$  is the ratio of the transmitted direct radiation to the total radiation incident on the top of the atmosphere. This factor can be calculated as follows:

$$\tau_b = \frac{G_{cb}}{G_o} = a_0 + a_1 \times e^{\left(\frac{-k}{\cos \theta_z}\right)} \quad (3.10)$$

Where:

$G_o = G_{on} \times \cos(\theta_z)$ , and the factors  $a_0$ ,  $a_1$ ,  $k$  are constants calculated from the following equations.

$$a_0 = r_0 \times (0.4237 - 0.00821 \times (6 - A)^2) \quad (3.11)$$

$$a_1 = r_1 \times (0.5055 - 0.00595 \times (6.5 - A)^2) \quad (3.12)$$

$$k = r_k \times (0.2711 - 0.01858 \times (2.5 - A)^2) \quad (3.13)$$

Where:

$A$  is the height above sea level. The above equations can only be used for  $A < 2.5$ . The values of the coefficients  $r_0$ ,  $r_1$ ,  $r_k$  are constants that are selected appropriately for a given area (Table 3.1).

**Table 3.1.** Coefficients for climate type and sample location [15,116].

Climate type	$r_0$	$r_1$	$r_k$	Sample location
Tropical	0.95	0.98	1.02	Nairobi
Midlatitude summer	0.97	0.99	1.02	Rome
Subarctic summer	0.99	0.99	1.01	Ny-Ålesund
Midlatitude winter	1.03	1.01	1.00	Gliwice

Diffuse radiation can be calculated using the following formula:

$$G_{cd} = \tau_d \times G_{on} \times [\cos(\varphi) \times \cos(\delta) \times \cos(\omega) + \sin(\varphi) \times \sin(\delta)] \quad (3.14)$$

Where:

$\tau_d$  is the ratio of the transmitted diffuse radiation to the total radiation incident on the top of the atmosphere. This factor can be calculated as follows:

$$\tau_d = \frac{G_{cd}}{G_o} = 0.271 - 0.294 \times \tau_b \quad (3.15)$$

Using the previous equations, it can be calculated the value of total radiation — irradiation. Total irradiation allows to define an input values to the solar cell, which can be written as:

$$\begin{aligned} G_c &= G_{cb} + G_{cd} \\ &= (\tau_b + \tau_d) \times G_{sc} \times \left[ 1 + 0.033 \times \cos \frac{360 \times n}{365} \right] \\ &\times [\cos(\varphi) \times \cos(\delta) \times \cos(\omega) + \sin(\varphi) \times \sin(\delta)] \end{aligned} \quad (3.16)$$

It is the value that falls on the extraterrestrial horizontal surface. In the case of total hourly radiation  $I_c$ , the equation is extended by the time range.

$$\begin{aligned}
I_c = & \frac{12 \times 3600}{\pi} \times (\tau_b + \tau_d) \times G_{sc} \times \left[ 1 + 0.033 \times \cos \frac{360 \times n}{365} \right] \\
& \times \left[ \cos(\varphi) \times \cos(\delta) \times (\sin \omega_2 - \sin \omega_1) \right. \\
& \left. + \frac{\pi \times (\omega_2 - \omega_1)}{180} \times \sin \varphi \times \sin \delta \right]
\end{aligned} \tag{3.17}$$

The above equations are the basis of the source code, which was then implemented into the simulation environment. The equations allow to obtain the irradiation value for a given time and location. The result of the above equations is the value for a given horizontal surface.

### 3.2.1 Solar Energy Limitations

The energy obtained by photovoltaic cells depends not only on direct and indirect radiation, but is also subject to external limitations. The obtained irradiation value in the above subsection shows the formula for ideal weather conditions. In fact, such conditions rarely exist outside of certain areas. We often deal with clouds that limit the access of sunlight, which causes limitations in energy production. Clouds can be divided into three main types:

1. Cirrus;
2. Cumulus;
3. Stratus.

The scale of cloud cover changes depending on the type of clouds. Cloud cover is measured on the okta scale [117]. The unit, or octane, means 1/8 of the sky. Depending on the size of the cloud, an appropriate cloud cover value is assigned (from 0 — no clouds to 8 — full cloud cover). The percentage of solar power reduction can be written as: 0—100%, 1—98%, 2—94%, 3—88%, 4—79%, 5—70%, 6—54%, 7—50%, 8—7% [118]. The cloud cover scale of 9/8 means the sky is obscured (9—0%) by fog or other meteorological phenomena [118,119,120].

The second type of limitation is temperature. Temperature fluctuations affect the efficiency of photovoltaic cells. The higher solar cell temperature, the lower their efficiency [39,115,121]. The decrease in efficiency is caused by the heating of the PV panels under the influence of sunlight and the reduction of the heat dissipation capacity during operation at elevated ambient temperatures [39,122,123]. The operation of photovoltaic panels at high temperatures not only results in lower electric power, but also accelerates the process of degradation of photovoltaic cells [123].

It can be seen that high temperature often guarantees a clear sky, although on the other hand it results in deterioration of the parameters of the solar cell. Each solar cell has a temperature coefficient that is related to voltage, current, and power [115]. As the temperature increases, the parameters of the solar cell deteriorate, reducing its power and efficiency (Figure 3.7).

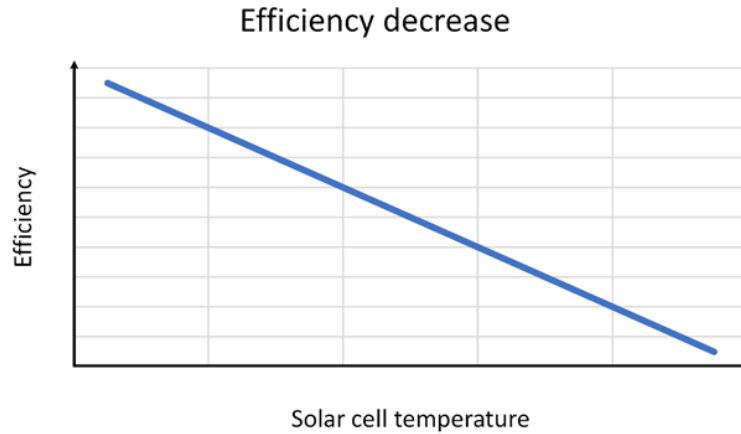


**Figure 3.7.** Efficiency decrease with the increase of solar cell temperature [15].

For flying vehicles, the decrease in temperature with increasing altitude must be taken into account. The distribution of air temperature depends mainly on latitude, height above sea level, season, and topography. The value of temperature drop can be defined as  $0.5^{\circ}\text{C}$ — $1^{\circ}\text{C}$  for every 100 meters [124]. Such approximations of the temperature drop can be used up to the tropopause.

Then, from the beginning of the stratosphere, a constant temperature value of  $-51^{\circ}\text{C}$  can be assumed up to 20 km [124]. Such a simplification is sufficient for HALE UAVs that fly up to a ceiling of about 20 km. In order to calculate the current temperature for a given altitude, it can be used as the following formula.

$$T_C = T_I - [H_R \times (T_D \times 100)] \quad (3.18)$$

Where:

$T_C$  is the current temperature at the flight altitude,  $T_I$  is the temperature on earth,  $H_R$  is the relative flight altitude in meters,  $T_D$  is the temperature drop. The value  $T_D$  can be assumed as  $\sim 1^{\circ}\text{C}$  for a dry-adiabatic temperature gradient and  $\sim 0,6^{\circ}$  for a moist adiabatic temperature gradient [125].

Air pollution and pollution of photovoltaic cells are other elements limiting the efficiency of PV panels. These data are measurable, but difficult to determine their exact value. These include layers of dust, pollen, smog, frost, and even snow or raindrops. These values are also constantly changing. In order to more precisely determine the contaminants and the possibility of encountering them at a given time and location, they should be grouped. The aim is to facilitate the identification of the places and times of such contamination. The intensity and impact on the operation of the solar-powered UAV power supply system would also need to be determined. Sometimes this kind of pollution is temporary and won't matter much in the scale of the entire mission.

### 3.3 PV System Model

Using the built-in PV Array library [126] in MATLAB/Simulink system, a single model of the solar cell was developed.

In order to obtain a precise and reliable result, the model had to be configured according to the data of a specific single solar cell. At this stage, a decision was made to choose a SunPower crystalline solar cell. The SunPower Maxeon solar cell is a pioneer in

regard to flexible crystalline photovoltaic cells. It is quickly available for purchase on the market and has very good parameters. According to the manufacturer, the SunPower Maxeon Ne3 provides an efficiency of over 24.34% [127]. The PV Array library was configured according to the parameters of the SunPower Maxeon Ne3 solar cell. Input data for the model were taken from the data sheet [128]. Earlier versions of this solar cell were also used in other UAVs and gliders [37,49,108].

The model of the MPPT controller was also used from MATLAB resources [129]. The exact operation of the model is described in article [130]. This kind of Maximum Power Point Tracking is based on Perturbation & Observation (P&O) algorithm [129]. The Perturb and Observe method is one of the most used control methods in commercial MPPT controllers [131]. The model had to be properly adapted to the UAV power supply system. Defining the appropriate parameters of the MPPT regulator will be determined only after the selection related to the system voltage and the MPPT model.

At this stage of the work, it was decided that in the initial simulations a commercial MPPT from Genasun company [132] will be selected as the model of the MPPT. The exact type of device will be selected only after selecting the appropriate parameters of the power supply system. The reason for choosing Genasun device was market availability, low weight, and size of the MPPT modules, that is especially important in UAVs. An additional advantage of the Genasun MPPT regulator is the use of the P&O algorithm in the products of this brand [133].

### 3.4 Battery Model

As in the case of the solar cell model and the MPPT, also in this case a ready library called the Generic Battery Model in the Simulink add-on was used [134].

The model had to be configured according to the data of a specific battery cell. The choice fell on the Li-ion NMC battery cell — Samsung INR18650-35E. The advantage of this battery cell is a high value of energy density, a wide range of operating temperatures, and performance.

Another advantage was the ability to buy this type of battery cell with solder tabs (Figure 3.8). This solution is important when building a flexible battery pack. Rigid welding of nickel plates can cause stresses during the buckling of the wings in which the battery cells are to be located. The use of battery cells with solder tabs allows them to be connected with a flexible cable, thanks to which the flexibility of the battery module increases. The Generic Battery Model was matched to the parameters of the Samsung INR18650-35E [135].



**Figure 3.8.** Samsung INR18650 35E with solder tabs.

## 3.5 Model Simplifications

### 3.5.1 Irradiance Model Simplification

In the case of changing the inclination of the PV cell to a horizontal surface, the inclination angle  $\beta$  must also be taken into account (Figure 3.9). In addition to the inclination angle  $\beta$ , the solar azimuth angle  $\gamma_s$  should also be taken into account. Solar azimuth angle is responsible for the direction of the location of the PV panel relative to the south direction.

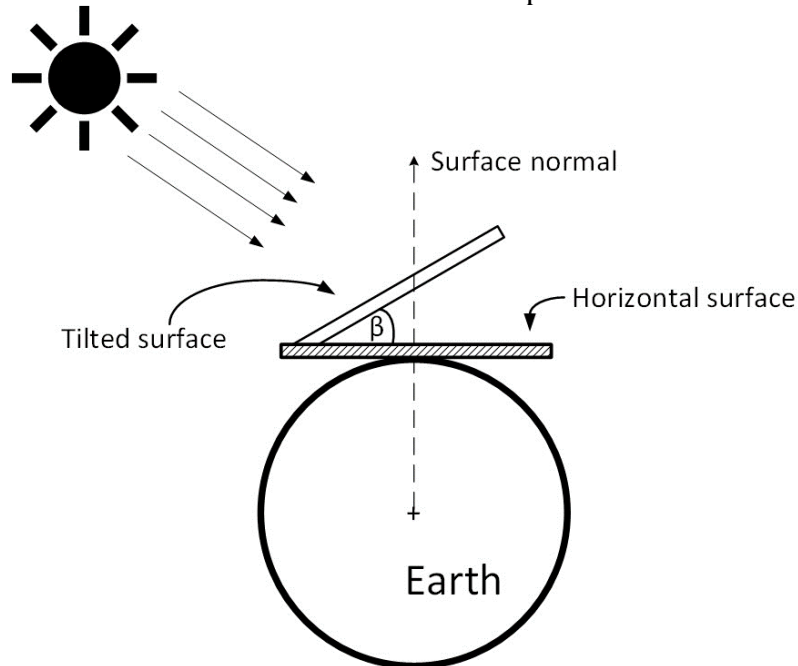


Figure 3.9. Tilted surface angle.

Depending on the value of the angles  $\beta$  and  $\gamma_s$  and the side of the hemisphere (north or south), equation 3.3 should be modified. Appropriate transformations have been applied in publications [39,115].

Due to the almost impossible to simulate the exact flight conditions, depending on the direction and speed of the wind, and the flight planning paths, the angle of inclination and the angle of the solar azimuth were omitted.

Another reason for omitting these variables in the calculations is the small values of flight path angle for UAVs. Large angle values are rarely used for the optimal flight path. Such a flight trajectory is not accurate in the case of the endeavor to obtain UAV's flight long-endurance. Even if large flight path angle values occur, they are rather temporary and insignificant compared to the rest of the flight.

The drone surface covered with solar cells was depicted as a material point. Depending on the airfoil, the surface is not straight but convex. To simplify the calculations and simulations, the curvature of the wing was not taken into account.

Winglet and tail angles were also not taken into account in the simulation model. Simplification was also not taking into account the shaded areas of photovoltaic cells by winglets and fuselages during low angles of the sun's elevation above the horizon.

Each of these simplifications should be verified during the research on the test stands and during the UAV flights. During approaching to the issue of extending the UAV flight, such simplifications seem justified at least in the initial phase of developing the methodology.

### *3.5.2 PV Model Simplification*

In the case of a photovoltaic system, the simplification concerned the MPPT. Depending on the model of the MPPT system, its efficiency can reach up to 99.85% [136] and the standard is to work with efficiency around 95%.

Ultimately, individual systems such as solar-powered UAV strive to develop a dedicated solution and not using a commercial device. A commercial device is a good solution at the prototype construction stage. Due to certain restrictions, these devices may not fully use their capabilities for dedicated UAVs.

The simulation model does not use any efficiency of the system, which makes it work with 100% efficiency.

### *3.5.3 Battery Model Simplification*

The battery model was developed on the basis of a single lithium-ion battery cell. The first simplification of the model was the "freezing" of the temperature value. The temperature range and its reference to the conditions outside the UAV were not taken into account. The operating temperature was set to an optimal value of 20°C. The conditions inside the battery housing are controlled by thermistors. Improving the thermal permeability of the battery module walls is to ensure that they are covered with a layer of material with a low  $\lambda$  coefficient (coefficient of thermal conductivity). Single battery cells will also be embedded in a stabilizing foam that will allow the module to deform in the event of wing buckling. Such a cover will additionally insulate the battery cells against low temperatures. In order to ensure optimal working conditions, the entire battery module will be equipped with a heating foil. In low temperatures, it will allow to heat up the temperature inside the battery housing.

Batteries generate heat during operation. Good thermal insulation should allow the battery module to accumulate thermal energy inside the battery pack. High temperatures are not as much taken into account as low. Mainly due to the ceilings at which UAVs are to fly.

The second simplification is not taking into account the aging effect of the battery. In the case of a specific system such as UAV, this effect can be omitted. After several hundred charging cycles, the batteries will be replaced if their parameters deteriorate. Moreover, the working conditions in which the batteries will work are difficult to analyze without a demonstrator that will reflect the working conditions of the batteries.

Only performing flights at high altitudes will make it possible to verify whether the simplifications of the model can be accepted or whether the simulation model should be refined.

## 4. Preliminary Verification Results

### 4.1 Irradiance Model

The irradiation model allowed to obtain the value of energy that reaches a given location in a given time. The equations contained in subsection 3.2 allowed for the development of a script that calculates the value of irradiation directly reaching the earth.

Ultimately, all simulations that will be carried out will be carried out for the location of Gliwice in Poland (northern hemisphere). Depending on the seasons and periods taken into account, the value of irradiation will change. In Figure 4.1 shows how the value of irradiation will change on the days that start successive seasons.

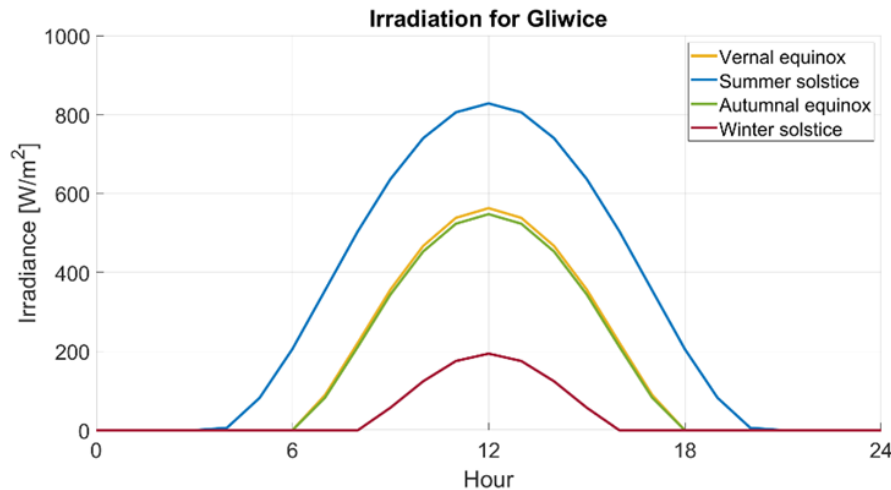


**Figure 4.1.** Irradiation for Gliwice for different days beginning seasons of the year [15].

In order to illustrate the changes in irradiation values in different places around the world at the same time, an additional 4 random locations were selected:

- Ny-Ålesund (Norway; Svalbard) – latitude:  $78^{\circ} 55' 30''$  N; longitude:  $11^{\circ} 55' 20''$  E;
- Gliwice (Poland) – latitude:  $50^{\circ} 17' 32''$  N; longitude:  $18^{\circ} 40' 3''$  E;
- Rome (Italy) – latitude:  $41^{\circ} 53' 36''$  N; longitude:  $12^{\circ} 28' 58''$  E;
- Mexico City (Mexico) – latitude:  $19^{\circ} 26' 0''$  N; longitude:  $99^{\circ} 8' 0''$  W;
- Nairobi (Kenya) – latitude:  $1^{\circ} 17' 11''$  S; longitude:  $36^{\circ} 49' 02''$  E.

Coordinates for the above location were obtained from the GeoHack website [137]. Calculations for the vernal equinox were performed for each location. On this day, everywhere in the world, the day lasts 12 hours. Figure 4.2 illustrates how important the location is in the case of solar-powered UAVs.

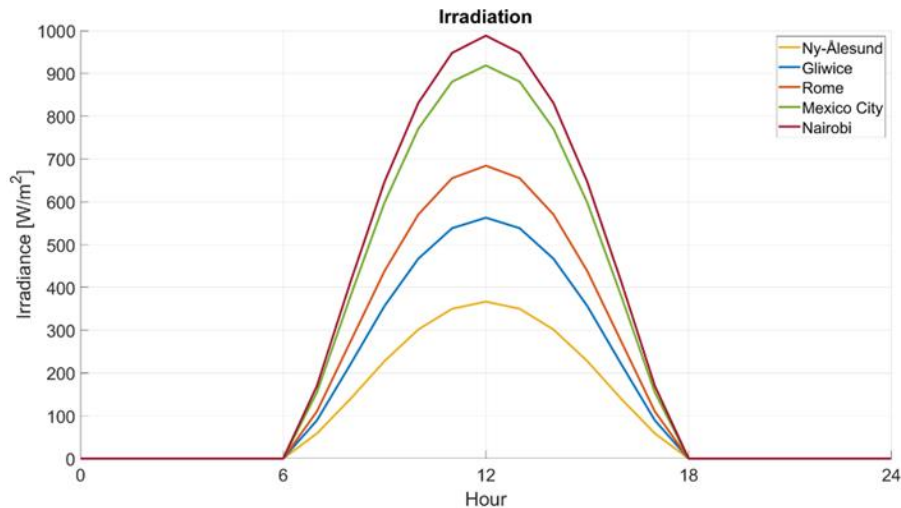


**Figure 4.2.** Irradiation for different locations in the Vernal equinox [15].

Two more locations have been added to the previous locations:

- Sydney (Australia) – latitude: 33° 52' 04" S; longitude: 151° 12' 36" E;
- Buenos Aires (Argentina) – latitude: 34° 35' 0" S; longitude: 58° 55' 0" W.

Their addition is to find out the value of irradiation also in the southern hemisphere. The calculated value is the daily energy incident per square meter.

Calculations were made for days beginning a new season. Table 4.1 presents the value of the daily value of energy that reaches the earth on these days. The table includes only the location without the altitude above sea level. The default height for each location is 0 meters.

For each of the listed locations, appropriate coefficients from Table 3.1 were selected. Choosing the wrong coefficients related to the geographical zone causes changes of a maximum of 1.5% in relation to the presented values.

**Table 4.1.** Daily irradiation for different locations and date in kWh to square meter.

Location	21 III	21 VI	23 IX	22 XII
<b>Ny-Ålesund</b>	2.52	7.11	2.4	0.1
<b>Gliwice</b>	3.88	7.46	3.75	0.92
<b>Rome</b>	4.75	7.63	4.62	1.81
<b>Mexico City</b>	6.41	7.22	6.3	4.4
<b>Nairobi</b>	6.92	5.88	6.85	6.5
<b>Sydney</b>	5.58	2.58	5.59	8.14
<b>Buenos Aires</b>	5.52	2.5	5.53	8.14

Another comparison and variable that significantly affects the irradiation result is the value of height above sea level. For each of the previous characteristics, this value was equal to 0. This was mainly due to the comparison only impact of geographic coordinates. Comparison of other altitude values is shown in Figure 4.3 for the location of Gliwice.

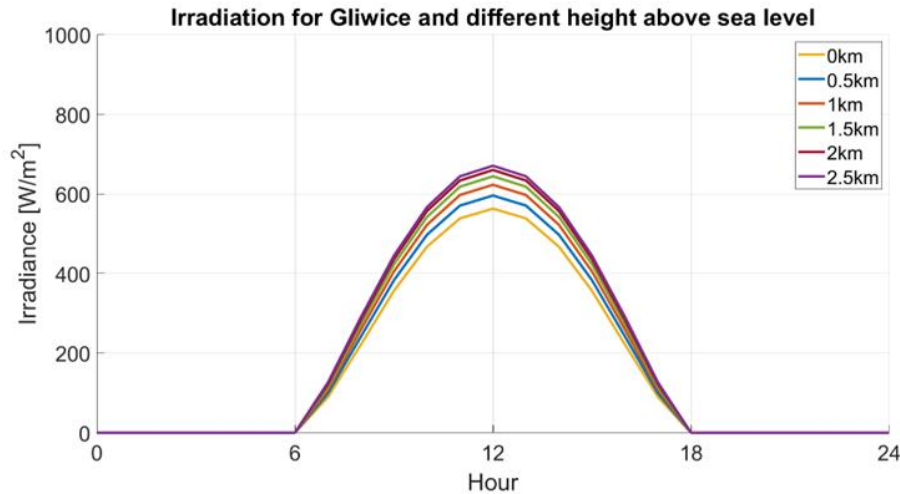


**Figure 4.3.** Irradiation for Gliwice at vernal equinox for different altitudes [15].

Analyzing formula 3.13, it can be seen that the height above sea level can be referred to a maximum height of 2.5 km taking into account the Hottel's estimation method. [39,115,116].

For the 0 – 2.5 km the range of height, the peak values, and daily irradiation were as follows:

- 0 km — 563 W/m<sup>2</sup> — 3.91 kWh/m<sup>2</sup>;
- 0.5 km — 596 W/m<sup>2</sup> — 4.18 kWh/m<sup>2</sup>;
- 1 km — 623 W/m<sup>2</sup> — 4.4 kWh/m<sup>2</sup>;
- 1.5 km — 644 W/m<sup>2</sup> — 4.58 kWh/m<sup>2</sup>;
- 2 km — 660 W/m<sup>2</sup> — 4.72 kWh/m<sup>2</sup>;
- 2.5 km — 670 W/m<sup>2</sup> — 4.81 kWh/m<sup>2</sup>.

The difference is the highest in the lowest altitudes. It is equal respectively 6.9% between 0.5 km and 0 km and 5.3% between 1 km and 0.5 km in the daily irradiation value. In the last range between 2.5 km and 2 km, the difference is smaller and it is equal to 1.9%.

The difference between peak values from 0 and 2.5 km is equal 19% and 23% in the daily irradiation value.

For each location, time of measurement, and altitude level, the irradiation values will vary. Figure 4.3 shows the general relationship between altitude and sea level — flight altitude matter and allows for better parameters and performance of the PV system.

The last comparison is a comparison of the daily irradiation characteristics and the so-called full solar tracking. Full solar tracking consists in continuous tracking of the incidence of sunlight so that the angle between the beam of direct radiation and the PV panel is equal to 90°.

From the point of view of the UAV, full solar tracking is impossible to implement, because in the case of sunrise or sunset, the UAV would have to climb vertically or nose-dive. The goal is to illustrate how continuous tracking of the movement of the sun's rays can improve the performance of a photovoltaic system. The UAV can gradually track the movement of the sun's rays, provided that the weather conditions allow it, e.g., wind or permits of the relevant services supervising air zones.

By changing the flight path angle or sink rate, it can keep up with direct sunlight to a greater extent. In practice, it will be more common to meet single-axis solar tracking, i.e., keeping up with the flight in a specific direction. Such a flight scenario can be implemented if both the flight path planning and weather conditions allow it. The analysis

was also performed for the location of Gliwice at the spring equinox and summer solstice (Figure 4.4).

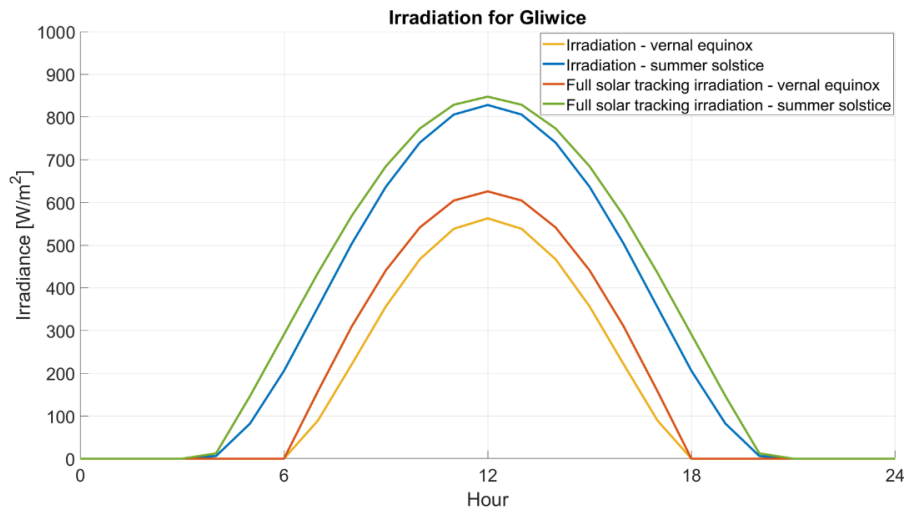


**Figure 4.4.** Irradiation for Gliwice at vernal equinox for different altitudes compared to the full solar tracking.

The results of the developed analyzes are as follows:

- Irradiation — vernal equinox — 3.88 kWh/m<sup>2</sup>;
- Irradiation — summer solstice — 7.46 kWh/m<sup>2</sup>;
- Full solar tracking irradiation — vernal equinox — 4.72 kWh/m<sup>2</sup>;
- Full solar tracking irradiation — summer solstice — 8.29 kWh/m<sup>2</sup>.

Differences in the value of energy obtained with full solar tracking will vary depending on the date and location. For Gliwice, the increase in value was 21% at the spring equinox and 11% on the summer solstice.

## 4.2 PV System Model

The result of the photovoltaic system model can be the current-voltage (I-V), power-voltage (P-V) characteristics, and their variations in different irradiation values and temperature conditions.

Figure 4.5 shows the I-V and P-V characteristics for the SunPower Maxeon Ne3 solar cell for various irradiation values according to the data entered into the model contained in the manufacturer's data sheet [127,128]. Changing the level of irradiation allows to verify what output parameters the solar cell will have during different dates, times or in the event of cloudiness.

## Characteristics of SunPower Maxeon Ne3

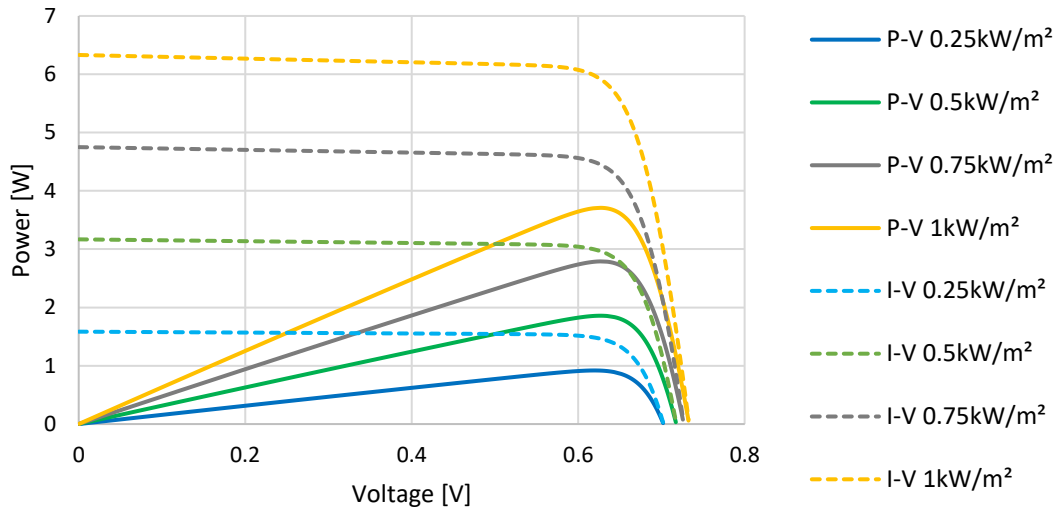


**Figure 4.5.** I-V and P-V characteristics of SunPower Maxeon Ne3 depending on irradiation.

Temperature fluctuations affect the efficiency of the solar cell and thus also its I-V and P-V characteristics. Figure 4.6 shows characteristics for irradiation equal  $1000 \text{ W/m}^2$  in four temperature values:  $0^\circ\text{C}$ ,  $25^\circ\text{C}$ ,  $50^\circ\text{C}$ , and  $75^\circ\text{C}$ .

## Characteristics of SunPower Maxeon Ne3

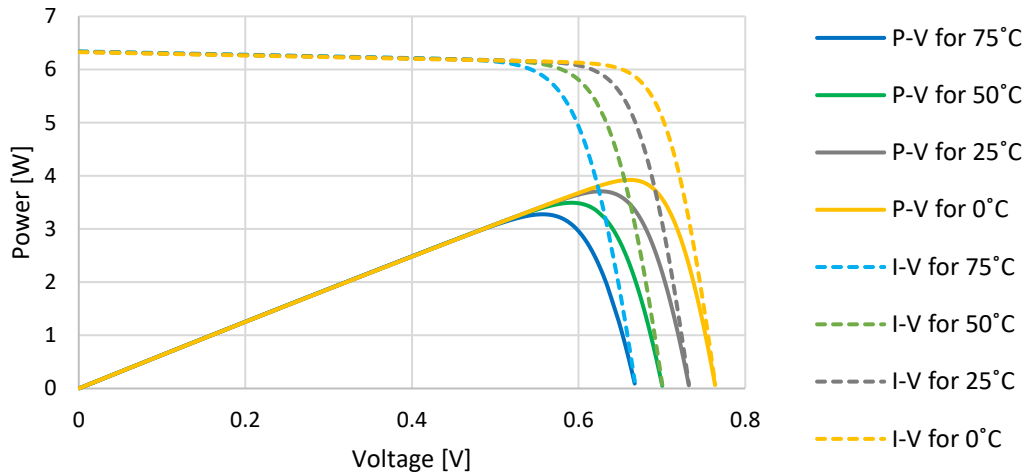


**Figure 4.6.** I-V and P-V characteristics of SunPower Maxeon Ne3 depending on temperature.

The correctness of the model operation can be seen both from the decrease in efficiency at lower irradiation values and in the increase of the solar cell operating temperature.

The solar cell model developed in this way was connected to the MPPT system. Due to the need to connect the energy storage (batteries) in order to simulate the correct operation of the PV system, several solar cells had to be connected in series so that they were able to charge the battery.

10 pcs. of solar cells were connected in series. The value of the voltage  $V_{mpp}$  in the system, depending on irradiation and temperature. It should oscillate between 5-7 volts. Single Li-ion cells with a nominal voltage of 3.6V were used as the battery.

Table 4.2 shows the results comparing the power from a single solar cell with the results from the MPPT system. The power from the MPPT system was divided by 10, which is the number of solar cells in the solar power supply chain.

**Table 4.2.** Comparison of solar cell and MPPT power

<b>Irradiation (W/m<sup>2</sup>)</b>	<b>Temperature (°C)</b>	<b>Solar cell power (W)</b>	<b>MPPT power (W)</b>
1000		3.78	3.78
750	25	2.83	2.82
500		1.88	1.87
250		0.92	0.91
		0	4.02
1000	25	3.78	3.78
	50	3.53	3.5
	75	3.28	2.99

By analyzing the results contained in Table 4.2, it can be concluded the correct operation of the MPPT system. Almost 100% efficiency of the system occurs when the system is analyzed at a temperature equal 25°C and below 25°C, even with significant fluctuations in the irradiance value. On the other hand, the efficiency of the system decreases with increasing temperature. For an irradiance of 1000 W/m<sup>2</sup> and a temperature of 75°C, the efficiency was 91%.

### 4.3 Battery Model

The results of the energy storage model are the charging and discharging characteristics of the battery cell. Figure 4.7 shows the discharge characteristics of the battery cell, where on the x-axis the unit is the capacity expressed in ampere-hour (Ah). On the other hand, the unit on the x-axis of the battery cell discharge characteristics shown in Figure 4.8 is the time expressed in hours.

The data entered into the Generic Battery Model library can take the form of constant values, but also parametric variables.

## Samsung INR 18650-35E discharge characteristics

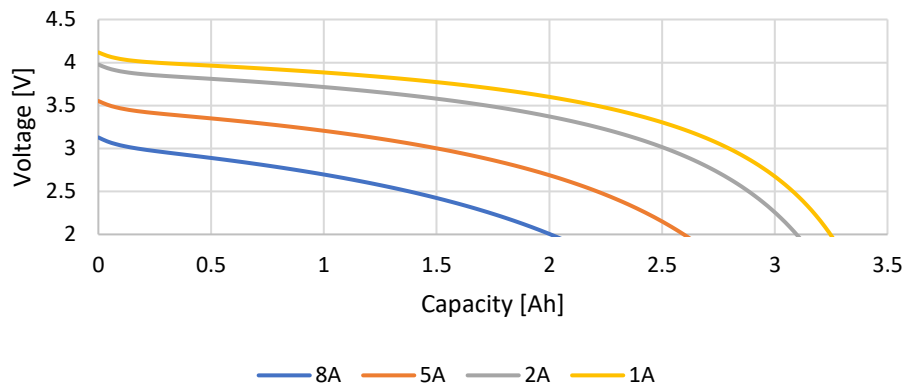


Figure 4.7. Initial discharge characteristics of Samsung INR18650-35E.

## Samsung INR 18650-35E discharge characteristics

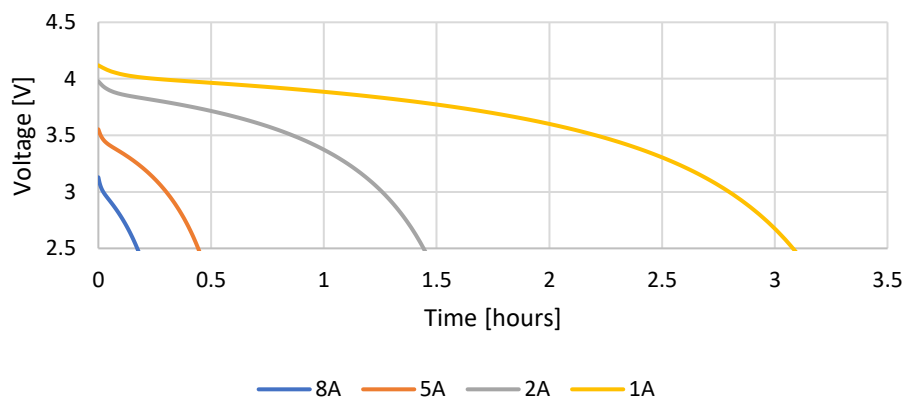


Figure 4.8. Initial discharge characteristics of Samsung INR18650-35E.

The correct operation of this part of the power supply system can be seen by analyzing Figure 4.8 where the time changes more or less proportionally to the value of the load current of the system. Moreover, the voltage drop associated with a higher current load allows to verify the correct operation of the simulation model.

The simulation model largely idealizes the characteristics of the values, which will often not agree with real measurements. In Figure 4.7 maximum load characteristic (8A) reduces the capacity of the battery cell by almost 40% compared to 1A load, which is unheard of in real systems.

## 4.4 Summary

The preliminary results verifying the operation of the systems were the basis for checking the correct operation of the system components and their tuning. The next stage was also aimed at integrating individual systems into one system representing SPMS.

Tuning the models will consist in carrying out tests and measurements of the photovoltaic system and batteries, and then implementing these data into the simulation environment.

## 5. Case Study

The doctoral dissertation focused on two types of UAVs. The first was a fixed-wing UAV belonging to the UAV family called Twin Stratos (TS), the second was a tail-sitter VTOL. The Twin Stratos UAVs were designed as a double-hull with two electric motors. The empennage is based on an inverted-v-shaped tail. Photovoltaic cells have been placed on the wings of the TS, which allow the UAV to extend its operating time. TS is a project implemented by Polish and Norwegian research institutes and companies [138]. Several units in different scales have been developed for research, testing, and verification of individual subsystems:

- Twin Stratos 110 (TS110) — 1:10 scale — UAV for testing the control system and familiarizing with the specifics of controlling this type of drone;
- TS18 — UAV for testing the power supply system and the energy consumption system;
- TS17 — UAV for testing the power supply system, verification of the simulation model of the power supply system, and assembly technology (Figure 5.1.);
- TS12 — UAV for long endurance flights, verification of flight parameters and energy autonomy performance. Intended for research tests;
- TS — target UAV intended for research and commercial services [139].

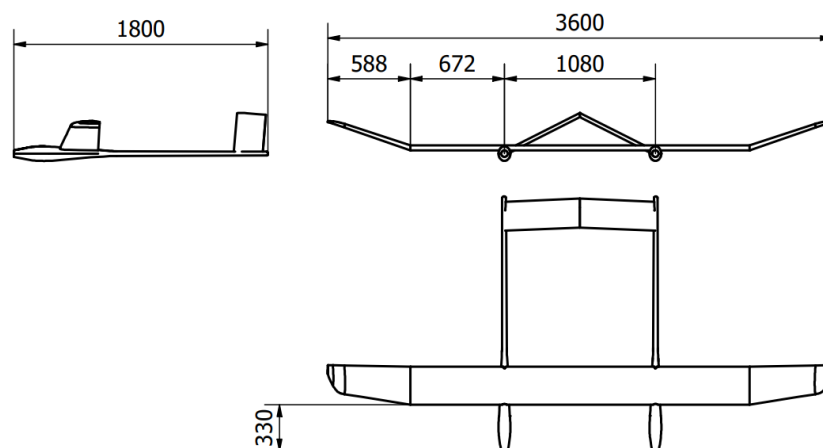


**Figure 5.1.** TS17 dimensions; courtesy of Kamil Zenowicz

In the doctoral dissertation, two Twin Stratos models were used for the calculations: TS17 and TS12. The aim was to determine how the difference in scale will affect energy production and energy consumption. What ratio will be maintained between energy produced and energy demand taking into account the difference in maximum ceilings due to a different class of the facility. TS17 can be classified as LALE UAV, while TS12 as HALE UAV.

In the TS airfoil is mixed. Depending on the part of the wing, it can be Hq-w 12x2.5 (in the center wing) and configurations of the Hq-w 11x2.5 and Hq-w 10x3.

The second considered case study is VTOL. Based on the existing solutions and products, a conceptual model of the VTOL tail-sitter was developed. The conceptual UAV based on the existing structure was used to explore the possibility of extending the flight time by installing PV panels on its structure. The design is based on SkyX commercial VTOL (Figure 5.2). The difference lies in the use of two electric motors and not four as in the case of SkyX. Such a combination was configured by combining two VTOLs: SkyX [29] and WingtraOne [32].



**Figure 5.2.** UAV SkyX [29]: (a) front view; (b) 3D view.

The tail-sitter is dimensionally similar to the TS17. The wingspan is 2.5m and the chord is just over 0.5m. Compared to the TS, the VTOL airfoil is symmetrical. NACA0010 was used as the airfoil.

Basic parameters of TS17, TS12, and VTOL are presented in Table 5.1. The values of individual parameters were calculated by aircraft designers and were taken into account during the work related to the design of the power supply system and modeling of the simulation environment.

**Table 5.1.** Case studies parameters; courtesy of Kamil Zenowicz and Magdalena Peciak

Parameter	TS17	TS12	VTOL
Maximum Take-off Weight (MTOW)	12	45	10
Wingspan (m)	3.6	12.4	2.5
Payload (kg)	2.5	2.5	0
Maximum power supply system mass (kg) (with payload included)	5	15	4
Estimated battery weight (kg)	2.5	12.5	4
Wing area (m <sup>2</sup> )	0.896	8.6	1.25
Propeller diameter (m)	0.4	0.9	0.75
Motor number	2	2	2
Angle of Attack range (°)	-3 to 8	-3 to 5	4.25
Maximum altitude (km)	8	20	4

<b>Take-off, climb, cruise, descent</b>			
Rate of Climb (ROC) (m/s)	0.999	1.5	2.5
Rate of Descent (ROD) (m/s)	0.41	0.26	0.5
Climb speed (m/s)	13.3	11.1	8.3
Cruise speed (m/s)	13	13.9	13.9
Descend speed (m/s)	6.5	9.5	8.5
Vertical T/O speed (m/s)	—	—	5

For each UAV, aircraft designers fixed the angle of climb and descent. By the calculated speed, they were able to calculate the rate of climb and rate of descent.

During the commencement of the work related to the power supply system, guidelines were received that the structure of the tested UAVs could not be changed. Their structure is rigid and should not be modified. A certain strict construction of the UAV was imposed and the results of the analyzes should indicate the advantages and disadvantages of this construction. Work related to the design of the power supply system should take into account these limitations and adapt to this type of construction.

In order to correctly verify the developed configuration of the solar-powered UAV power supply system and the general method of building the power supply system, it was decided to use the experience of other teams that had already developed solar-powered aircraft [18,19,37,41,94,140].

## **5.1 Energy Consumption**

The value of energy demand has been developed for Maximum Take-off Weight (MTOW) and parameters from Table 5.1. The value of energy consumption has been divided into two components. The first is electric motors. They consume most of the energy during flight. Depending on the flight stage and the aviation mission scenario, the power and efficiency of the electric motors change. Power consumption data for each stage was calculated by aircraft designers.

For verification, the results of analytical calculations were compared with the results of the simulation model. The developed simulation model, thanks to which the energy demand data was obtained, was described in more detail in the article [107]. The accuracy of simulation results was 95% compared to the analytical calculations.

The ultimately selected MBD methodology is based on simulation models. It caused that data from simulation (not analytical calculations) were adopted as those to which it was intended to refer in the developed methodology. The developed results already included the efficiency of the type of propeller that was ultimately used. The efficiency of the electric motors had to be additionally taken into account in the further stage of work.

### *5.1.1 Twin Stratos 17*

The energy demand for TS17 was divided into 3 parts. For each of the flight stage i.e., climb, cruise flight, and glide. The characteristics of the power needed to climb to a certain altitude are shown in Figure 5.3.

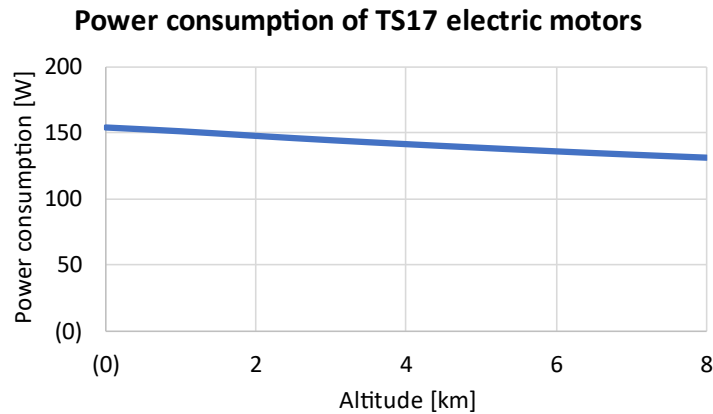


**Figure 5.3.** Power consumption of TS17 during climbing.

The value of the power decreases with the increase in altitude at the set flight parameters. However, this is a small difference, which is only 10% between the highest ceiling of 8,000 meters and sea level — from 150 watts to 130 watts.

The maximum energy demand of the TS17 is approximately 150 watts. However, this value may change depending on the prevailing conditions. For this reason, it was necessary to provide an additional power reserves, which the UAV would be able to use during sudden, unexpected situations. For the initial calculations, an electric motor with a nominal power of 100 watts each was assumed (2 electric motors will provide a nominal power of 200 W).

In the case of electric motor operation, the efficiency of the drive system must be taken into account. For TS17 and each subsequent case study, the efficiency value was taken from maps of proportions of the expected load to the nominal load [141]. In the case of climbing, the efficiency of the electric motors was defined as 90%.

Another characteristic taken into account was flight at different altitudes. For cruise flight, the needed power results are shown in Figure 5.4.

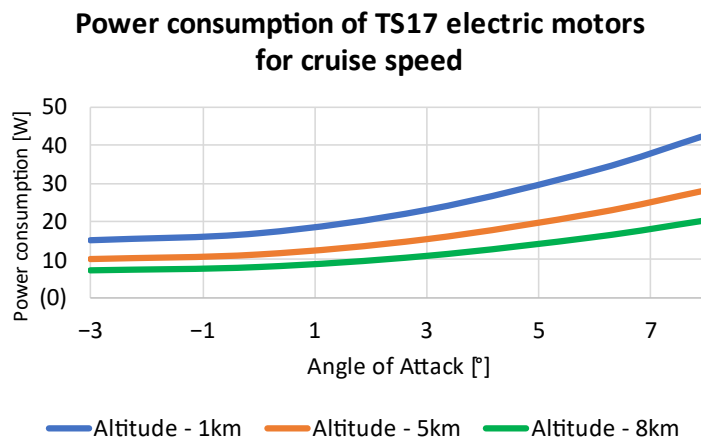


**Figure 5.4.** Power consumption of TS17 during cruise flight.

Comparing the power values needed for cruise flight, it can be stated that depending on the setting of the angle of attack, ceiling and the cruise speed variable, the power value will change. The power range for the considered cruise flight cases is in the range of 10-20% of the climb values. In this case, regardless of whether the flight would

occur at an altitude of 1 km, 5 km, or 8 km, the efficiency of the electric motors was set at 50%.

Another issue was connected to the additional equipment on board the TS17. The devices that the UAV was to be equipped with include Pixhawk, NVIDIA Jetson Nano, telemetry system, GPS module, airspeed sensor — pitot tube, MPPT, and two servos.

The value of on-board equipment energy demand is difficult to define. It was decided that the power value will be a constant value. For each subsequent case study, the power value will be taken into account in the same way.

In order to calculate the power of the devices, the maximum operating power of each device was summed up. The power that had to be taken into account for the TS17 was 20 watts. This value will be added to the climb and cruise flight stages. During gliding, when the electric motors do not draw any energy from the batteries, the value of 20 watts will be constantly consumed by the on-board devices.

A summary of the TS17 energy needs is presented in Table 5.2.

**Table 5.2.** TS17 power consumption summary.

	<b>Climbing</b>	<b>Cruise</b>	<b>Gliding</b>
<b>Electric motor power consumption (W)</b>	135-150	10-43	—
<b>Efficiency (%)</b>	90%	50%	—
<b>Power consumption from energy storage (W)</b>	150 - 167	20-86	—
<b>Summary power consumption including electronics (W)</b>	170-187	40-106	20

### 5.1.2 Twin Stratos 12

Power values during the climb for TS12 were performed in the same way as for TS17 (Figure 5.5.).

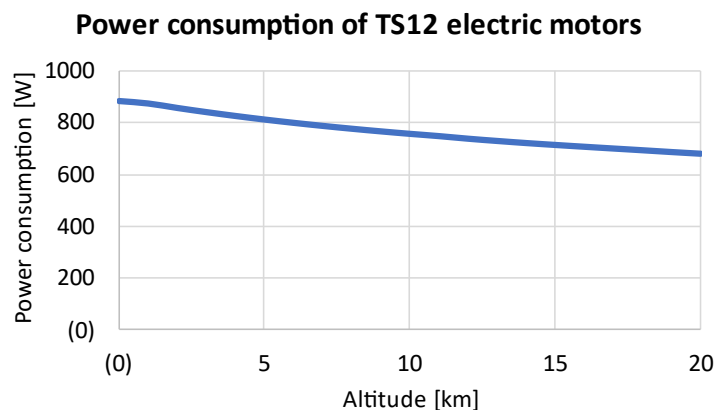


**Figure 5.5.** Power consumption of TS12 during climbing.

The power during take-off is 885 watts, while for 20 km it is 680 watts. A difference of 20,000 meters reduces the power requirements by 25% during climbing.

It was decided to choose two identical electric motors with a total nominal power of 1000 watts. Moreover, in this case, the efficiency during climbing was set at 90%.

Figure 5.6. shows the power values needed for horizontal flight at certain altitudes.

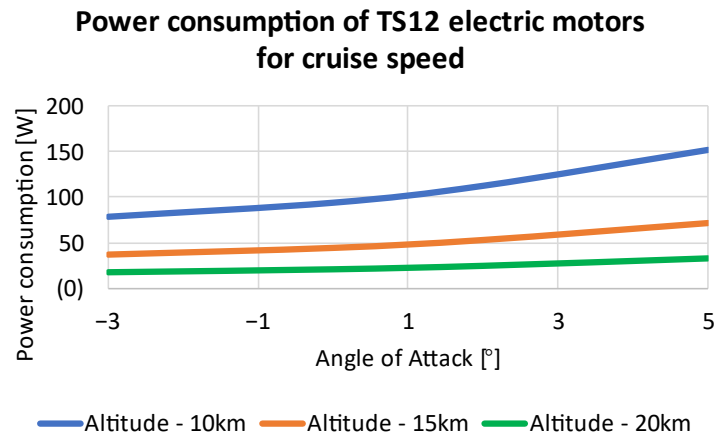


**Figure 5.6.** Power consumption of TS12 during cruise flight.

Power values for different angle of attack can change even several times. This is especially evident on the example of flight characteristics at an altitude of 10 km. Comparing the values for cruise flight with the values for climb, it can be seen that the differences at 10 km, 15 km, and 20 km are greater than in the case of TS17 (Figure 5.4.). When analyzing the graph, it was assumed that the reference value for determining the efficiency will be the median of each graph. For 10 km — 100 W, for 15 km — 50 W, for 20 km — 20 W. Cruise flight efficiency was defined as 50% at 10 km, 30% at 15 km and 10% at 20 km.

The larger scale of TS12 than TS17 and a slightly different application mean that numerous measuring devices for research purposes will be on board. For this reason, the energy demand of TS12 will be slightly different than in the case of the smaller TS facility.

All devices that the TS17 is equipped with will also be on board the TS12 with minor changes to the models, e.g., MPPT, servos, NVIDIA computer. One of the target applications of TS12 is the possibility of making measurements related to the assessment of air pollution profiles [138]. Additional devices in which UAV will be equipped are numerous sensors:

- Pyranometer SP-510-SS and SP-610-SS;
- RS92SGP or RS41 radiosonde;
- AE-51, OPC-N3 air pollution sensors;
- Nephelometer;
- Gas sensors.

Summing up the power values, it was decided to provide an additional power reserve, which would enable the attachment of further measuring, control or monitoring devices due to the large space inside the TS12 as well as due to the possibility of attaching the nacelle to the UAV. The value of the constant power that will be taken from the energy storage is estimated at 50 watts.

A summary of the TS12 energy demand is shown in Table 5.3.

**Table 5.3.** TS12 power consumption summary.

	Climbing	Cruise			Gliding
		10 km	15 km	20 km	
<b>Electric motor power consumption (W)</b>	680-885	79-151	37-71	17-32	—
<b>Efficiency (%)</b>	90%	50%	30%	10%	—
<b>Power consumption from energy storage (W)</b>	756-983	158-302	123-237	170-320	—
<b>Summary power consumption including electronics (W)</b>	806-1033	208-352	173-287	220-370	50

### 5.1.3 VTOL Tail-Sitter

Slightly different flight mechanics of the VTOL compared to the Twin Stratos UAVs cause that it does not ascend gradually, but takes off vertically, and after reaching a certain height, it switches to horizontal flight. Figure 5.7 has been used for better illustration.

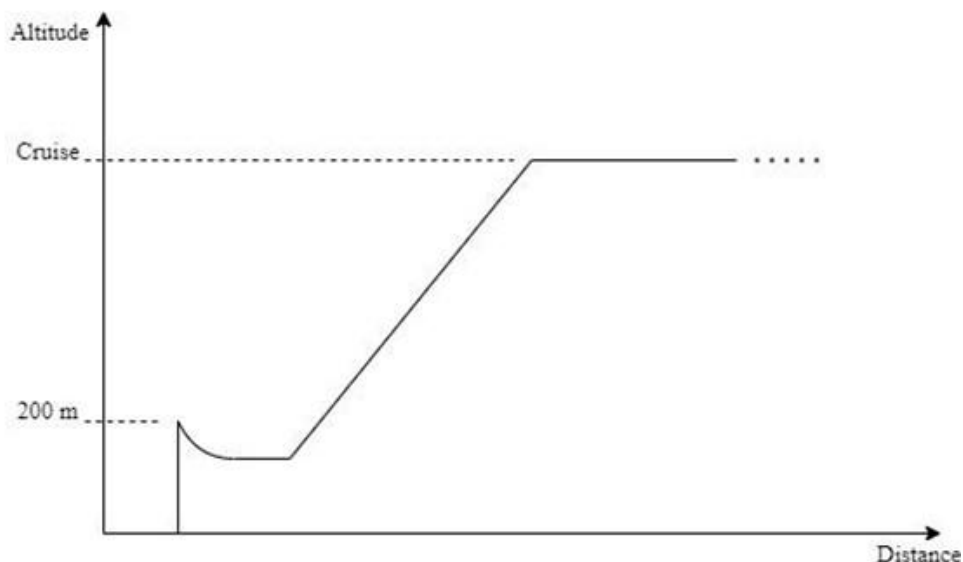


**Figure 5.7.** A diagram of the vertical take-off and further climbing as fixed-wing UAV until the cruise altitude [27].

In the case of the analyzed tail-sitter, aviation constructors developed a take-off method consisting in a vertical take-off to a height of 200 meters, and then VTOL changes

the angle and starts the climb phase analogous to that of the TS UAV. The moment of changing the angle is associated with the loss of height and the need to accelerate the vehicle to the appropriate speed using gravity (this can be compared to a glider recovering from a stall) [27]. Then, leveling off occurs and the climb begins in the new flight configuration to the cruising altitude.

Figure 5.8. shows a graph of the power needed to take-off and climb to a maximum ceiling of 4,000 meters.

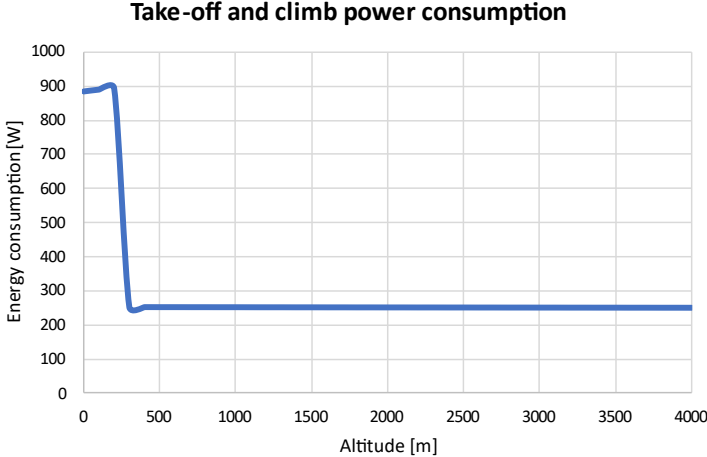


**Figure 5.8.** Power consumption of VTOL during climbing.

The power needed for a vertical take-off is 3.5 times higher than the power needed for a climb. Vertical take-off consumes approximately 900 watts of power when during a constant ROC climb uses 250 watts.

Reaching the set ceiling allows to start the cruise flight stage. Figure 5.9 presents the power needed for a horizontal flight depending on the altitude.

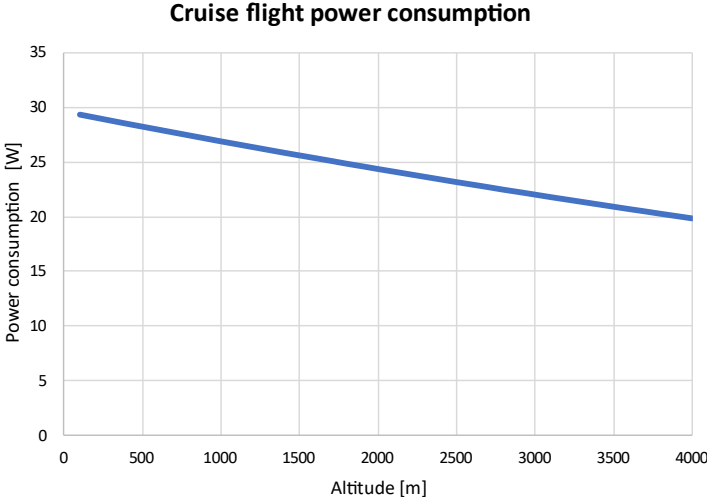


**Figure 5.9.** Power consumption of VTOL during cruise flight.

The minimum height for which the calculations were made is 100 meters. Then the propulsion system needs 29.5 watts, while at an altitude of 4,000 meters this value decreases to 20 watts.

The selection of electric motor power for VTOL was carried out slightly differently than for Twin Stratos UAVs. Due to the fact that the power of about 900 watts is necessary

only for a vertical take-off lasting several dozen seconds, it was decided to choose two electric motors with a peak power of 1000 watts. The selection of such a drive causes that the rated power of the motor is much lower than the peak at which the motor can operate for a short time. Depending on the type, size, construction, and manufacturer of the electric motor, this time can be a few seconds or minutes, and the difference between the peak and nominal value can change several times. Based on different types of electric motors, it has been estimated that the approximate nominal power of the motor will be 250 watts for each (total rated power equals 500 watts) [142].

The electric motors efficiency for the individual stages of the flight were selected as follows. At take-off, due to continuous maximum power, an efficiency of 50% was taken into account, for climb due to optimal load 90%, for cruise flight 20%.

The value of the on-board devices power demand will be roughly comparable to TS17. For this reason, it was decided to use a constant input power of 20 watts. A summary of the VTOL's power requirements is shown in Table 5.4.

**Table 5.4.** VTOL power consumption summary.

	<b>Vertical take-off</b>	<b>Climbing</b>	<b>Cruise</b>	<b>Gliding</b>
<b>Electric motor power consumption (W)</b>	885-900	250	20-29.5	—
<b>Efficiency (%)</b>	50%	90%	20%	—
<b>Power consumption from energy storage</b>	1770-1800	278	100-147.5	—
<b>Summary power consumption including electronics</b>	1790-1820	298	120-167.5	20

## 5.2 Photovoltaic Energy

For each of the tested UAVs, two aspects were taken into account: location and flight date. Gliwice was chosen as the place of flights and missions. The temperate climate causes that both cold winter and hot summer can be encountered. The flight period has been shortened to the spring-autumn period. In winter, the irradiation, duration of the day and weather conditions are not favorable not only for photovoltaic systems, but also for monitoring devices. In the case of observations, snow can cover the monitored object. Cloud cover is significant, which limits the visibility and the sense of conducting some types of research.

The assumptions take into account that the UAVs flight would occur in stable weather conditions. It was decided that the winter period would not be taken into account in the tests and simulations for practical reasons. In addition, due to the almost symmetry of time between the spring equinox — summer solstice and the summer solstice — autumn equinox, it was decided to consider the spring — summer period in order to simplify the research. The irradiation values are more or less periodically symmetrical,

i.e., the value in January is close to December, February to November, March to October, etc.

Initial analyzes regarding the value of energy that can be produced by the PV system began with the surface of the UAV wings. The available surface of the wings allows to calculate the value of energy that can be produced by photovoltaic panels located on the UAV's surface. Data from publication [143] were used as input values. It contains the average monthly solar radiation values in Poland. In addition to the wing area and the value of the visible light intensity, the efficiency of the PV panels also had to be taken into account. The data used for the initial calculations are presented in Table 5.5.

**Table 5.5.** Average energy produced by solar-powered UAVs during months.

<b>Parameter</b>	<b>TS17</b>	<b>TS12</b>	<b>VTOL</b>
Wing area (m <sup>2</sup> )	0.896	8.6	1.25
Monthly average insolation (kWh/m <sup>2</sup> )			
• March		2.78	
• April		4.17	
• May		4.86	
• June		5.83	
Predicted solar cells efficiency (%)		20	
Predicted average produced energy in 24 hours (kWh)			
• March	0.5	4.78	0.7
• April	0.75	7.17	1.04
• May	0.87	8.36	1.22
• June	1.04	10.03	1.46

Data presented in Table 5.5. contain some imperfections, e.g., there is no information about the highest daily value of solar radiation, e.g., on the summer solstice, but only the monthly average value. This value takes into account cloud cover and unfavorable weather conditions during the specified period. Due to the long duration of flight, such situations should also be taken into account when modeling the power supply system.

Data from Table 5.5. can be compared with the UAV energy demand values in order to calculate the daily energy balance. The predicted efficiency of the solar cells was an estimate. It took into account the decrease in efficiency caused by the lamination film.

Knowing the available area of each UAV, it was possible to determine the number of photovoltaic cells that could be placed on the drones. TS17 can accommodate a maximum of 40 pcs. of solar cells, TS12 350 pcs., and VTOL 80 pcs. The number of photovoltaic cells allows to initially estimate the available power that the PV system will be able to generate during the flight. The given number of solar cells will be included in

the simulation model for each UAV. The exact configuration including series and parallel connections of the system will be defined at a later stage of work.

### **5.3 Batteries**

In the case of UAVs powered by solar cells, the optimization of the energy storage in terms of weight and capacity is related to the choice of a specific battery configuration. Due to the many variables that occur in the UAV environment, it is difficult to estimate the conditions in which the UAV will fly. It is simplified from the assumptions that the UAV will not fly in very windy weather, in bad weather conditions, which not only make piloting difficult, but may also cause permanent damage to the UAV structure.

The battery is correlated with the payload of the UAV. The total weight available for use is the sum of the estimated battery weight and the payload. This value was calculated by aircraft designers. This is the mass of energy storage, measuring equipment, control devices, etc. By increasing the mass of the battery, we extend the flight time, but it will not always be the optimal choice. There may be a situation where the PV energy will not be able to charge the battery to 100% SOC. By reducing the battery capacity, the number of measuring devices on board the UAV can be increased, but the flight time can be shortened.

The golden mean is to enable both charging the battery to 100%, using the energy produced by PV in certain phases of flight and to provide space for the necessary equipment that should be on board the aircraft. Due to changing weather conditions and, above all, the change of seasons, the optimization is limited to a certain extent.

By choosing the capacity of the energy storage, it was decided in what time frame the UAV will be able to fly continuously, ensuring energy autonomy (if possible), when the flight time will be able to extend, and when the photovoltaics used on the UAV's surface will be redundant.

Under ideal, repeated conditions, precise optimization can be made. Due to the constant changes and uncertainties related to the expected flight conditions, a choice must be made that cannot be precisely optimized in terms of battery capacity.

The capacity of the battery should be compared with the energy from the PV panels and the energy consumption of the electric motors and other on-board devices. Initial calculations should take into account under what conditions (date and time) the UAV's power supply system is able to charge the SOC to 100% and in what phase of flight this may occur (climb, cruise, glide). By successively verifying and comparing the SOC with PV energy and energy consumption, a choice related to battery capacity should be made.

It was decided that the choice regarding the battery capacity would be made only after the development of the simulation model of the power supply system. The ability to compare several configurations will allow to more closely examine the battery pack also in terms of weight.

### **5.4 Summary**

Preliminary calculations comparing the possible production of energy from the PV system with the energy consumed by the electric motors during the flight were intended to show whether the daily energy from PV is greater than the energy demand.

For this purpose, the power diagrams from chapter 5.1 were used to calculate the energy demand, just like the tables from chapter 5.1, ROC and climb speed values. These

values will allow to calculate the flight path angle, i.e., the angle with which the UAV will ascend. This is necessary to calculate the initial UAV climb time.

The simplified flight scenario was to include a flight with an altitude of 5 km for TS17, 10 km for TS12, and 1 km for VTOL. After reaching the set ceiling, the UAV would perform a cruise flight. Table 5.6 presents the energy demand for three UAV types.

**Table 5.6.** Energy consume by UAVs during simplified flight.

	<b>TS17</b>	<b>TS12</b>	<b>VTOL</b>
Rate of Climb (ROC) (m/s)	0.999	1.5	2.5
Climb speed (m/s)	13.3	11.1	8.3
Flight path angle	4.3	7.7	16.7
Time to 1 km flight climb	—	—	~7m
Time to 5 km flight climb	~1h30m	—	—
Time to 10 km flight climb	—	~2h	—
Energy cons. for climb (kWh)	0.28	2.07	0.05
Energy cons. for 24h cruise at mentioned kilometers height (kWh)	1.2	6	3.6

In the calculations for the climb, the maximum power value was assumed, and for cruise flight the value was averaged. Comparing the values in Table 5.6 and in Table 5.5, it can be concluded that a positive energy balance will be the easiest to achieve in TS12. In the case of TS17, it is close to achieving a positive daily balance in June. However, VTOL is the worst. Its daily energy demand is more than twice the production capacity.

## 6. Fine-Tuning of Simulation Models

The purpose of tuning the simulation models and their individual components is to reflect the behavior of the system during operation as realistically as possible. For this purpose, a number of tests and analyzes were carried out, which are described in the following subsections.

### 6.1 Planned Scenarios

One of the key parameters is to plan the flight path in the most realistic way as possible. When planning it, all stages (take-off, climb, cruise flight, gliding, landing), duration of a given stage, and energy consumption should be taken into account. In addition, each operation must provide feedback on the current flight altitude, ambient temperature. This subchapter has been divided into 3 parts. The first concerns the scenarios prepared for LALE UAV, i.e., for TS17. The second concerns HALE UAV, i.e., TS12. The last part is about the VTOL tail-sitter.

#### 6.1.1 *Twin Stratos 17*

Two main target scenarios were developed for the TS17. Their aim was to extend the duration of the flight as much as possible. Their representation is shown in Figure 6.1.

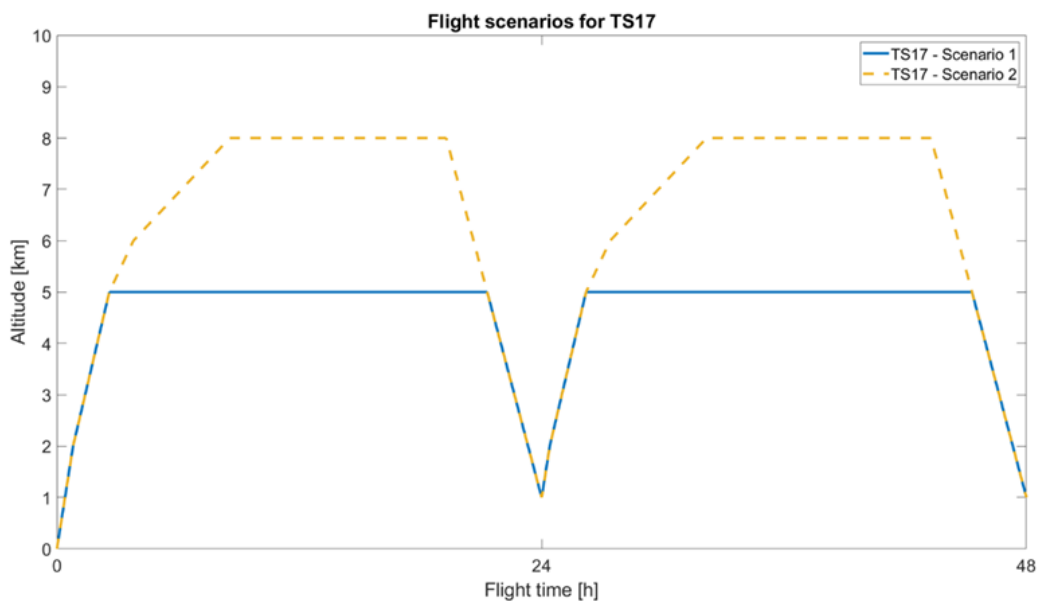


**Figure 6.1.** Example scenarios that will be considered in TS17 [15].

For TS17, two milestones are defined. The first was to enable the UAV to fly to an altitude of at least 5 km. The second was related to the endurance of the flight and was supposed to allow the flight to last for at least 24 hours.

By analyzing the graphs concerning the UAV energy demand from subchapter 5.1, it was noticed that the energy consumption of electric motors decreases with increasing altitude. For this reason, the developed target scenarios were mainly based on the longest possible flight at the highest possible altitude, while minimizing energy consumption.

Scenario no. 1 involved climbing TS17 to a height of 5 km and then maintaining this ceiling. The UAV started gliding to a height of 1 km in such a way that it reached the altitude of 1000 meters 24 hours after the start of the flight. Then from the ceiling of 1 km, it climbs again to a height of 5 km.

The height of 1 km was chosen as a kind of time buffer. In the event of failure or low SOC, the gliding will allow the UAV to land safely in a safe location.

Scenario no. 2 was developed analogously to scenario no. 1. The only difference is that the UAV climbs higher, up to 8 km. The 8 km ceiling has been calculated as the maximum TS17 ceiling which UAV is able to achieve.

### 6.1.2 *Twin Stratos 12*

Due to the much wider possibilities regarding the flight of TS12, the scenarios developed for HALE UAV have been divided into 3 main flight paths planning (Figure 6.2).

For TS12, milestones have also been set. The first concerned the possibility of reaching the ceiling of 20 km, the second flight for at least 24 hours.

The developed scenarios are analogous to TS17. Achieving long-endurance flight is mainly based on high-altitude flight. For this reason, the TS12 flight path included much higher altitudes than in the case of TS17.

Scenario no. 1 involved take-off and ascent to 10 km, then maintaining this altitude. Gliding was carried out in such a way that its completion occurred at an altitude of 1 km, 24 hours after the start of the flight. Then the ascent to a height of 10 km was resumed.

Scenario no. 2 was developed in the same way as scenario no. 1 with the difference that the ceiling to which TS12 rises is 15 km.

The last scenario — no. 3 included the maximum ceiling to be reached by TS12 — 20 km. Due to the very long gliding time from the height of 20 km, this time it was decided not to descend to the level of 1 km (it would be the end of the day — evening), but to the height of 5 km. Thanks to this, TS12 will rise again to a height of 20 km during the second day after the start of the mission.

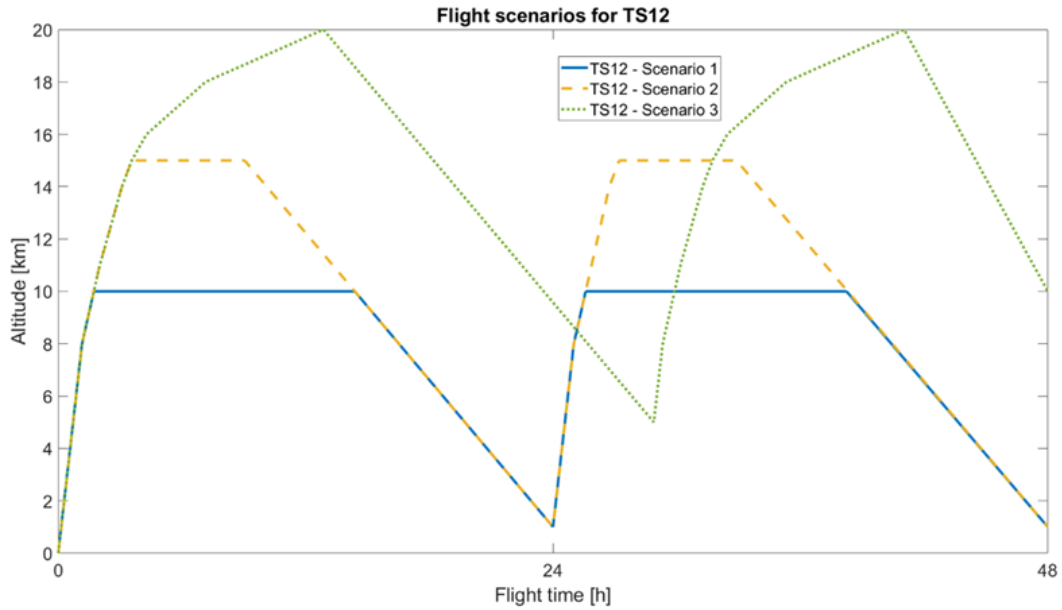


**Figure 6.2.** Example scenarios that will be considered in TS12 [15].

The energy demand during the cruise flight of TS12 is several times lower than in the case of TS17 in relation to the energy needed to climb the UAV. The discrepancy increases with higher horizontal flight altitude. It was considered that the second alternative would be continuous flight at a constant altitude. After taking-off and climbing to the set altitude — the ceilings were set as before, i.e., 10, 15, and 20 km — the UAV will start a cruise flight.

### 6.1.3 VTOL

In the case of VTOL, due to its different purpose, construction, and flight mechanics, scenarios were developed based on lower ceilings than in the case of TS17 and TS12 (Figure 6.3).

The first scenario concerns an exemplary target application of VTOL, e.g., monitoring leaks from pipelines. In this case, climbing to an altitude of 1 km and continuous flight at this altitude will allow for the implementation of the target mission.

The second scenario takes into account climbing the VTOL to the maximum ceiling level — 4 km — and then maintaining this ceiling. The potential energy accumulated in altitude should allow for longer flight time, and a higher ceiling will reduce energy consumption. In this scenario, it is intended to test how the VTOL is able to maximize its flight endurance performance.

No specific milestones have been defined for VTOL due to the early stage of project development. In the case of VTOL, there is more talk about the impact of photovoltaics on the operation of the UAV power supply system, i.e., the time that the VTOL will be able to work longer than about full energy autonomy.

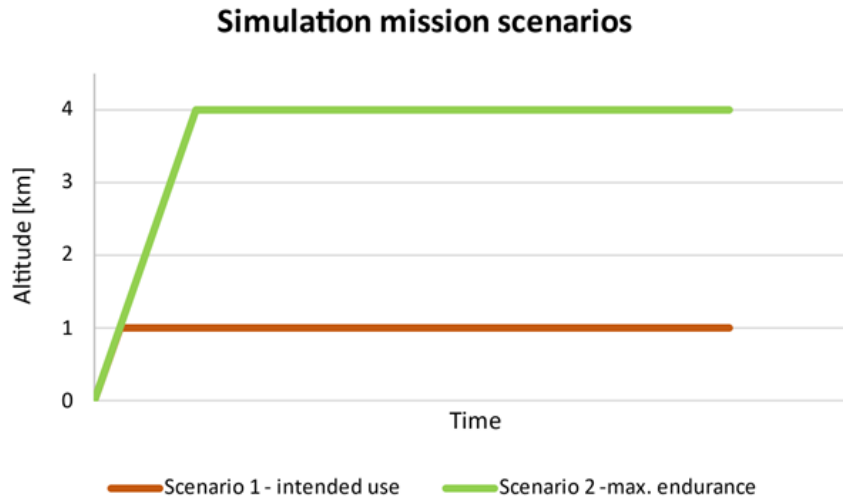


**Figure 6.3.** Example scenarios that will be considered in VTOL [27].

#### 6.1.4 Summary

Sunrise was initially set as the start time for the all UAVs' scenarios. Starting the mission at this time allows for the gradual elimination of losses related to the discrepancy between energy consumption and energy production by PV panels.

Take-off and climb involve the highest energy consumption, making the energy balance negative. If the batteries drain before reaching the set altitude, it will be needed to change the start time.

All scenarios were considered within 48 hours, unless after 24 hours from the start the SOC would be equal to 0%. A period of two days will allow to analyze whether and how the SOC level changes between consecutive days.

In the case of flight at the spring equinox, the temperature on earth was defined as 15°C. On the summer solstice, the temperature value was changed to 25°C.

Airspeed data and ROC and ROD values are given in Table 5.1. The values that were the most important from the point of view of developing the flight scenario were the time to climb to a given altitude and the energy consumption for this maneuver. The climb speed and ROC values were used to calculate the flight path angle.

For TS17, the flight path angle is 4.3°, for TS12 7.7°, for VTOL 16.7°. Ensuring adequate lift was ensured by using a constant Angle of Attack of 6° for TS17, 3.5° for TS12, and 4.25° for VTOL.

In the initial phase of flight, TS17 and TS12 can climb quickly at high climb angles. By ascending to higher altitudes, the flight path angle values will decrease. Change is necessary due to the decrease in air density and pressure. This results in lower energy consumption, however, the time of the climb stage at a higher altitude is extended by reducing the flight path angle.

The lower density of the air means that the speed of the UAV must be increased. The increasing speed will increase the power consumption. To simplify the simulation model, it was assumed that the energy consumption data would be the same as those obtained in the drive system simulation model (data from subchapter 5.1). They take into account the fixed value of airspeed, ROC, and flight path angle. This simplification can be applied as the increase in power associated with higher speed will be reduced by using a lower flight path angle.

Table 6.1 presents the flight path angle used in the simulation model of the power supply system. These values were used to calculate the climb time between specific altitudes and to calculate the energy consumption during these flight stages.

**Table 6.1.** Flight path angles included in the simulation

Altitude (km)	TS17	Altitude (km)	TS12	Altitude (m)	VTOL
From 0 to 2	3°	From 0 to 10	5°	From 0 to 200	90°
From 2 to 5	2°	From 10 to 15	4°	From 200 to 4,000	16.7°
From 5 to 6	1°	From 15 to 17	2°		
From 6 to 8	0.5°	From 17 to 20	1°		

## 6.2 Photovoltaic Cell

The test stand (Figure 6.4a) for collecting the I-V and P-V characteristics consisted of a light source in the form of a xenon flash lamp with a power of 1430 watts, a measuring table, and measuring probes. The light source, after passing through the filter ("Air Mass Filter") and the optical system, evenly illuminated the measuring table (Figure 6.4b). A more detailed description of the apparatus and software used to perform the measurements can be found on the research laboratory website [144].

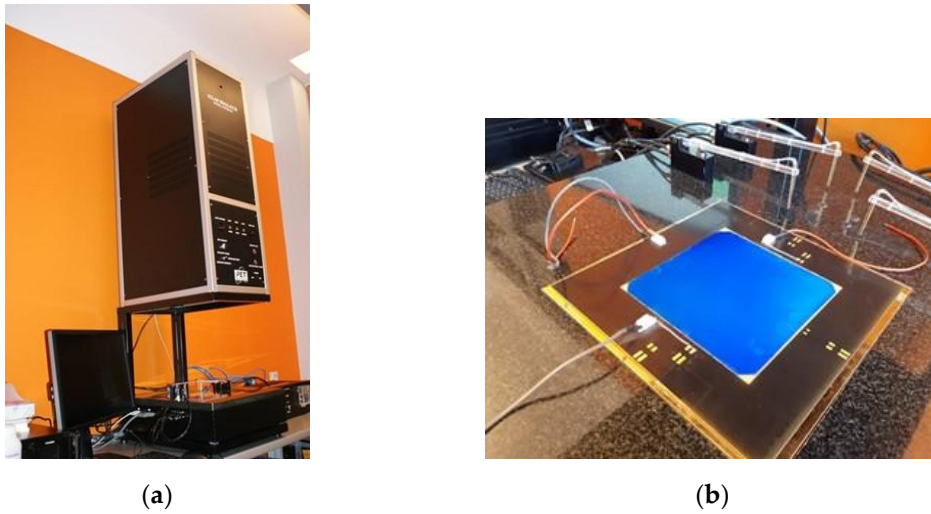


**Figure 6.4.** Test stand: (a) solar simulator with a xenon flash lamp, measuring table, and computer for downloading current-voltage characteristics; (b) research conducted on flexible solar cells placed on the measuring table [35].

The test stand made it possible to obtain measurements in the STC (Standard Test Conditions) [145] — irradiated with a power of  $1000 \text{ W/m}^2$  at a temperature of  $25^\circ\text{C}$  and an air mass spectrum of 1.5 (AM 1.5G) defined by the European standard IEC 60904-3 [146]. The system for measuring the current-voltage characteristics of solar cells meets all the requirements of the IEC 60904-1 standard [147].

The selected flexible silicon SunPower Maxeon Ne3 solar cell, according to the manufacturer's data, provides an efficiency of at least 24.34% [127]. Under STC conditions, it generates 3.77 watts of power. Getting to know the I-V (Figure 6.5) and P-V (Figure 6.6) characteristics of the photovoltaic cell was to verify the correctness of these data. 25 pcs. of solar cells were tested.

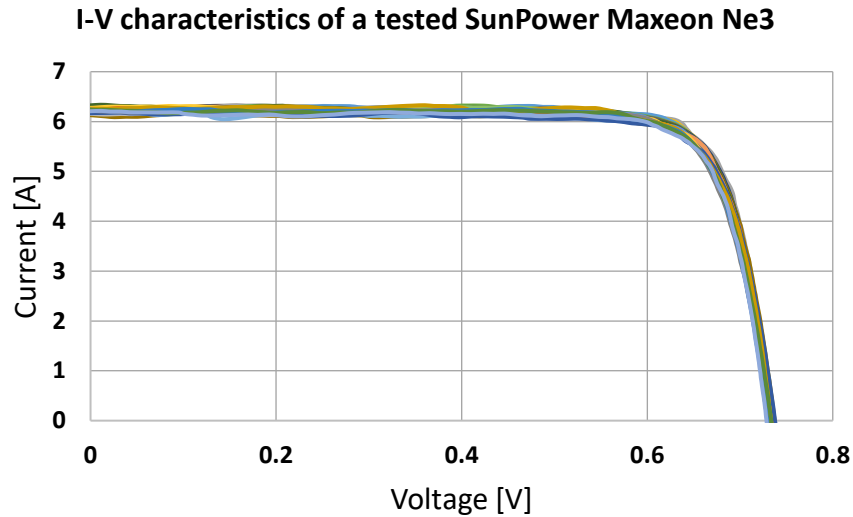


**Figure 6.5.** I-V characteristics of tested SunPower Maxeon Ne3.

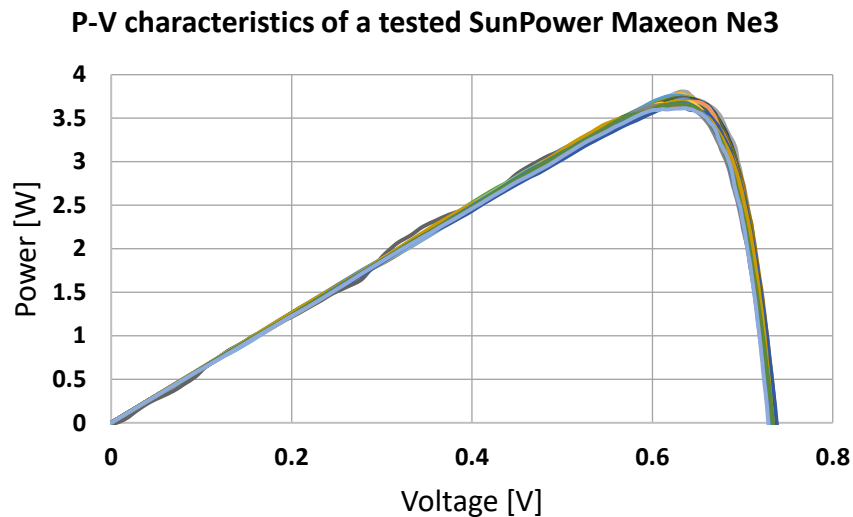


**Figure 6.6.** P-V characteristics of tested SunPower Maxeon Ne3.

### 6.2.1 Laminating Film

The decision and the entire process of proceeding, research, and analysis regarding the selection of the appropriate laminating film to cover solar cells, as well as research regarding the lamination process are described in detail in the article [35].

The selected PVC (Polyvinyl Chloride) film with a thickness of 100 microns was tested on the Evolution 220 spectrophotometer (Thermo Fisher Scientific, Waltham, MA, USA) to measure the characteristics of transmission, absorption, and reflection of the film. The spectrophotometer allowed for the determination of the characteristics in wavelengths ranging from 190 to 1100 nm, so it can measure the whole range of the visible light which is the most important in the case of solar cell research [35].

The SunPower Maxeon Ne3 data sheet contains the spectral response of the solar cell, which is the ratio of the current generated by the solar cell to the power incident on the solar cell [148]. In order to better illustrate the operation of the solar cell, primarily in the visible light range, this characteristic is shown in Figure 6.7a.

Tests carried out with a spectrophotometer allowed to obtain the characteristics of absorption, reflection, and transmission. They are appropriately placed in Figures 6.7b-d.

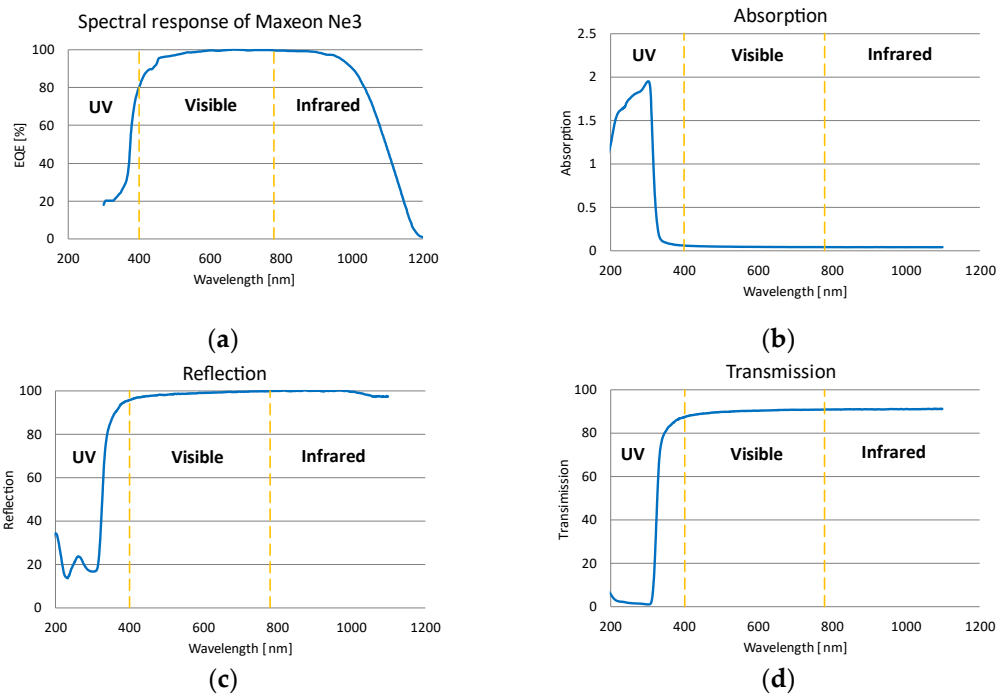


**Figure 6.7.** Characteristics of: (a) spectral response of Maxeon Ne3; (b) 100µm film absorption; (c) 100µm film reflection; (d) 100µm film transmission.

During the analysis of the graphs, the main observations concerned the range of wavelengths and the places where changes in characteristics occurred. In terms of solar energy supplied to solar cells, changes in the UV and infrared range are not as significant as in the visible light range.

There are some variations in UV wavelengths for transmission, absorption, and reflection. From the value of about 300 nm, the characteristics stabilize at one level in the entire range of visible light up to the final value of 1100 nm. Studies carried out on the laminated film explained the changes in reflection, absorption, and transmission in the visible light range. A uniform value of the characteristics in the range from 300 to 780 nm proves that the parameters of the solar cell in the visible light range will be constant. This information allows to conclude that the system will operate with similar efficiency in the entire range of visible light, and sunlight will reach beyond the laminating film to the PV panels. Lack of 100% permeability allows to conclude that the system will show worse values of electrical parameters and system efficiency. For this purpose, the laminated solar cells were tested on the test stand described in section 6.2.

### 6.2.2 Research of Laminated Photovoltaic Cells

The process of lamination and selection of the type and thickness of the film is presented and described in more detail in the article [35]. Figure 6.8. shows a laminated solar cell ready for testing on a test stand.



**Figure 6.8.** Laminated solar cell prepared for tests [15].

Laminated photovoltaic cells were tested on the test stand in the same way as non-laminated solar cells. 25 samples of laminated solar cells were tested. I-V and P-V characteristics are shown in Figures 6.9 and 6.10.

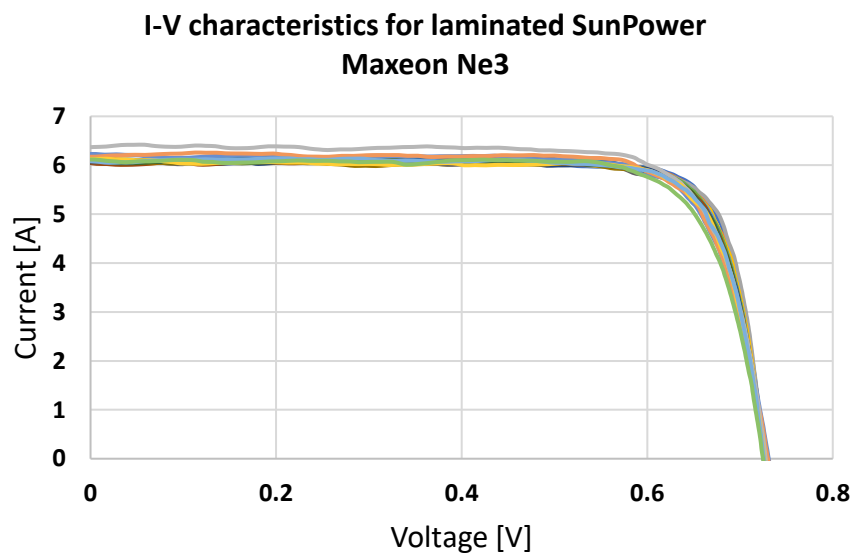


**Figure 6.9.** I-V characteristics of tested laminated SunPower Maxeon Ne3.

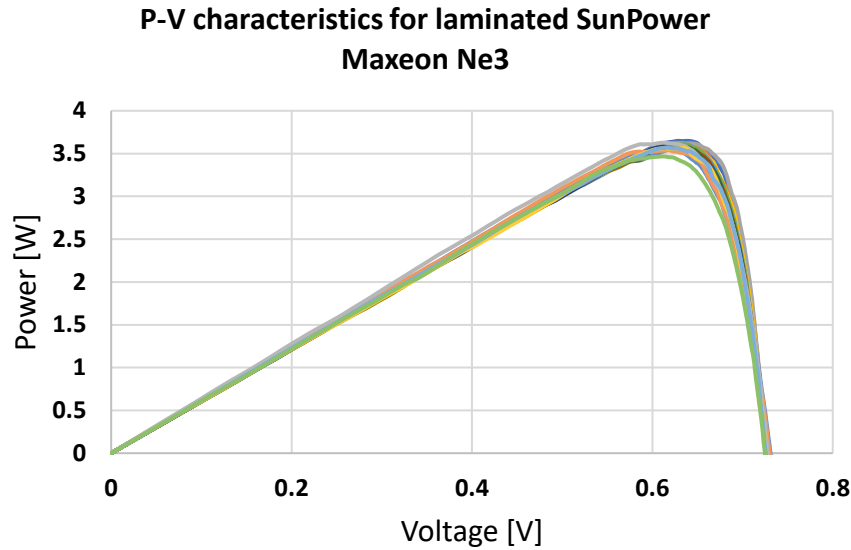


**Figure 6.10.** P-V characteristics of tested laminated SunPower Maxeon Ne3.

The relative standard deviation (RSD) and the minimum and maximum values obtained during the tests for both laminated and non-laminated samples are presented in Table 6.2.

**Table 6.2.** Specification of tested SunPower Maxeon Ne3 solar cells [35].

Data	Non-laminated			Laminated (100 $\mu$ m film)		
	Min	Max	RSD (%)	Min	Max	RSD (%)
$V_{oc}$ (V)	0.728	0.738	0.77	0.725	0.731	1.81
$I_{sc}$ (A)	6.109	6.33	0.28	6.032	6.421	0.24
$V_{mp}$ (V)	0.616	0.639	1.04	0.604	0.629	1.47
$I_{mp}$ (A)	5.793	6.039	0.79	5.724	6.05	1.15
$P_{mpp}$ (W)	3.619	3.82	1.32	3.51	3.7	1.27
Fill Factor (%)	79.9	84.2	1.23	77.1	82.2	1.9
Efficiency (%)	24	24.77	1.12	23.01	23.79	0.85

The data obtained during the tests were averaged. Parameters values are shown in Table 6.3 and their characteristics in Figure 6.11. Data from the tested laminated solar cells was used in the simulation model.

**Table 6.3.** Electrical specifications of tested SunPower Maxeon Ne3 solar cells [35].

Data	Manufacturer data (non-laminated)	Non-laminated	Laminated (100 $\mu$ m film)
$V_{oc}$ (V)	>0.731	0.733	0.726
$I_{sc}$ (A)	>6.382	6.330	6.061
$V_{mp}$ (V)	>0.625	0.627	0.624
$I_{mp}$ (A)	>6.050	5.92	5.747
$P_{mpp}$ (W)	>3.77	3.71	3.589
Fill Factor (%)	80.5	80.8	81
Efficiency (%)	>24.34	24.29	23.33

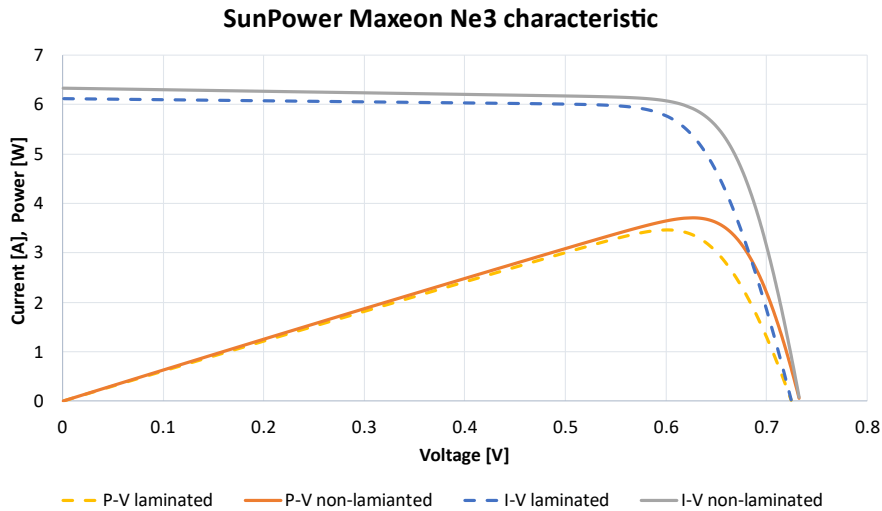


**Figure 6.11.** Final I-V and P-V characteristics of the tested SunPower Maxeon Ne3 cells used in the tuned simulation model [15].

### 6.2.3 Observations of a Solar Cell on a Microscopic Scale

Checking the photovoltaic cells both before and after lamination on a microscopic scale was aimed at comparing the structure of the solar cell and verifying whether the structure was damaged due to the lamination process. The exclusion of microcracks would allow for a definitive statement that the change in the characteristics, efficiency, and parameters of the solar cell results only from the lamination and the cover of solar cell with the layer of film. Figure 6.12 shows microscale of front surface of solar cell when Figure 6.14a and 6.14b rear surface. Macroscopic scale of the rear side of the solar cell is presented in the Figure 6.13.

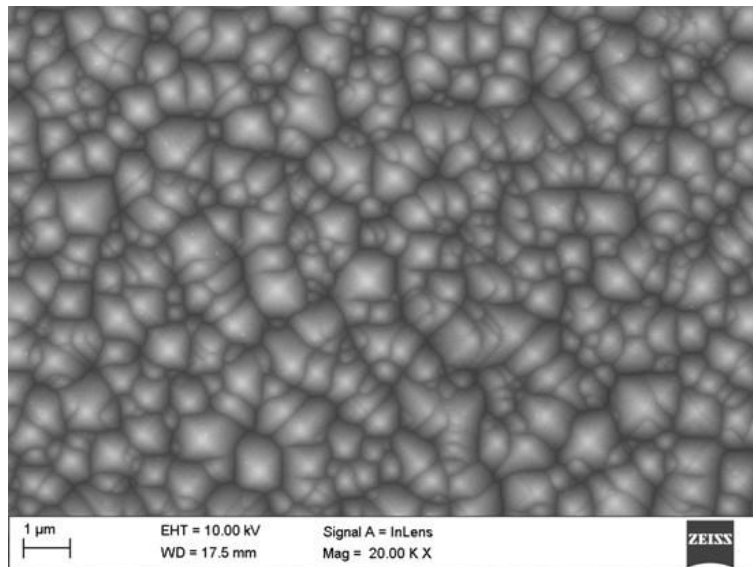


**Figure 6.12.** SEM textured surface topography of the N-type monocrystalline silicon solar cell [35].



**Figure 6.13.** Rear surface of Maxeon Ne3 with visible connectors in the lower part [35].

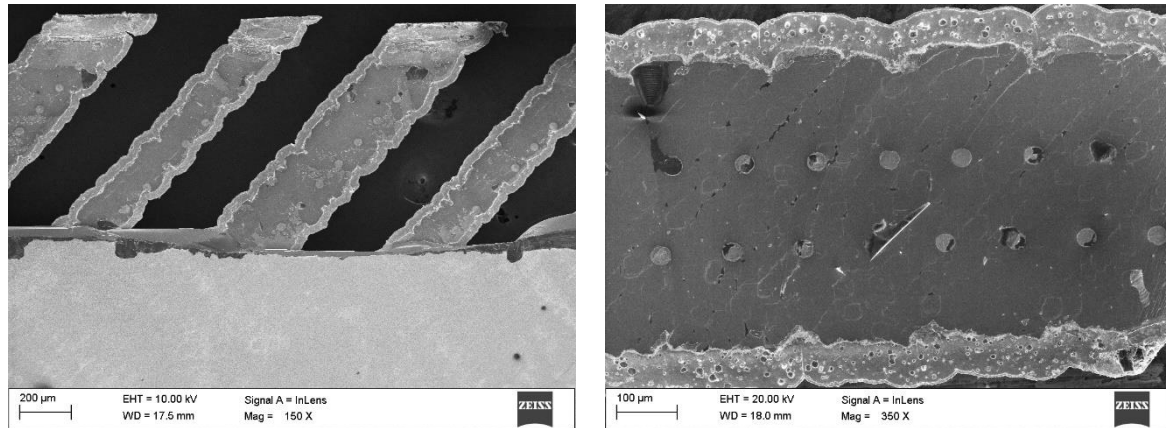


**Figure 6.14.** Topography of the electrical contact surface of a monocrystalline silicon photovoltaic cell of the N-type: (a) contact of fingers (grid lines) with connectors; (b) finger (grid line) [35].

When analyzing the structure of the solar cell before and after the lamination process, no traces of microcracks were observed. The temperature changes during lamination and the force generated by rollers pressing the film to the solar cell did not damage the upper surface layer and the electrical connections of the solar cell. The decrease in the efficiency of the solar cell is therefore not due to microcracks, but only due to the properties of the layer of film applied during lamination. The lower efficiency and deterioration of electrical parameters are related to the light transmittance factor of the film [35].

### 6.3 Batteries

The selected model of the Samsung INR 18650-35E battery cell had to be tuned for the correct operation of the system and to reflect its correct characteristics. Preliminary model tuning data were taken from the website that reviewed Samsung battery cells [149]. The characteristics that are presented there are shown in Figure 6.15.

### Samsung 35e discharge characteristics

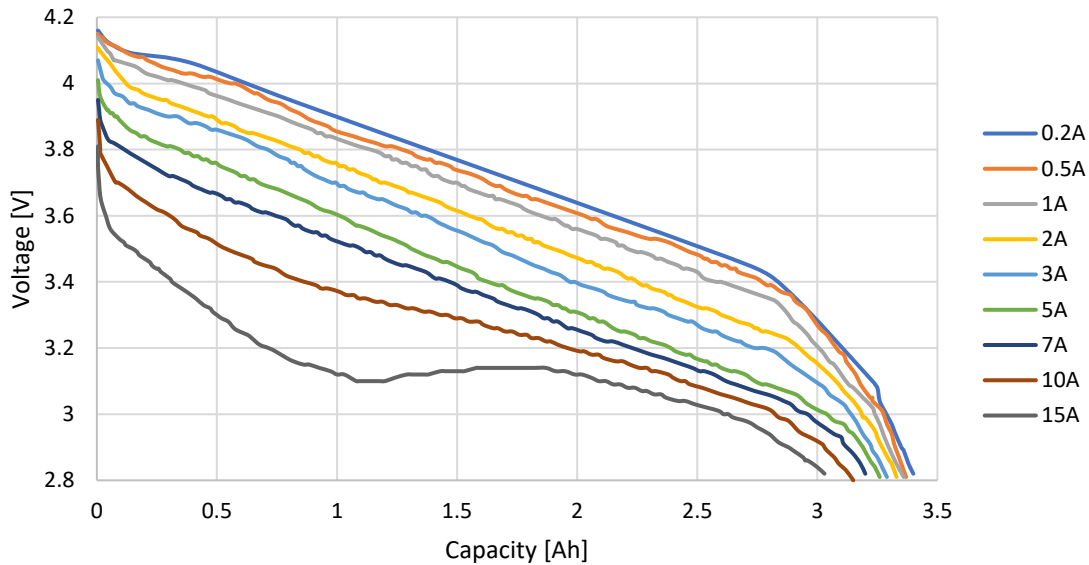


Figure 6.15. Discharge characteristics of Samsung INR18650-35E [149].

Fine-tuning the energy storage system required defining the exact parameters of the batteries from the very beginning. The voltage of each of the tested UAV cases — TS17, TS12, and VTOL was determined on the basis of the voltage closest to the motors, so that the voltage did not have to be additionally "passed" by additional DC-to-DC converters.

The power ranges of electric motors of different manufacturers and the rated voltage of these motors were analyzed. Such verification allowed to determine that for TS17 it will be 4S voltage (4 Li-ion battery cells connected in series — rated voltage equal 14.4V) and for TS12 and VTOL 12S (43.2V).

The choice of the exact value of the battery capacity was made on the basis of a simulation taking into account the complete power supply system. The simulation also included exemplary flight scenarios — contained in section 6.1.

The value of the current that will flow in the system should be related to the C-rated current value, which directly depends on the battery capacity — single battery cell C-rating is based on nominal capacity: 1C is equal 3.5 A for Samsung INR18650-35E.

In the initial simulation, the battery model was configured according to the 0.5A (~0.14C) characteristic from Figure 6.15. More precisely, the model will be fine-tuned only after selecting the battery configuration.

Using the example of the analysis presented for TS17, the process of making a decision regarding the selection of the appropriate battery configuration will be explained. The entire process is presented in a similar way in Figure 6.16 and its dependence on the energy balance, which is presented in Figure 6.17, also had to be taken into account. For TS12 and VTOL, this process was carried out in an analogous manner.

The parallel connection, on which the battery capacity directly depended, had to be verified in terms of weight, working time, and charging possibilities. Three points were developed to which the power supply system was to be adapted:

- Possibly low weight;
- Capacity enabling the use of energy from the PV system — charging to the highest possible SOC value;
- Dimensional aspect — the battery pack must fit to the space into UAV.

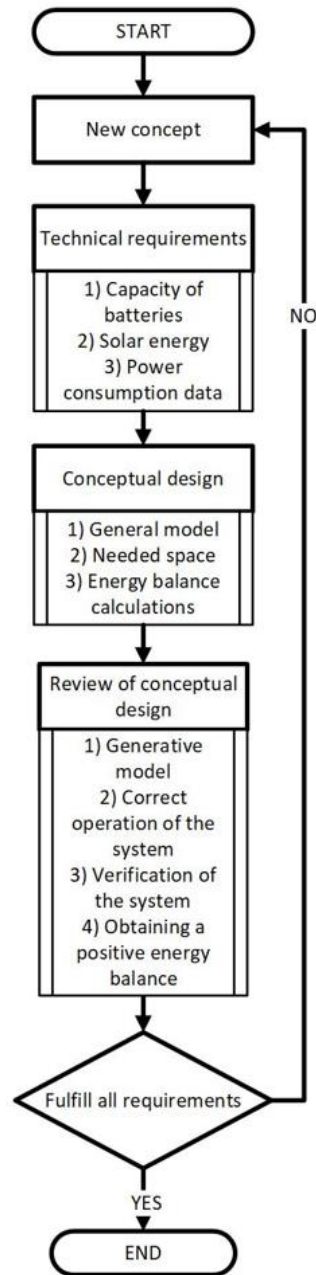


**Figure 6.16.** Flow chart of choosing the parameters of the power supply system [15].

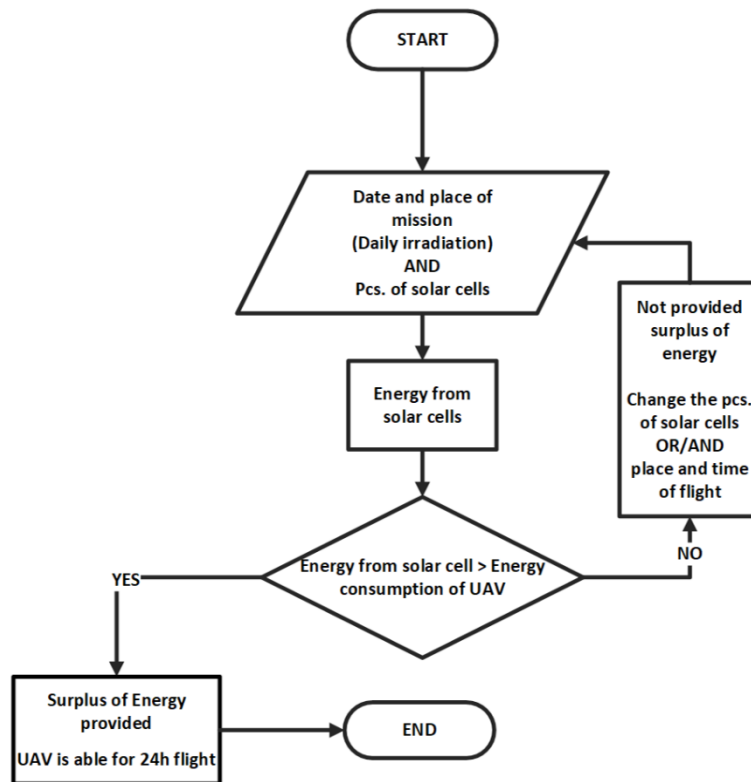


**Figure 6.17.** Flow chart of the energy balance of the UAV [15].

In the article [41], the optimization of UAV flight endurance can be achieved, e.g., by analyzing different battery capacities. Similarly, in the analysis of this doctoral thesis case studies, this way of matching the battery size for the UAVs was taken into account.

The maximum mass of the batteries could also "take away" the available mass for the payload. Based on the assumptions presented in Table 5.1, it was assumed that the payload weight for TS17 and TS12 should be 2.5kg. For VTOL, due to a different application, no additional payload was included. If necessary, the mass of the payload can be allocated to the power supply system, increasing the maximum mass of the batteries to 5kg for TS17 and 15kg for TS12.

The simulations were divided into two parts. The first is to perform sample scenarios at the spring equinox, the second is to perform a flight on the summer solstice.

The first flight scenario was concerned on the continuous flight at an altitude of 1 km. Such a scenario is not important from the point of view of flight endurance, but it is important from the point of application and performance of tests, measurements, and monitoring of areas. It is more of a scenario for performing temporary tests and, as in the case of VTOL (Figure 6.3), showing an example of a target application. In this case, the scenario of the VTOL flight was borrowed (from Figure 6.3).

The scenario of continuous flight at an altitude of 1 km does not represent any of the scenarios presented in chapter 6.1.1, however, it is intended to additionally help in the proper selection of battery capacity and weight.

Figure 6.18 shows the discharge of the UAV power supply system at the vernal equinox for different battery capacities during steady flight at 1 km altitude. The unit of capacity at this stage has been omitted and replaced with mass, which is more important from the point of view of UAVs and the available payload.

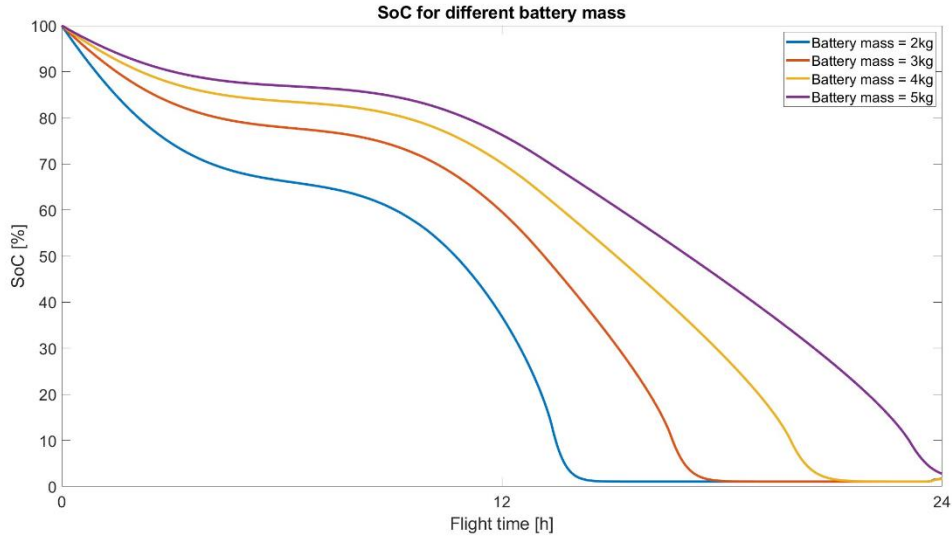


**Figure 6.18.** SoC for different battery mass during 1 km flight at vernal equinox (refers to TS17).

The battery is gradually discharging. For such a scenario, no PV system is unable to achieve a positive energy balance at the vernal equinox. The duration of the flight depends on the capacity and weight of the battery. In this case, the bigger it is, the longer the flight will take (what could have been foreseen).

Figure 6.19 also shows the vernal equinox scenario, with the difference that it already shows the full scenario from the moment of take-off until reaching the height of 5 km and then maintaining this ceiling (identical to the scenario presented in Figure 6.1).

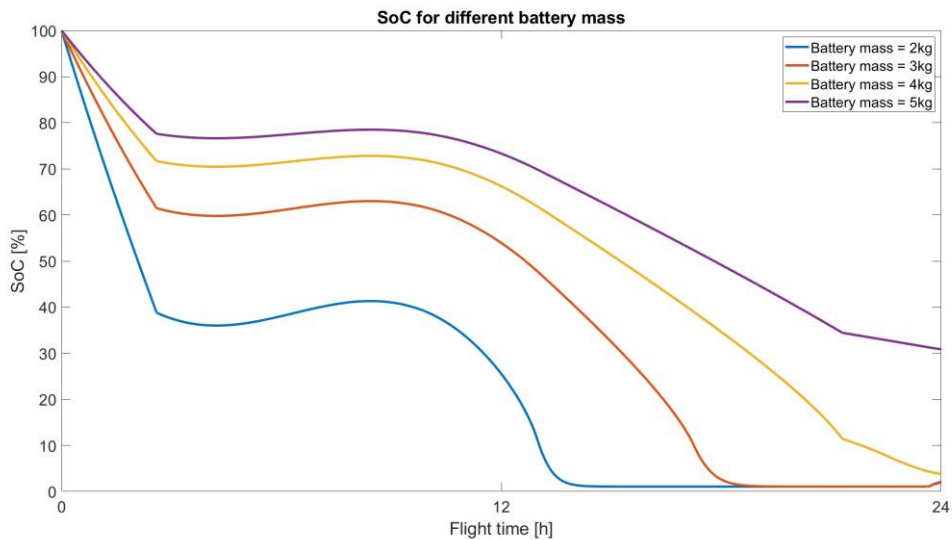


**Figure 6.19.** SoC for different battery mass during 5 km flight at vernal equinox (refers to TS17).

In the case of climbing in the initial phase, it can be noticed a significant decrease in SoC. Lower energy consumption started at the altitude of 5 km during the cruise flight allowed to achieve a positive energy balance and to slightly recharge the batteries. With the increase in battery capacity (mass), the degree of SoC growth decreased.

The last sample of flight at the vernal equinox was performed for scenario no. 2 in Figure 6.1 — a flight to an altitude of 8 km (Figure 6.20).

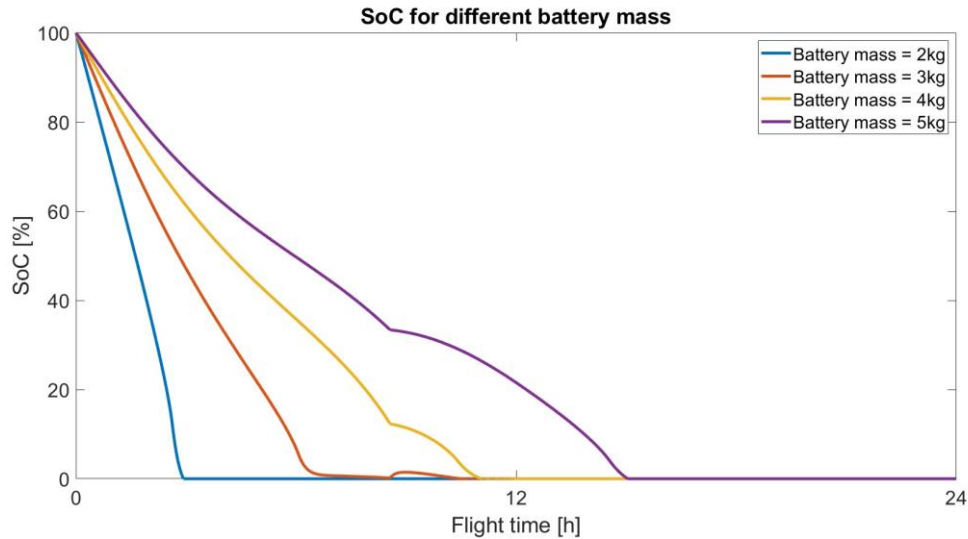


**Figure 6.20.** SOC for different battery mass during 8 km flight at vernal equinox (refers to TS17).

Due to the longer climb time, and thus greater energy consumption, the UAV operation time was shortened. The time needed to reach the altitude of 8,000 meters is 8.5 hours. It can be seen that at this point (8.5 hours from the start) the discharge characteristics of the batteries change. The weight of the battery equal 2kg and 3kg makes it impossible to fly to an altitude of 8 km during the spring equinox. The weight of 4kg and 5kg allows the TS17 to fly to an altitude of 8,000 meters. After reaching the altitude of 8 km, the energy demand needed for cruise flight is greater than the PV system can produce at this time. The energy balance is therefore negative all the time and only allows to extend the time without the possibility of recharging the batteries.

The second part of the scenarios presents identical 3 scenarios, i.e., a flight at an altitude of 1 km, 5 km, and 8 km on the summer solstice. The execution of flight scenarios in this period allows to know the maximum duration of the UAV flight. The continuous flight scenario at 1 km is shown in Figure 6.21.

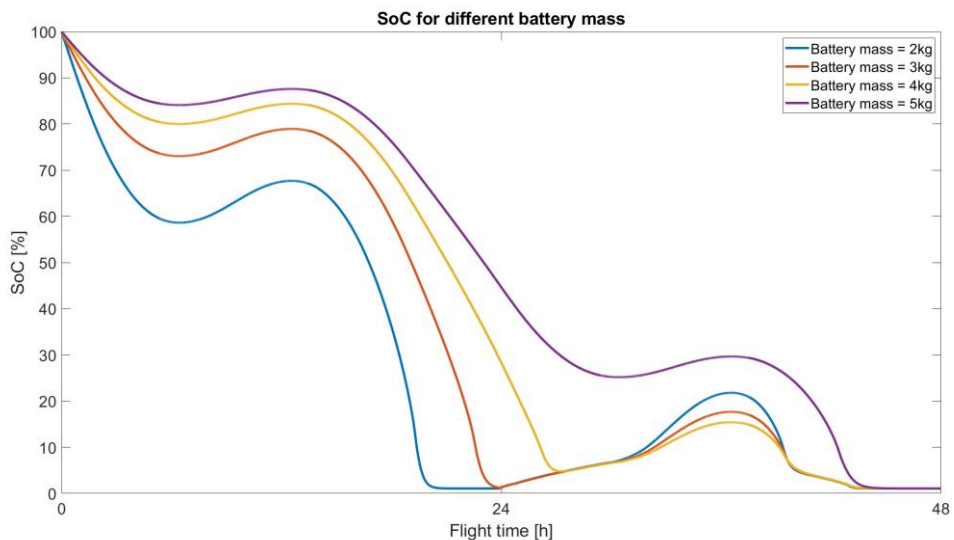


**Figure 5.21.** SOC for different battery mass during 1 km flight in summer solstice (refers to TS17).

Changing the time of the mission to the summer solstice allowed for a significant extension of the flight time. The higher irradiation value allowed the battery to be

recharged, which could not be observed for this scenario implemented at the spring equinox. Flight over 24 hours is possible with batteries weighing 4 kg and 5 kg. A battery weighing 2kg and 3kg is not able to fly for more than 24 hours.

Figure 5.22 presents the SOC results from the scenario no. 1 from Figure 6.1 in the summer solstice.

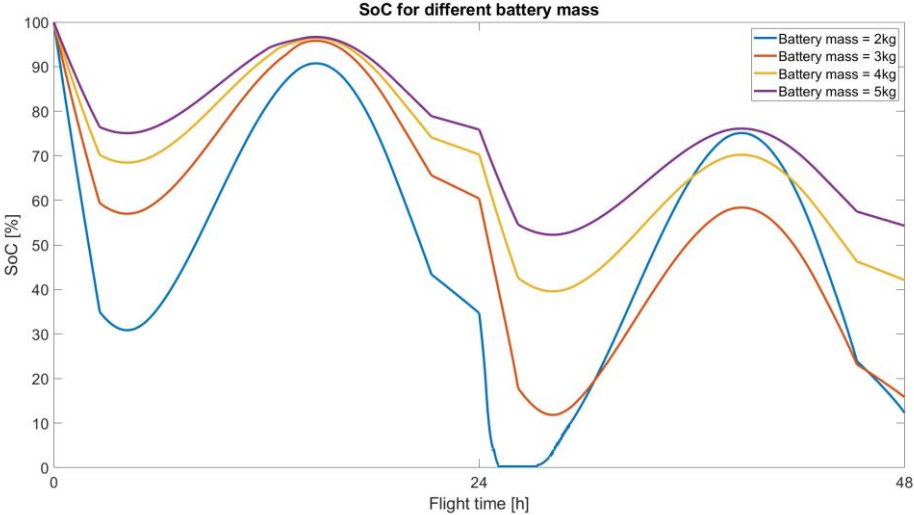


Figure 5.22. SOC for different battery mass during 5 km flight in summer solstice (refers to TS17).

From SOC characteristics it can be seen that each battery capacity allowed for a 24-hour flight. In the first 24 hours, almost each battery capacity was able to charge up to 90% of SOC. Three battery configurations were able to perform the 48-hour flight. The smallest configuration (lowest mass) was unable to provide sufficient capacity for the climb stage on the second day. The 2kg battery, due to its smaller capacity, was able to charge faster. The correct operation of the system can be noticed on the second day of the implemented scenario. The smaller capacity of the 2kg battery allowed for faster achievement of a higher SOC level than in other cases.

The last scenario — a flight to an altitude of 8 km — is shown in Figure 5.23. The high degree of battery discharge caused that only the largest battery configuration allowed for a 24-hour flight.

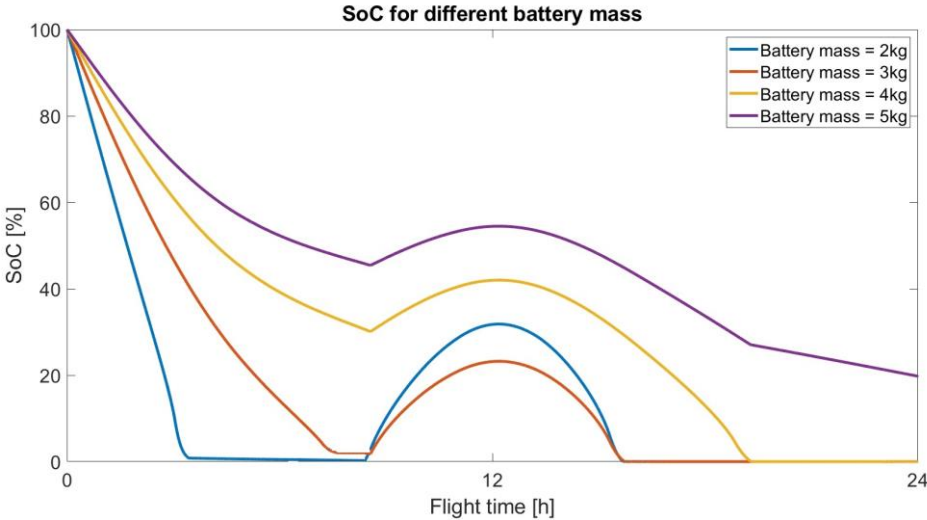


Figure 5.23. SOC for different battery mass during 8 km flight in summer solstice (refers to TS17).

It can be seen that the simulation works under rigid conditions. After drop SOC to 0%, the simulation does not turn off but continues the system operation. The reason for this kind of the operation of the system is to know the energy balance in the further stages of the flight and to verify the correct operation of the simulation system.

After such analyzes presented only on the example of TS17, a decision was made which, according to the assumptions, was to best harmonize between ensuring the long-endurance of the flight in the period between the spring equinox — summer solstice — autumn equinox and also providing additional payload for placing UAV accessories.

The result of these simulations was the selection and final configuration of UAV batteries:

- TS17 — 4S12P;
- TS12 — 12S18P;
- VTOL — 12S6P.

Such a combination of battery cells made it possible to determine what C-rated current values occur for these three case studies (TS17, TS12, VTOL) during the flight. By analyzing the values of energy demand during take-off, climb, and cruise flight, the range of C-rated current was given. This range is presented in Table 6.4. In the table the gliding stage was omitted. Avionics consumes negligible energy, and during gliding only this kind of load occurs.

The weight of the TS17 battery was 2.4 kg, for the TS12 it was 10.8 kg, and for the VTOL 3.6 kg.

**Table 6.4.** C-rated range of current values for UAVs in different stages of flight

	<b>TAKE-OFF</b>	<b>CLIMB</b>	<b>CRUISE</b>
TS17	-	0.3C	0.1C
TS12	-	0.3C	0.1C
VTOL	2C	0.3C	0.1-0.2C

Data which are presented in Table 6.4 show the current values which will discharge the batteries during the flight. For this purpose, the Samsung INR18650-35E battery cell was measured on the test stand. The data that will be obtained will eventually be implemented in the simulation model.

In addition to taking typical current-voltage characteristics, the temperature of the battery cell was also controlled. The battery cell heats up during operation. Understanding the heating characteristics of the battery cell is important from the point of view of long-distance flights at high altitudes, where the temperature reaches minus tens of degrees Celsius. The tests were carried out in a polystyrene insulating layer — more or less in the same layer in which the battery cell in the UAV will be placed (Figure 6.24).

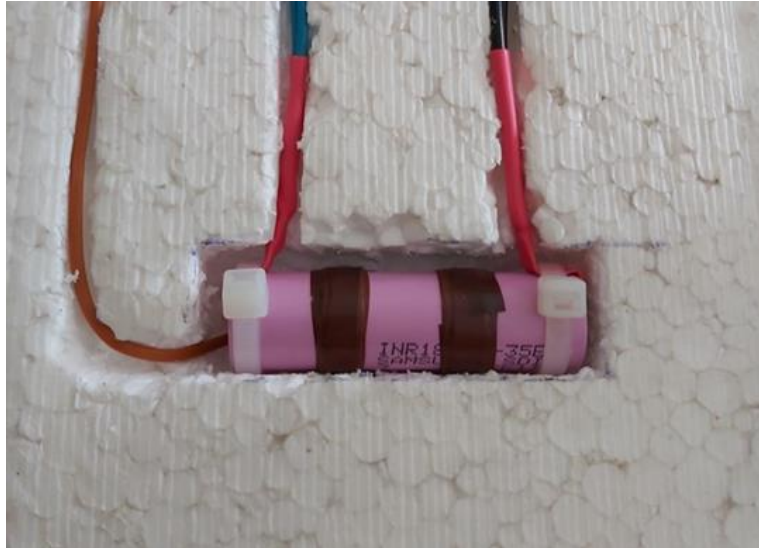


**Figure 6.24.** Tested Samsung INR18650-35E.

Two most important characteristics were taken: 0.2C (0.7 ampere) and 0.5C (1.75 ampere). During a cruise flight, when the value has been defined as even 0.1C, its value may increase due to on-board devices that constantly draw energy from the batteries, as well as in the event of unfavorable weather conditions forcing an increase in power.

For a VTOL, a 2C-rated current discharge takes only 40 seconds only during a vertical take-off to an altitude of 200 meters. Therefore, the measurement of this characteristic was omitted.

The discharge and temperature characteristics are shown in Figure 6.25. The x-axis shows the time when y-axis shows the SOC level and the temperature of battery cell.

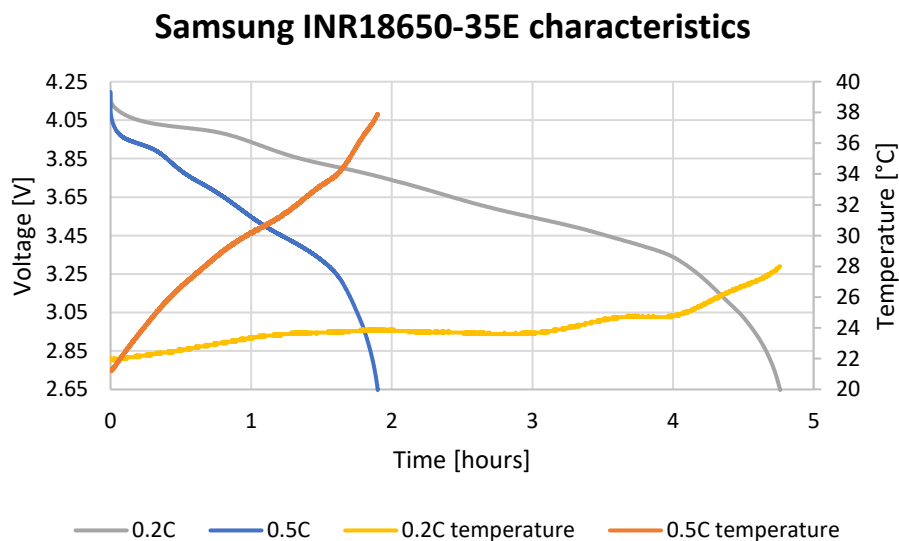


**Figure 6.25.** Temperature and discharge characteristics of the tested Samsung INR18650-35E.

In order to tune the Generic Battery Model library, the characteristics were also taken in the form where the x-axis is marked with the battery capacity in ampere-hour. It is presented in Figure 6.26.

## Discharge characteristics of Samsung INR18650-35E

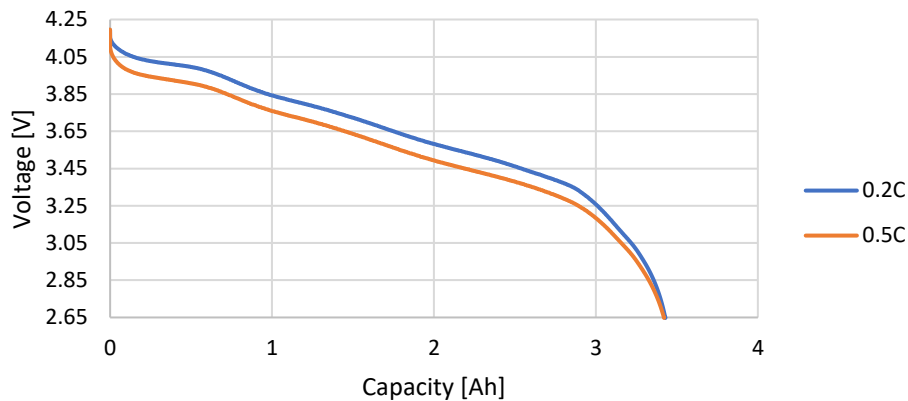


**Figure 6.26.** Discharge characteristics of the tested Samsung INR18650-35E implemented in the simulation model.

The fine-tuning of the model consisted in defining the parameters of the Generic Battery Model library in a way that would best reflect the real characteristics of the Li-ion battery cell during the battery discharge simulation.

Figure 6.27 shows the tuning of the simulation to the actual discharge characteristics of the Samsung INR18650-35E battery cell.

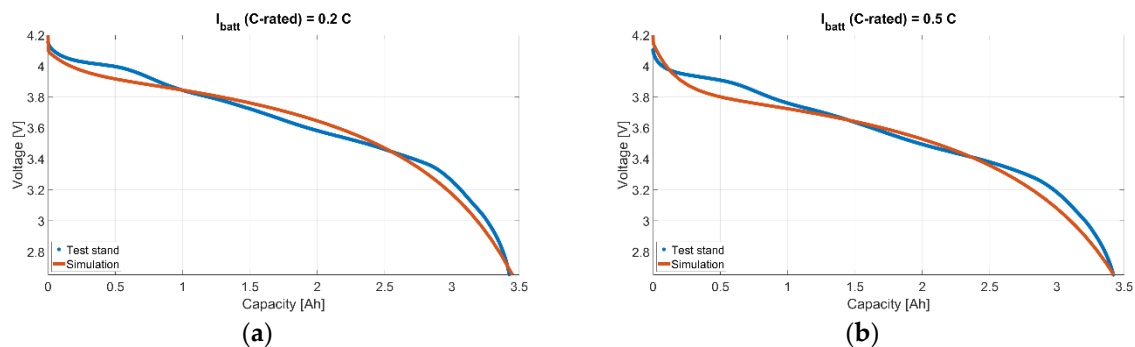


**Figure 6.27.** Characteristics of tuned: (a) 0.2C; (b) 0.5C.

In addition to tuning the battery model to the load system, it was necessary to verify how the PV system would charge the battery cells and what the C-rated current value would be during charging. For this purpose, the entire range of irradiation power from 0 watts up to almost 900 watts (peak value for Gliwice in the summer solstice) had to be used. Each of the analyzed UAVs had to be considered separately. In order to simplify model, it was decided not to complicate the power supply system and do not split the charge and discharge characteristics at this stage of work.

In order to verify and learn about the differences in characteristics for different values introduced into the simulation model, a comparison of identical flight scenarios was carried out with the introduction of changes to the Generic Battery Model library.

Only the phenomenon based on TS17 is presented. Identical simulations were performed in TS12 and VTOL. Exemplary simulations were performed for both the spring equinox (Figure 6.28) and the summer solstice (Figure 6.29).

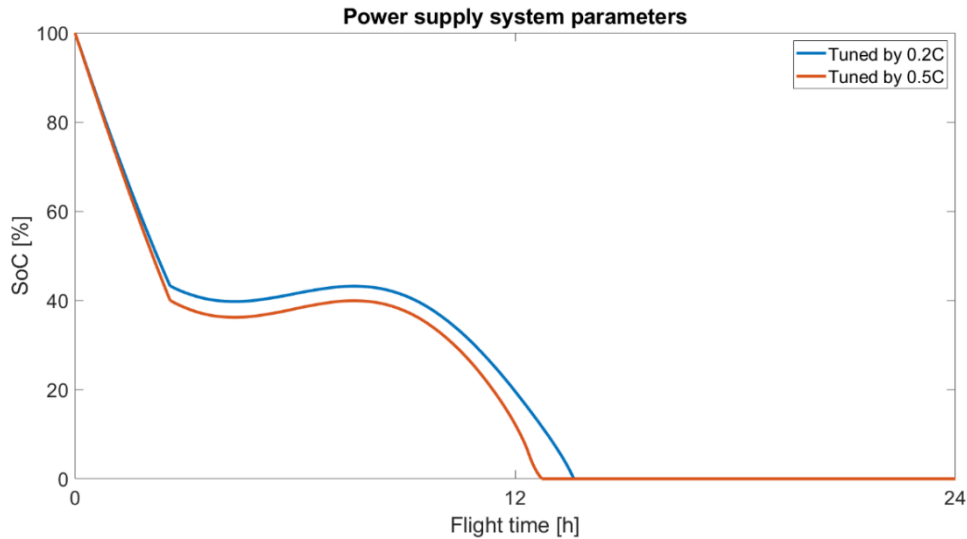


**Figure 6.28.** SOC parameters of the 5 km mission at the vernal equinox (refers to TS17).

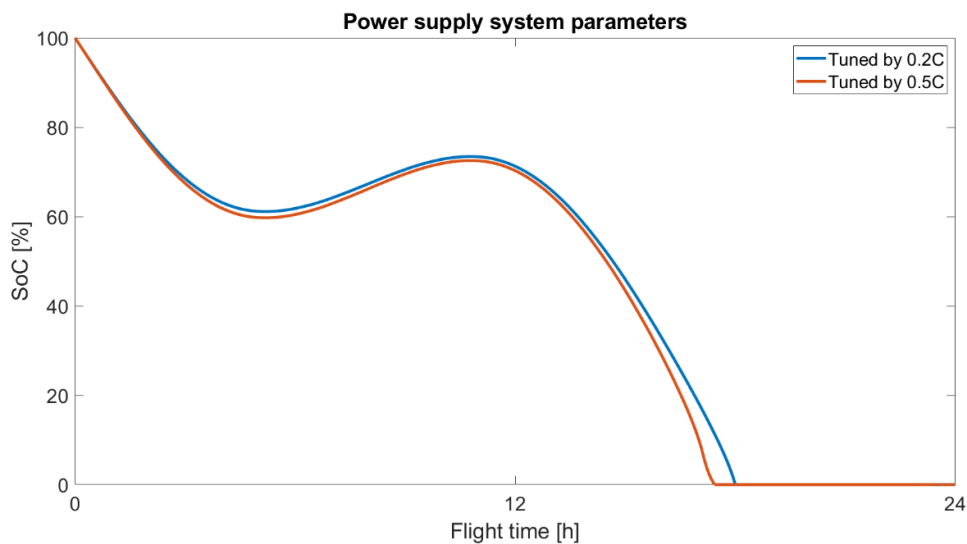


**Figure 6.29.** SOC parameters of the 5 km mission in the summer solstice (refers to TS17).

The analysis of both characteristics allows to observe that tuning the model to the discharge parameters with 0.5C current shortens the mission time — the SOC discharges faster. It can be seen in Figure 6.29 that during a positive energy balance, tuning the system to the 0.5C characteristic causes the charging to proceed slightly faster than when tuning to the 0.2C characteristic. This is due to the simplification that is implemented in the Generic Battery Model library — charging is the reverse of discharging. Tuning to the characteristics of a higher charging current causes the SOC to reach a higher charge level faster.

The analysis also allows to observe that when the UAV is climbing, the system should actually be tuned to 0.5C. At this stage, the SOC drops more clearly than in the case of tuning to the 0.2C characteristic. However, in the case of cruise flight, both systems have almost parallel characteristics. The change deepens again in the final phase — the final discharge to 0% SOC.

Due to the fact that climb loads the system the most, it was decided to tune the model to the value of 0.5C. Such a simplification can be made due to the small load fluctuations and the very low C-rated current which discharges the batteries. In the case

of UAVs, these simplifications still reliably calculate the true SOC value. In the case of much greater fluctuations in the discharge, the system should be divided into individual subsystems that would change the settings to the conditions of the load.

At an early stage, which will be finalized by verification on a prototype, as many simplifications as possible should be sought, so that the system is not complicated and possible changes can be quickly implemented to the model and the systems included in it.

Similarly to the TS17 simulation model, the power supply systems in the TS12 and VTOL were tuned. The changes occurred in the same places. What should be taken into account in this case are slightly worse output parameters — the system discharges a bit faster. This buffer can be taken into account when performing missions. Winds occurring during the flight, unfavorable weather conditions occurring temporarily can increase energy consumption, and thus worsen the ideal conditions included in the simulation.

It was decided that both for the two Twin Stratos and for the VTOL, the entire system would be tuned to 0.5C-rated current characteristics.

## 6.4 Summary

Fine-tuning of the UAV power supply system allowed for the development of the configuration of solar cells and battery cells connections. Parameters of UAV solar power management system are presented in Table 6.5.

**Table 6.5.** Power supply system parameters

<b>Power supply system parameters</b>			
	<b>TS17</b>	<b>TS12</b>	<b>VTOL</b>
Battery capacity (kWh)	0.605	2.722	0.907
Battery connection	4S12P	12S18P	12S6P
Battery mass (kg)	2.4	10.8	3.6
Number of solar cells	40	350	80
Solar cells connection	20S2P	70S5P	40S2P
Solar cells mass (kg)	0.264	2.31	0.528

In the case of tuning the energy storage system, the PV system and the value of the current that flows to the batteries during the mission should also be taken into account. Due to the dynamic changes in the system, it would have to be tuned to specific characteristics. However, the charging values of the PV system are so low that they do not significantly affect the system. The biggest changes in the power supply system occur in the case of high charging and discharging currents. Low values make the system more stable. Therefore, in order to further simplify the model, this element has been omitted.

The configuration of the connection of the PV panels affects the basic values of the power supply system — current and voltage. The most important parameter verifying the energy balance is the output power of the system. The series connection of the system allows to achieve the voltage matched to the dedicated MPPT regulator. Parallel

connection provides system redundancy. The selected configurations were intended for practical use and should be adaptable to Genasun's MPPT regulators.

The mass of the entire SPMS system consists of the mass that has been allocated for the batteries, the mass of solar cells that are on the drones, the mass of BMS, MPPT, and cabling. Ultimately, in order to reduce the mass of the system, it is considered to get rid of the redundant housings of BMS and MPPT, because these devices will be placed inside the UAV anyway. Therefore, the initial estimates of the mass of the power supply system omitted the systems monitoring the operation of the PV and batteries. Cabling was also omitted at this stage of work. A summary of the weight of the SPMS system is listed in Table 6.6.

**Table 6.6.** Mass summary of the UAVs

<b>Power supply system parameters</b>			
	<b>TS17</b>	<b>TS12</b>	<b>VTOL</b>
Maximum mass (kg)	5	15	4
Batteries (kg)	2.4	10.8	3.6
Solar cells (kg)	0.264	2.31	0.528
Payload (kg)	2.5	2.5	0
SUMMARY — mass balance (kg) compared to estimated battery weight from Table 5.1.	-0.164	-0.61	-0.128

In the case of TS17 and TS12, the balance can be compensated by reducing the available payload. In this situation, the payload for the TS17 will be slightly more than 2.3 kg and about 1.9 kg for TS12. In the case of VTOL, there is not much to reduce the negative energy balance. The weight that has been exceeded is less than approx. 1-1.5% of the total weight of the vehicle. The mass of additional electronics managing the power supply system and cabling should be taken into account here. In the case of TS17 and TS12, there is still a mass buffer that can be used. VTOL does not have this capability.

The calculations were adjusted to previously calculated values. Depending on the arrangement of the systems inside the UAV, it may also be necessary to balance the UAV, and thus it is possible to increase the weight of the vehicle to some extent.

The results, which will be presented in Chapter 7, will take into account the data obtained at the design and conceptual stage.

## 7. Results

The results of the work presented in this chapter are intended to compare how the change of time and season will affect the endurance of the UAV flight. To what extent different designs, maximum flight altitudes, and UAV size will affect their endurance.

Each simulation included sunny clear weather for the UAV flight in Gliwice. The most important parameters that are given in the figures below are SOC, energy consumption at a specific stage of the flight and the current energy supplied by the photovoltaic system to the power supply system.

Comparing both the energy used and the energy produced makes it possible to determine the energy balance and verify in which stage of the flight, the UAV is able to recharge the batteries and in which situation the UAV uses the energy stored in the batteries.

The scenarios were performed only at two specific times — at the vernal equinox (March 21) and in the summer solstice (June 21).

The mission execution time is astronomical, i.e., it does not take into account the division of summer (local) time during performing flights on the summer solstice.

The duration of the day for the vernal equinox is 12 hours — sunrise is at 6 a.m. This is also the moment of starting the flight mission.

The duration of the day for the summer solstice is 16h — sunrise is at 4 a.m. This is also the moment of starting the flight mission.

In real life conditions, a specific SOC level should be taken into account at which the mission will be canceled and it will be necessary to abort the mission. It is necessary to safely bring the UAV to the ground. In the analysis of the results presented below, two SOC values were taken into account. The first is SOC equal to 0%. It aims to illustrate the maximization of results without maintaining appropriate safety measures. The second value is SOC equal 20%. Such a buffer allows to safely bring the UAV to the ground, enabling the operation of drives and servos (only for Twin Stratos) if necessary.

### 7.1 Twin Stratos UAVs

#### 7.1.1 *Twin Stratos 17*

The TS17 flight without the use of solar energy is possible in the event of a PV system failure, the need to fly at night or in unfavorable irradiation conditions. Table 7.1 shows the values of daily irradiation for the location of Gliwice during the spring equinox and summer solstice. Additionally, Table 7.1 takes into account the energy values that the PV system on board the TS17 can produce both on March 21 and June 21.

**Table 7.1.** Parameters of daily insolation and energy produced by TS17.

<b>Daily insolation value (kWh/m<sup>2</sup>)</b>	
Vernal equinox	4.02
Summer solstice	7.67
<b>Daily energy produced by TS17 (kWh)</b>	
Vernal equinox	0.59
Summer solstice	1.12

In order to be able to refer the impact of the PV on UAVs that do not use PV energy, the first simulations which took into account the two scenarios from in subchapter 6.1.1 were developed. The results are appropriately presented for scenario no. 1 in Figure 7.1. and for scenario no. 2 in Figure 7.2.

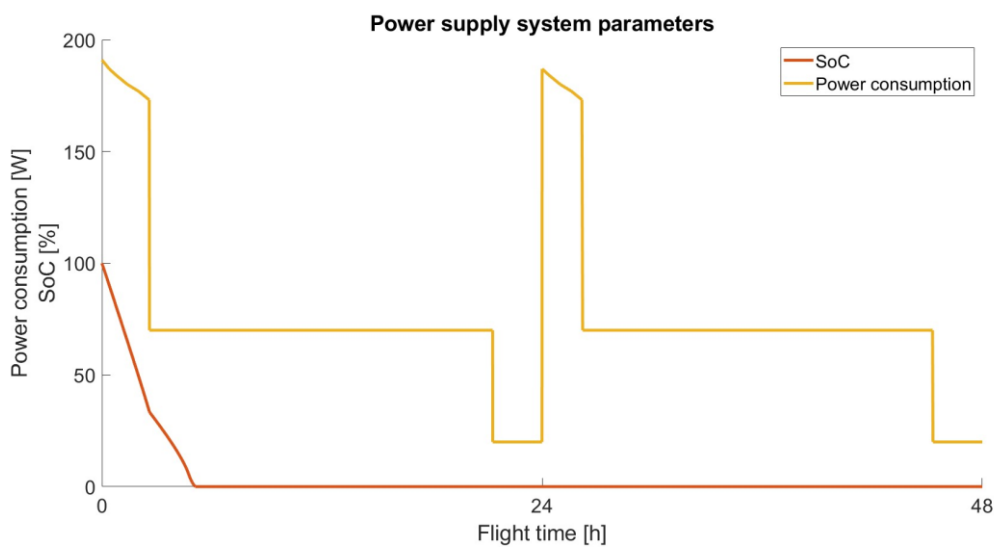


**Figure 7.1.** Twin Stratos 17 5 km scenario without PV.

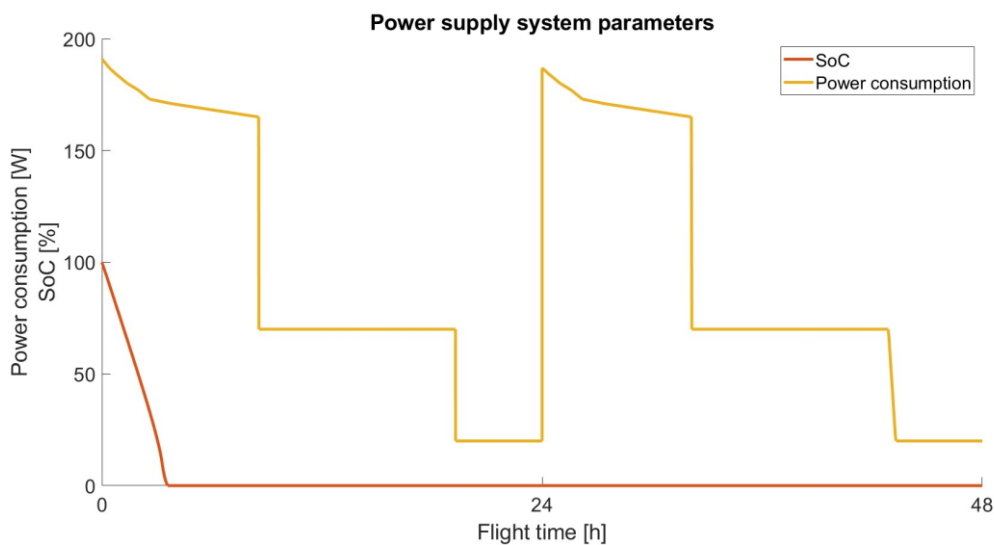


**Figure 7.2.** Twin Stratos 17 8 km scenario without PV.

The results which took into account the impact of PV on TS17 were divided into two stages. The first is the time of flight, i.e., the division into the spring equinox

(March 21) and the summer solstice (June 21). The second is directly related to the flight scenario — flight to the altitude of 5 km and to the altitude of 8 km.

During the vernal equinox, two simulations were performed — for two scenarios. Their results are presented in Figure 7.3, respectively for scenario no. 1 and Figure 7.4 for scenario no. 2.

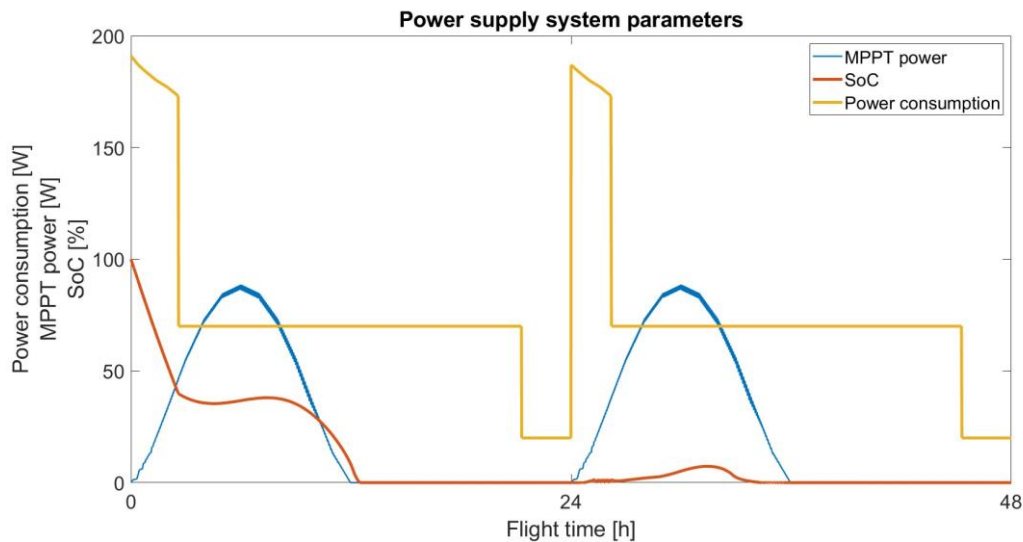


**Figure 7.3.** Twin Stratos 17 5 km scenario at the vernal equinox.

By analyzing the TS17 flight to an altitude of 5 km, it can be observed that this ceiling is possible to reach at the vernal equinox. The change in energy consumption from the ascent stage to the cruise flight stage allows for a period of about 4 hours to obtain a positive energy balance. A small surplus of the energy balance causes that the level of SOC increases slightly and remains almost at the same level of about 35%.

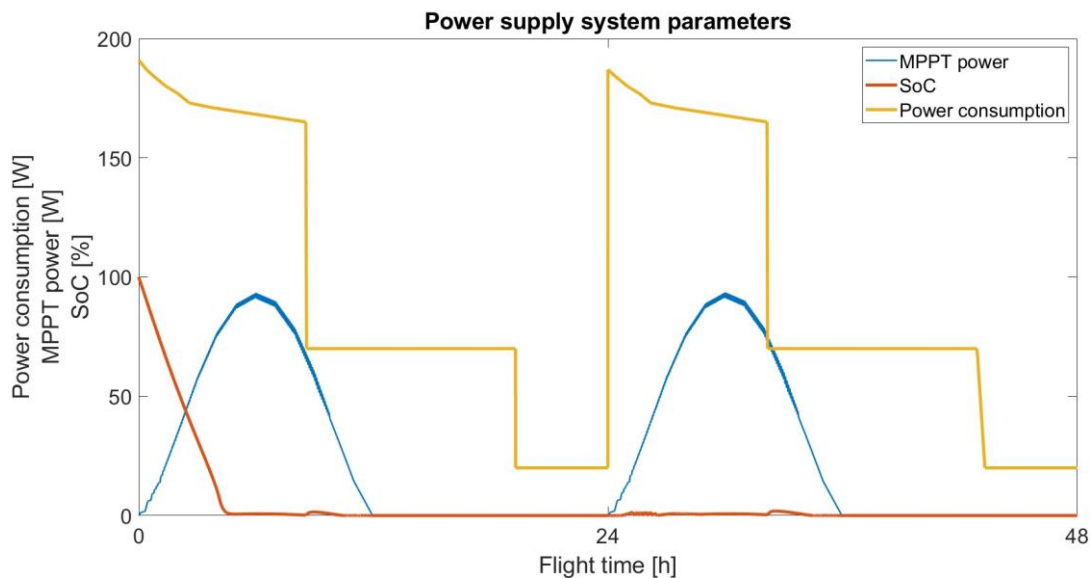


**Figure 7.4.** Twin Stratos 17 8 km scenario at the vernal equinox.

In the case of a flight to an altitude of 8 km, due to the high power consumption and reduced flight path angle in the last 3 km, the time of the climb operation was significantly extended. This makes the ceiling of 8 km impossible to achieve. At 6,300m, the SOC of the battery is drained. The scenario in which the take-off occurs with the

sunrise means that there is practically no situation in which the energy balance would be positive — apart from minor exceptions at 8.5 h and 32.5 h — where the line of energy consumption coincides with the line of energy produced.

Flights during the spring equinox allow for a continuous flight up to 12 hours. It should be noted that for scenario no. 1 at SOC 20% and 0% UAV is at height 5,000 meters, while the height in the second scenario will vary. Using the ROD value for TS17 (0.41m/s), it can be calculated the average descent time, which will be about 3 h and 20 min from a height of 5 km to the ground.

The change of time to the summer solstice is intended to present maximized results for the proposed flight scenarios. Below in Figure 7.5, a flight scenario to an altitude of 5 km was presented.

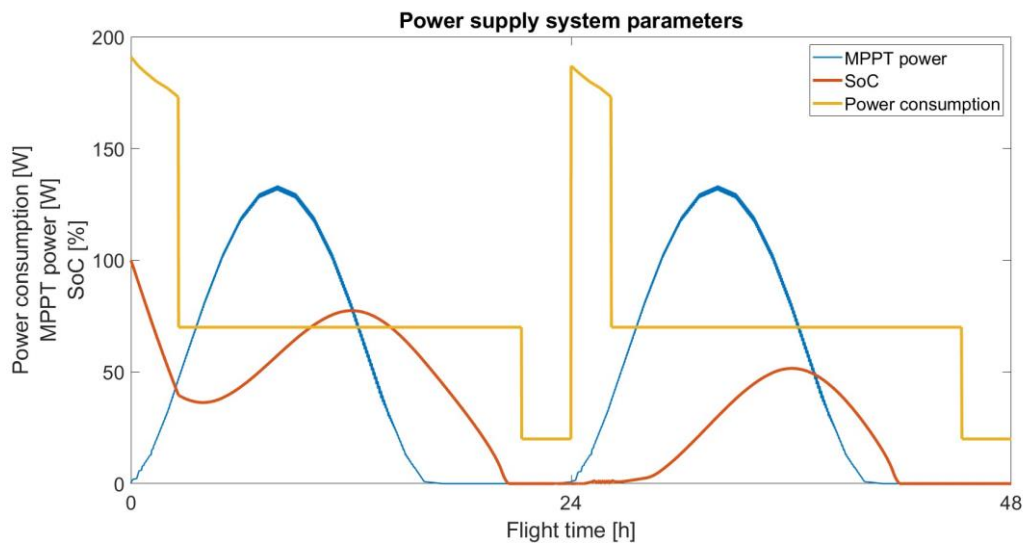


**Figure 7.5.** Twin Stratos 17 5 km scenario in the summer solstice.

In the case of the flight on June 22, it can be seen a much more visible moment when the batteries start charging. Due to the greater extreme of irradiation and the longer day time, the power supply system is able to recharge the batteries to the level of 77%.

The mission time change was also applied to the flight to 8,000 meters (Figure 7.6).

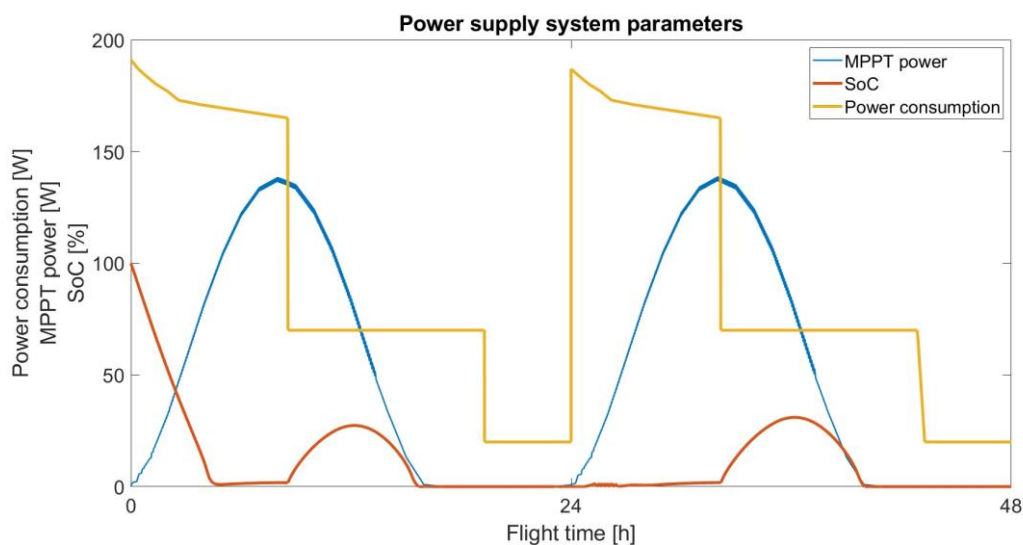


**Figure 7.6.** Twin Stratos 17 8 km scenario in the summer solstice.

The flight to an altitude of 8,000 meters was completed 4 h and 25 min after the take-off. Although it can be noticed in some phases of the flight that the energy from the MPPT system is able to be higher than the energy demand, the selection of the take-off time prevented the UAV from reaching the 8 km level. At 6,300 meters, the UAV's battery was completely discharged.

In order to increase the energy from the PV system, it was decided to change the take-off time. The total climb time of the TS17 from level 0 to level 8 km was 8.5 hours. For this reason, it was decided to average the time in such a way that half of the set time to reach the 8 km ceiling was at noon. The start was set for 7 a.m. The characteristics for scenario no. 2 are presented in Figure 7.7.

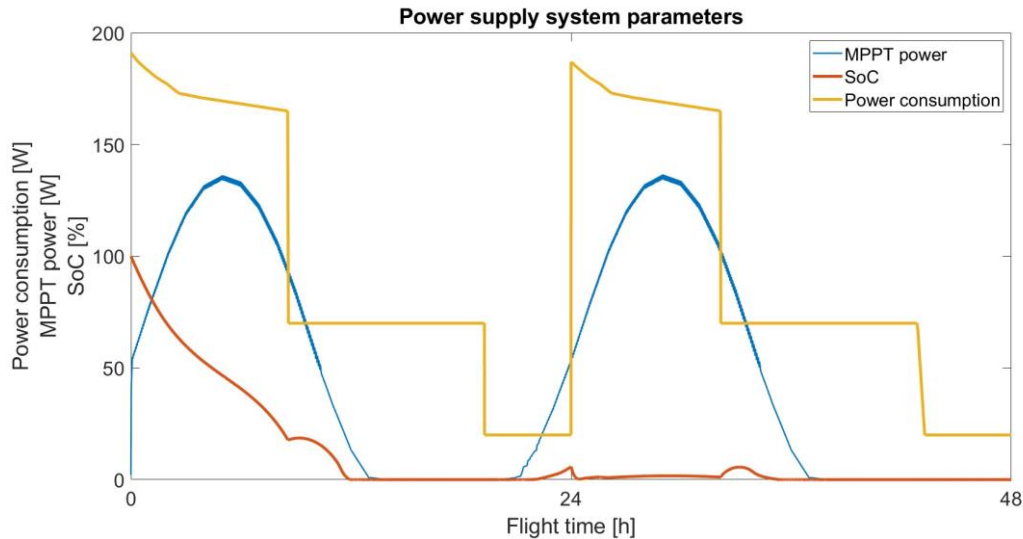


**Figure 7.7.** Twin Stratos 17 8 km scenario in the summer solstice – take-off at 7 a.m.

By analyzing the chart for the TS17 flight with the take-off delayed by 3 hours relative to sunrise (rise around 4.00 a.m.), it can be observed that the UAV is able to reach a ceiling of 8 km. After reaching an altitude of 8,000m, the SOC was 18%. The possible time of maintaining the flight at the height of 8 km can last up to about 3 hours. The energy consumption when TS17 is flying at an altitude of 8 km is less than at an altitude of 5 km. However, a less loaded motor operates with lower efficiency. As a result, the energy consumption for the power supply system was set at the same level for both the 5 km and 8 km ceilings. Table 7.2 summarizes the results for the TS17 power supply system regarding the SOC level and mission duration.

**Table 7.2.** Summary of the performed TS17 scenario simulations.

<b>SOC = 0%</b>			
	5 km	8 km	8 km take-off at 7 a.m.
no PV	5 h	3 h 30 min	—
Vernal equinox	12 h 20 min	4 h 25 min	—
Summer solstice	20 h 30 min	4 h 25 min	11 h 45 min
<b>SOC = 20%</b>			
no PV	3 h 45 min	3 h	—
Vernal equinox	11 h 05 min	3 h 30 min	—
Summer solstice	19 h 15 min	3 h 30 min	8 h 20 min

### 7.1.2 Twin Stratos 12

As in the case of TS17, also for TS12 a table was developed with the data of irradiation and the possibilities of energy production by the UAV power supply system (Table 7.3).

**Table 7.3.** Parameters of daily insolation and energy produced by TS12.

Daily insolation value (kWh/m <sup>2</sup> )	
Vernal equinox	4.02
Summer solstice	7.67
Daily energy produced by TS12 (kWh)	
Vernal equinox	5.13
Summer solstice	9.8

As in the case of TS17, the first simulation that was carried out concerned flights without the use of PV energy. The first graph — Figure 7.9 — presents the analysis carried out for scenario no. 1 (included in subchapter 6.1.2) — a flight to an altitude of 10 km.

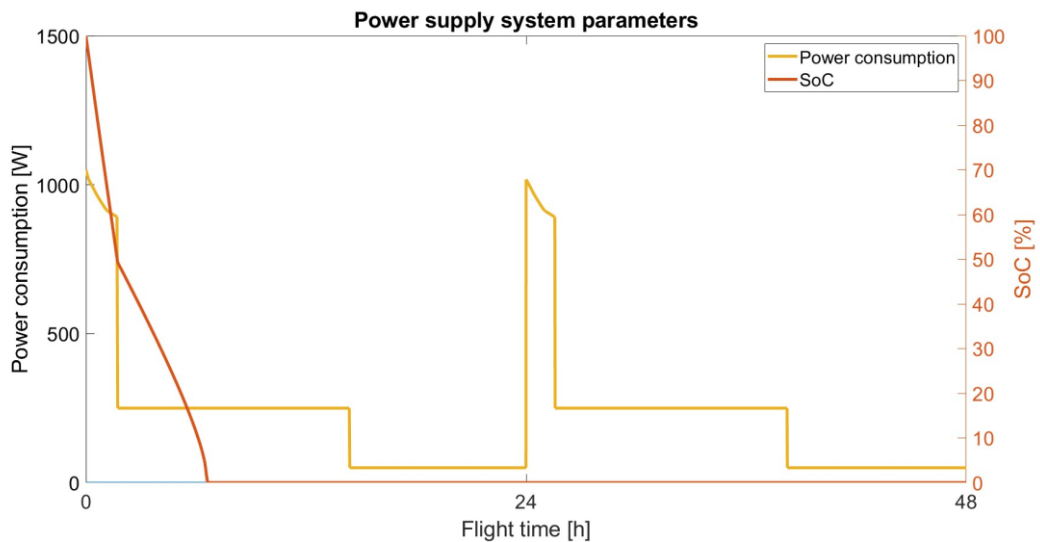


**Figure 7.9.** Twin Stratos 12 10 km scenario without PV.

The analysis of the SOC graph shows that even without the use of PV, the TS12 is able to reach the ceiling of 10 km and start the cruise flight stage. The battery will discharge after approx. 6 h and 35 min. An identical simulation was carried out for a flight to an altitude of 15 km — scenario no. 2.

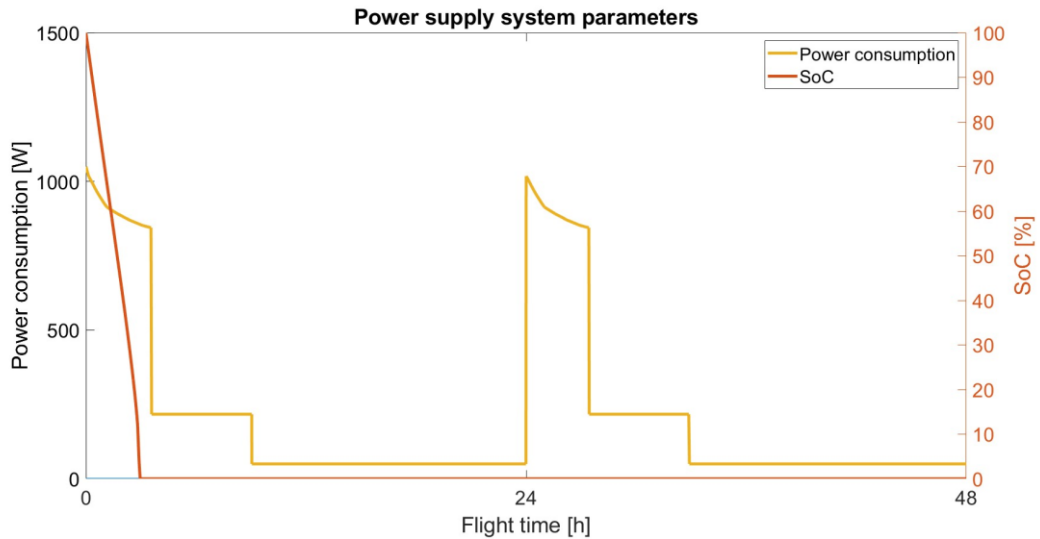


**Figure 7.10.** Twin Stratos 12 15 km scenario without PV.

Flight to an altitude of 15 km without PV is impossible. By the time the TS12 reaches the 15 km ceiling, the battery will be drained. The power supply system will behave in the same way for a simulation representing a flight to an altitude of 20 km — scenario no. 3. The parameters of the propulsion system and all energy-consuming elements will be the same up to the altitude of 15 km. The battery is fully discharged at an altitude of 13,700 meters — 3 hours from the starting of the mission.

Without PV, a maximum ceiling of 13,700 meters is possible. Subsequent simulations take into account the use of solar cells on the UAV surface. Each of the three scenarios is simulated during the spring equinox and summer solstice. The first of them — the scenario of a flight to an altitude of 10 km on March 21 — is presented in Figure 7.11.

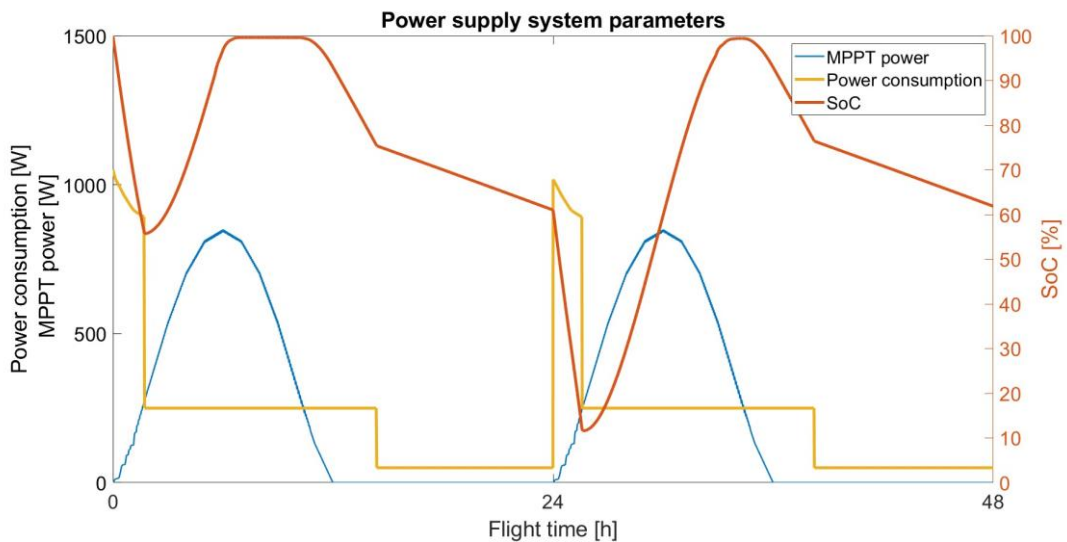


**Figure 7.11.** Twin Stratos 12 10 km scenario at the vernal equinox.

During take-off and climbing, the battery discharge, however, after transitioning to cruise flight, the reduced value of energy demand allows to obtain a positive energy balance. From 1 h and 45 min (7:45 a.m.) after the start of the flight, the energy balance remains positive until 10 h and 20 min of flight (4:20 p.m.). A negative energy balance causes the battery to gradually discharge. The lowest SOC value occurs on the second

flight day, when the TS12 performs the second climb stage. The SOC value is equal to 11.5% when the UAV reaches the ceiling of 10 km. The next stage of flight (cruise flight) allows the power system to charge the battery to 100% SOC. After 48 hours of flight, the SOC value is equal to 62%, i.e., the same value as in the previous day after 24 hours.

Scenario no. 1 was also simulated on June 21 (Figure 7.12).

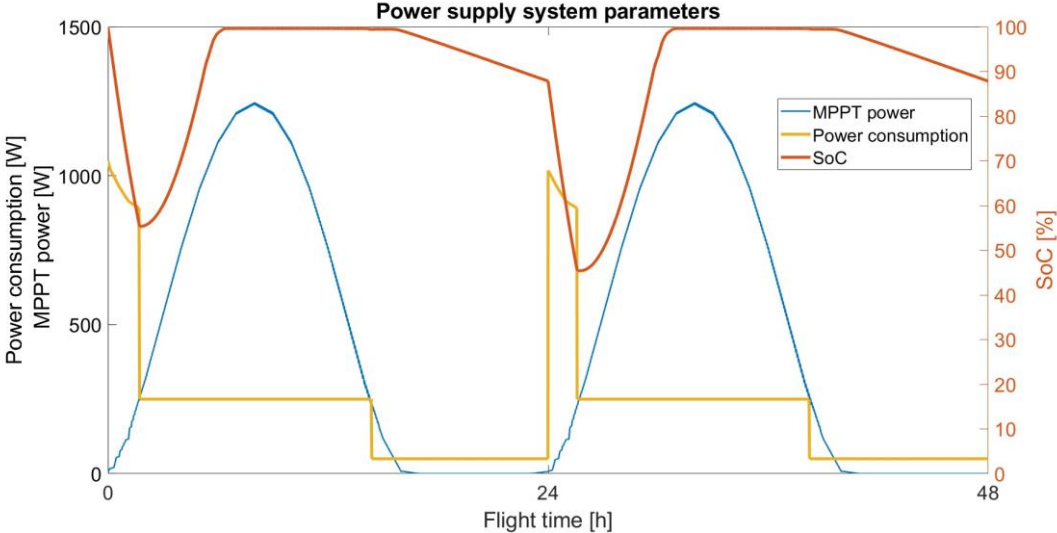


Figure 7.12. Twin Stratos 12 10 km scenario in the summer solstice.

Identically as in the case of the spring equinox flight, the TS12 power supply system discharges until it reaches 10 km altitude. Then the positive energy balance allows the battery to be charged to 100%. Due to the greater value of irradiation, the charging time is shorter and the longer duration of the day and the value of irradiation allow to maintain a fully charged battery for a longer time. Visible discharge begins only after sunset. Starting the ascent stage at sunrise on the second day causes that SOC drops more rapidly. Its lowest value after reaching the ceiling of 10 km is 45%. After 48 hours of flight, the SOC value is the same as 24 hours earlier and amounts to 88%.

The second scenario — a flight to a higher altitude of 15 km — was carried out for the spring equinox and is presented in Figure 7.13.

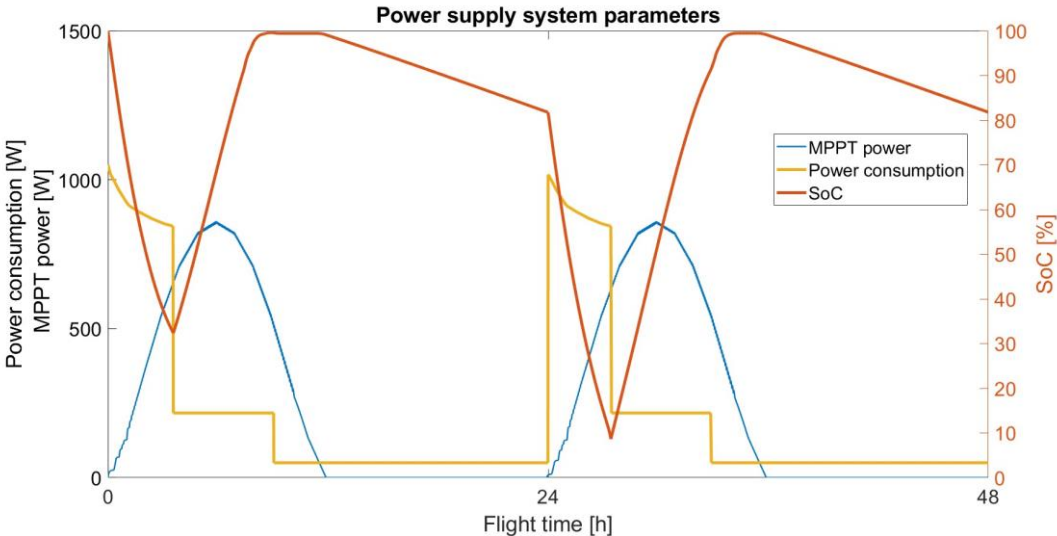
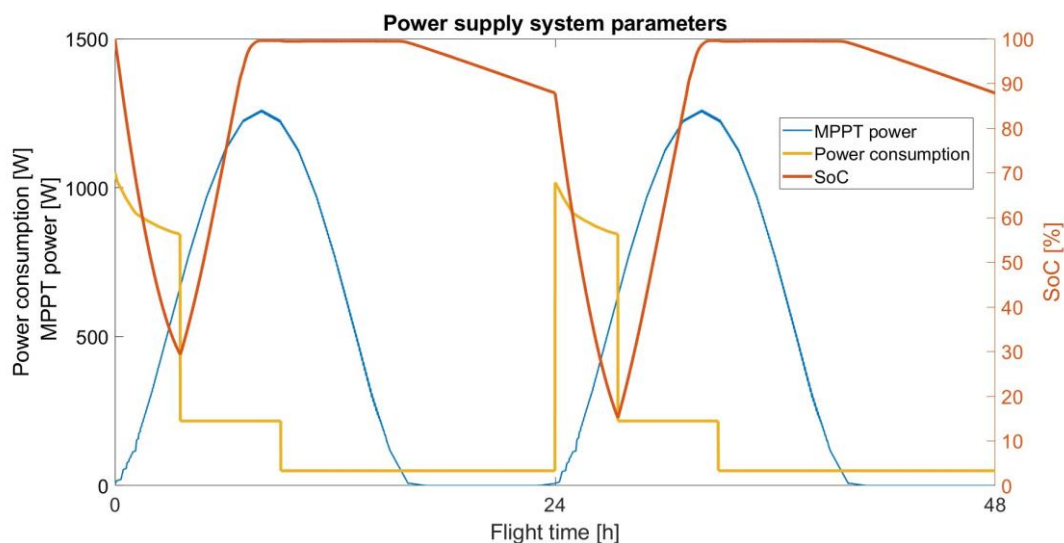


Figure 7.13. Twin Stratos 12 15 km scenario at the vernal equinox.

A longer climb time to a higher altitude causes a deeper discharge of the batteries. The SOC level after reaching the ceiling of 15 km is 32%. Lower energy consumption during cruise flight allows to charge the battery to 100%. After sunset, the TS12 starts the gliding stage. After 24 hours of flight, as well as after 48 hours of flight, the SOC of the battery is 81%. Climbing again from 1,000 meters to 15,000 meters puts a heavy load on the power supply system. Negative balance causes that after reaching the height of 15 km, the SOC level is equal to 8.5%.

The greater extreme of the power supply system discharge is due to the longer climb time than in the case of scenario no. 1. It is caused not only by the higher altitude, but also by the decrease of the flight path angle from the height of 10 km.

An identical simulation was carried out for scenario no. 2 on the summer solstice. Figure 7.14 shows the changed SOC and MPPT power characteristics.



**Figure 7.14.** Twin Stratos 12 15 km scenario in the summer solstice.

The characteristics of the proposed flight path on June 22 allow for finding an analogy between scenario no. 1 and no. 2 for the same two flight dates. Also in this case, the battery is continuously discharged until it reaches the ceiling of 15 km.

It can be seen that the gliding stage started at approx. 1 p.m. (9 hour flight). The flight path planned in this way is a waste from an energy point of view. While in the spring scenario, the shorter time of the day caused less loss, it was possible to delay the moment of gliding by 1.5 hours (the moment when UAV is able to obtain the positive energy balance and SOC level is equal 100%). In the case of planning a flight path to an altitude of 15 km on June 21, the moment of gliding should be delayed by at least 5 h and 30 min. Then the loss of energy possible use would be smaller. The lowest SOC level will also increase.

Reaching 100% of the SOC level should allow not only to maintain the flight at a specific altitude, but also to climb to a higher altitude, which is an additional time and energy buffer. The graph shows what power values the load system (propulsions and avionics) can take from the power supply system. The goal is to make the most of the prevailing conditions and UAV flight capabilities.

The state of charge of the battery after 24h and 48h does not change compared to the flight at the spring equinox and is then 88%. The minimum SOC level is reached again when reaching the highest altitude — 15 km — and is 15%.

The last scenario, which included a flight to an altitude of 20 km, is shown in Figure 7.15. This figure presents the simulation results for vernal equinox.

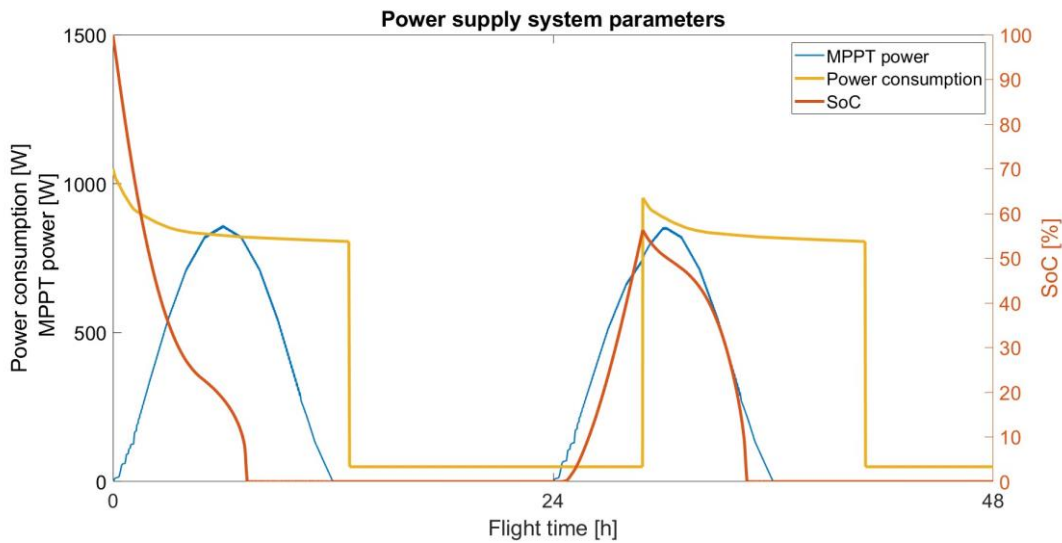


**Figure 7.15.** Twin Stratos 12 20 km scenario at the vernal equinox.

Reaching 20,000 meters with a sunrise take-off is impossible at the vernal equinox. Extended flight time, and especially reduced flight path angle, causes that the energy demand is greater than the energy from the energy storage and the energy produced by the PV system. During the flight, only for a moment at noon, the value of the energy produced by the PV system is greater than the energy demand. In order to check whether it is possible for the TS12 to reach the ceiling of 20 km, a flight simulation was conducted on the summer solstice. Figure 7.16 shows the characteristics obtained for the flight on June 21.

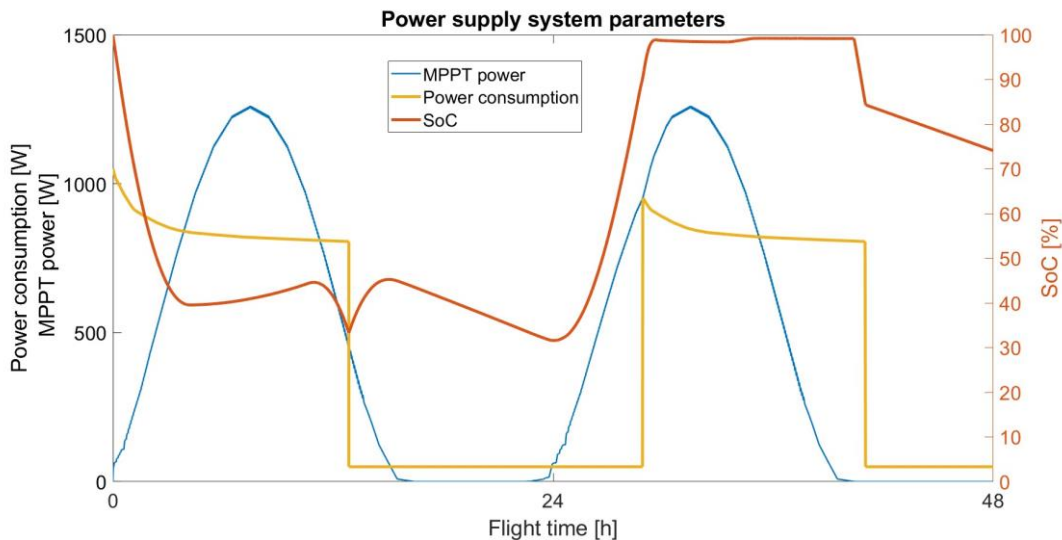


**Figure 7.16.** Twin Stratos 12 20 km scenario in the summer solstice.

An almost 13-hour flight to an altitude of 20 km is possible on the summer solstice. Due to the fact that gliding to the height of 1 km takes over 20 hours, it was decided to glide only to the level of 5 km, which takes 16 hours (as presented and explained in chapter 6.1.2).

TS12 finished gliding at approx. 9 a.m. the second day (29 hours of flight). Due to the gliding and minimal energy consumption, the PV system was able to start charging the

batteries at sunrise. For 5 hours — from the moment of sunrise to the moment of ascending again at 9:00 am — the positive energy balance allowed the batteries to be charged to 100% SOC. From 9 a.m., despite the considerable energy demand associated with climbing, there was also a positive energy balance.

It can be seen that in the 29th hour of the flight, the moment of changing the flight stage was almost perfectly set. The power supply system was charged to 100% and, additionally, a positive energy balance made it possible to achieve a higher ceiling by climbing. In this way, energy storage did not lose energy, and UAV used an energy from PV production.

Table 7.4 contains the most important values regarding the possible flight time of the TS12. These values take into account specific scenarios and mission execution time.

**Table 7.4.** Summary of the performed TS12 scenario simulations.

<b>SOC = 0%</b>			
	10 km	15 km	20 km
no PV	6 h 35 min	3 h	3 h
Vernal equinox	over 48 hours	over 48 hours	7 h 20 min
Summer solstice	over 48 hours	over 48 hours	over 48 hours
<b>SOC = 20%</b>			
no PV	5 h 10 min	2 h 40 min	2 h 40 min
Vernal equinox	25 h 15 min	26 h 40 min	5 h 40 min
Summer solstice	over 48 hours	27 h	over 48 hours

A comparison of the obtained results of scenarios no. 2 and no. 3 at the summer solstice shows that it is important from the point of view of energy autonomy to carefully plan the flight path.

While in the case of a flight to an altitude of 20,000 meters, the potential of solar energy and energy storage has been used, in the case of a flight to an altitude of 15,000 meters, unnecessary energy loss and a poorly planned scenario are visible. It is inaccurately synchronized with the flight time.

At the stage of developing exemplary flight scenarios (subchapter 6.1), no such problems were noticed. It was able to know this kind of shortcomings only after analyzing the simulation results.

It was decided to carry out one more type of simulation, which would omit the gliding stage, and would only take into account the take-off, climbing to a specific ceiling (as before 10 km, 15 km, 20 km) and maintaining this ceiling for as long as possible.

Such a scenario will make it possible to check whether maintaining the flight at altitude will be more efficient and cost-effective than energy savings when gliding, but also a high load when performing next climbing.

The scenario of climbing to a height of 10 km and maintaining this ceiling was the first simulation (Figure 7.17).

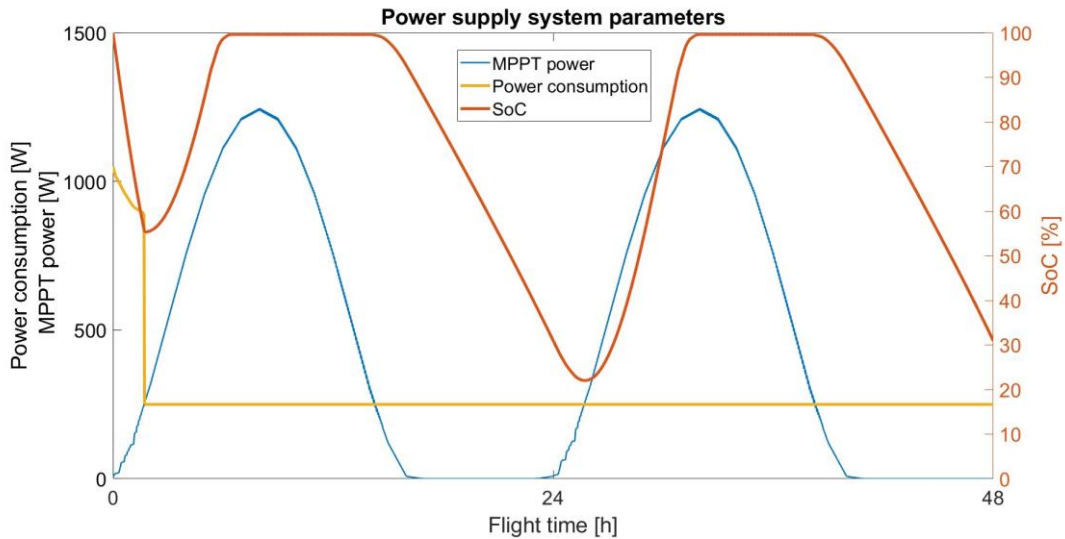


**Figure 7.17.** Twin Stratos 12 10 km scenario in the summer solstice for continuous flight.

After reaching the ceiling of 10,000 meters, the TS12 is able to start charging the batteries. Positive energy balance and at the same time 100% SOC level lasts until 6:15 p.m. (14 h and 15 min from the start of the flight). Next, the battery level slowly decreases until 5:45 a.m. the second day (25 h and 45 min after starting the flight). At the worst moment, the SOC level is 22%, and after 24 and 48 hours of flight, this level is 31%.

The advantage of such a solution is not only the possibility of obtaining energy autonomy in such conditions, but also the load of the power supply system with constant current. A battery discharged in this way will be exposed to smaller fluctuations, which should affect on the battery long-term operation. Another advantage of flying at a constant height is the practicality of using such a flight method, e.g., observation activity.

An identical flight plan was carried out for a flight to an altitude of 15,000 meters. After reaching the ceiling of 15 km, TS12 will start a cruise flight at this altitude (Figure 7.18).

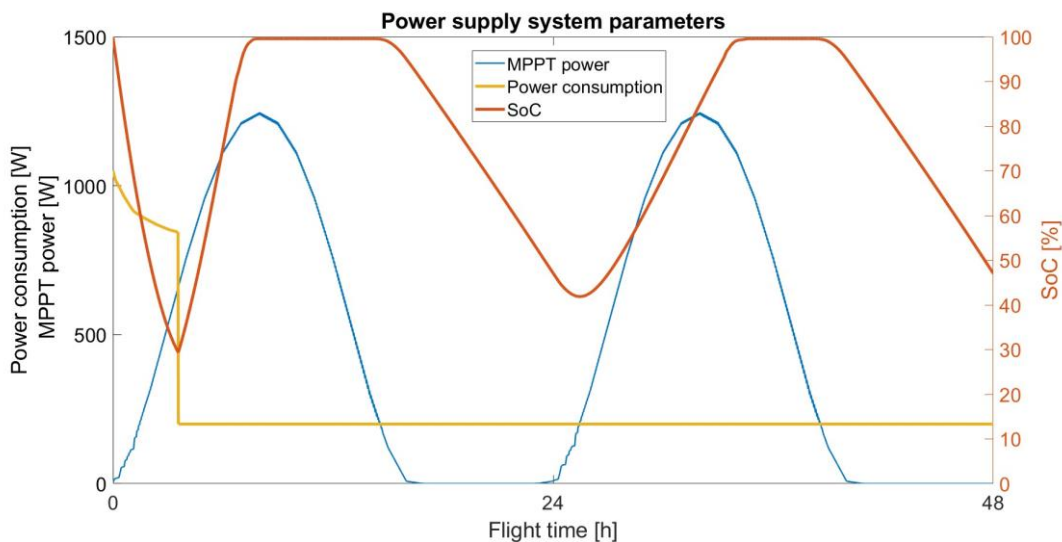


**Figure 7.18.** Twin Stratos 12 15 km scenario in the summer solstice for continuous flight.

The characteristics are analogous to the previous example with the difference that in the initial phase the SOC is discharged more. Lower energy demand at 15 km than at

10 km causes that the lowest discharge point during cruise flight to 41%. After 24 hours and 48 hours, the battery level is 47%.

Comparing the scenario of a flight at a constant altitude of 15 km, it can be concluded that it is more favorable than the scenario of a constant flight at an altitude of 10 km. In addition to the higher SOC value, an additional advantage is the flight at a higher altitude, which allows, e.g., a longer time to make a decision in the event of a malfunction.

The last exemplary scenario involved a flight to an altitude of 20 km and then maintaining the flight at this altitude (Figure 7.19).

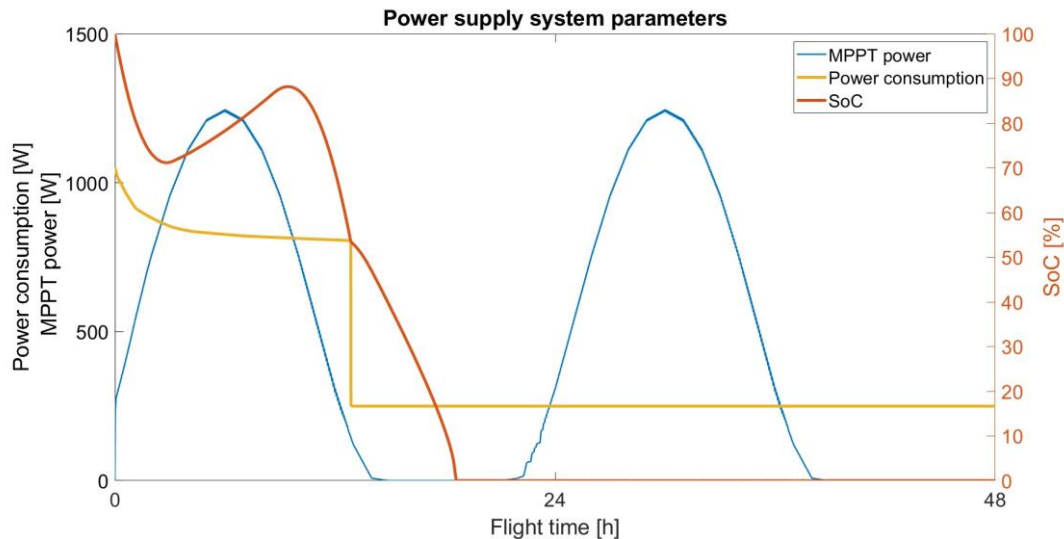


**Figure 7.19.** Twin Stratos 12 20 km scenario in the summer solstice for continuous flight.

Continuous flight at an altitude of 20 km is not possible. This is mainly due to the high energy demand at the very stage of reaching the ceiling of 20,000 meters. For the next stage of flight at a constant altitude, the power supply system consumes more energy than in the case of flight at an altitude of 15 km. This is due to the very low efficiency of the electric motors. The power needed to fly at an altitude of 20 km is small, but the low efficiency means that the actual energy consumption is almost 10 times higher.

The batteries were drained after 17 h and 45 min of flight. Still, in this type of scenario performed, the 20,000 meter altitude buffer should be kept in mind. The summer solstice analysis was conducted to maximize the TS12 achievement. Due to the impossibility of maintaining the flight at such a high altitude within this period, it can be concluded that continuous flight at this altitude in the location of Central Europe is impossible with the preselected assumptions.

Taking into account the flight to the maximum altitude with the possibility to operate the UAV at such a high ceiling, the flight path should be based on gliding no continuous flight.

## 7.2 VTOL

In the case of the previously tested TS UAVs, their design allowed, depending on the scale, to fly at an altitude above 5 km for TS17 and even reaching 20 km for TS12. For VTOL, the maximum flight ceiling was 4 km. The presented results will take into account two scenarios presented in subchapter 6.1.3 and their presentation will take into account the flight without PV at the vernal equinox and summer solstice. The first scenario involved a flight to an altitude of 1 km, and then a cruise flight at this altitude (Figure 7.20).

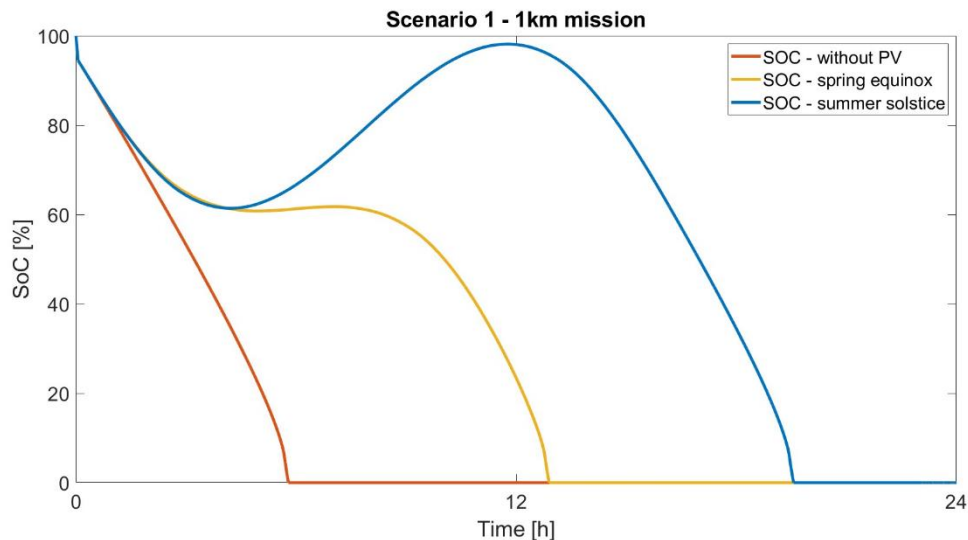


**Figure 7.20.** State of charge of the battery during the continuous flight at 1 km.

The analysis of the above characteristics shows a strong load on the power supply system in the initial phase of the vertical take-off and climb to a height of 1 km. Due to the short duration of this stage of the flight (reaching the ceiling of 1 km takes only 6 minutes), the batteries were discharged to 95%. This was followed by a gradually constant value of current discharge during the flight at a predetermined altitude of 1,000 meters. Analyzing the SOC charts depending on the flight date, it can be preliminarily concluded that the flight at the spring equinox extends the flight by 100%, and at the summer solstice twice.

In the case of the flight at the spring equinox, the PV system allowed to maintain the SOC on an equal level around noon (6 hours of flight), while on the summer solstice, the PV system was able to charge the power supply system to almost 100%. In order to analyze the energy balance, a graph comparing the energy demand and the energy possible to be produced by the PV system was used (Figure 7.21).

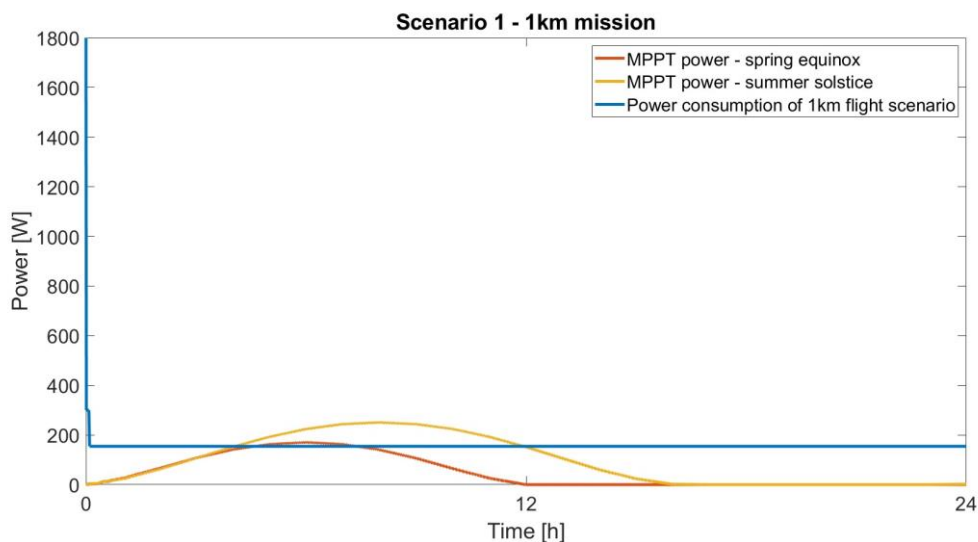


**Figure 7.21.** Power consumption and MPPT power produced by solar cells for the 1st scenario.

During the vernal equinox, a positive energy balance occurs for about 3 hours. However, this value is negligible, which makes it unable to charge the batteries. It can be seen in Figure 7.20. On the summer solstice, the positive energy balance occurs for about

8 hours. Longer irradiation time and greater amplitude than at the vernal equinox mean that the SOC of the battery is able to reach the level of 100%.

Scenario no. 1 for the VTOL was intended to present in the most realistic way an exemplary mission for the use of a tail-sitter. The second scenario was performed to enable the analysis of the maximum VTOL flight (Figure 7.22).

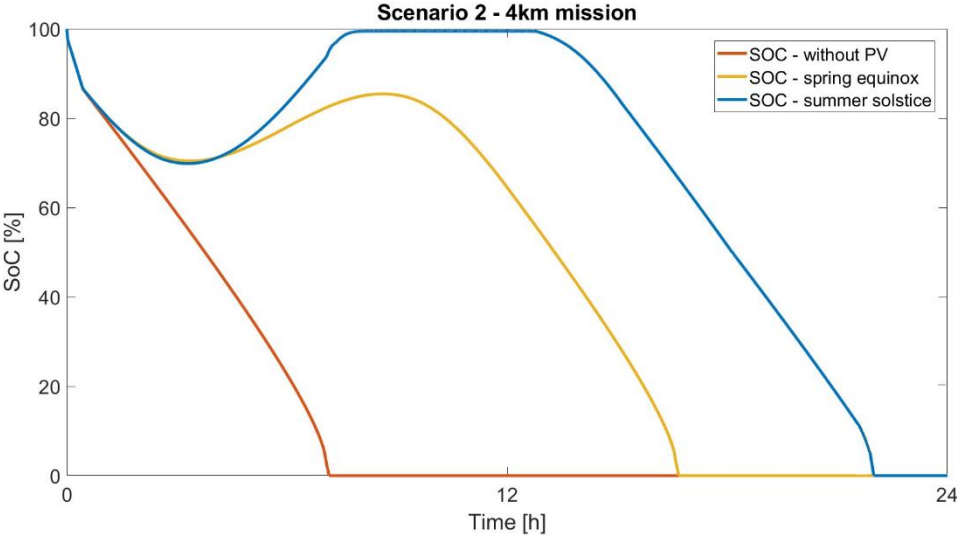


Figure 7.22. State of charge of the battery during the continuous flight at 4 km.

The characteristics of the SOC charts for a 4 km flight are different than in the previous scenario. The initial phase, due to the longer time needed to reach the ceiling of 4,000 meters, causes a greater reduction in the SOC level. Compared to scenario no.1, the graphs without the PV system are the most convergent. The use of solar cells means that both on March 21 and June 21 the flight at an altitude of 4 km lasts longer than at an altitude of 1 km. The lower value of the energy demand allowed to recharge the batteries even at the spring equinox (up to a maximum of 85%). On the summer solstice, the SOC reached 100% and maintained it for about 5 hours until the negative energy balance.

A comparison of the energy demand and the energy produced by the PV system is shown in Figure 7.23.

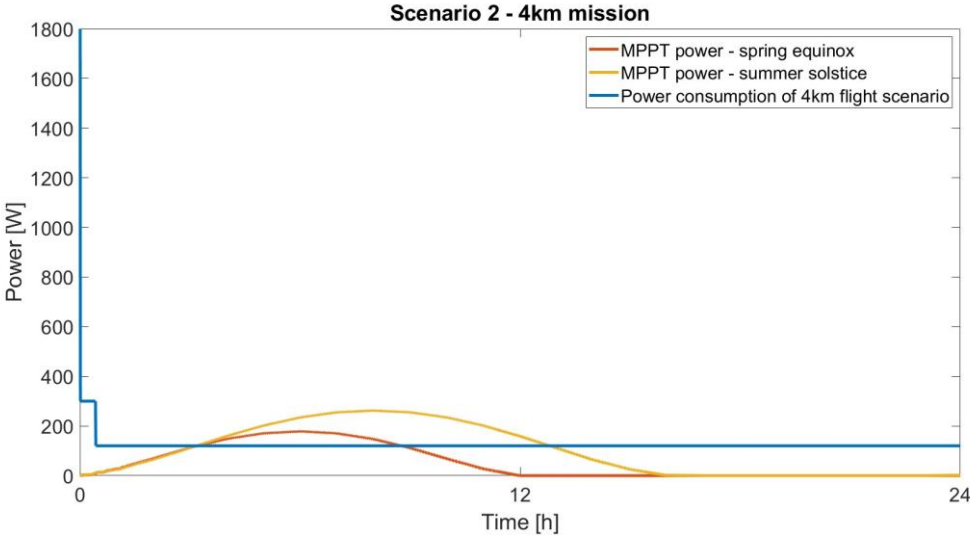


Figure 7.23. Power consumption and MPPT power produced by solar cells for the 2nd scenario.

The difference between Figure 7.20. and Figure 7.22. occurs only in the value of energy demand. Comparing both graphs, it can be seen the periods in which the energy balance is positive and negative. The lower energy consumption at higher altitudes allows to extend the flight time. The exact values for the SOC of 20% and 0% are shown in Table 7.5.

**Table 7.5.** Summary of the performed VTOL scenario simulations.

	<b>Without PV</b>	<b>Vernal equinox</b>	<b>Summer solstice</b>
Daily insolation value (kWh/m <sup>2</sup> )	—	4.02	7.67
Daily energy produced (kWh)	—	1.17	2.24
Time of day duration (hours)	—	12 h 15 min	16 h 25 min
<b>1 km flight</b>			
Flight time to 0% SOC (hours)	5 h 50 min	13 h	19 h 30 min
Flight time to 20% SOC (hours)	5 h 10 min	12 h 15 min	18 h 55 min
<b>4 km flight</b>			
Flight time to 0% SOC (hours)	6 h 25 min	16 h 30 min	22 h
Flight time to 20% SOC (hours)	5 h 30 min	15 h 30 min	21 h

### 7.3 Summary

In the case of the scenarios prepared for TS17, it can be stated that the flight to the height of the set milestone of 5 km is possible to achieve even without the use of solar cells. The flight to the limit altitude of 8 km had to occur not only on the summer solstice, but also during the day when the irradiation value was higher than in the case of the take-off at sunrise.

A 24-hour flight in the case of TS17 is impossible to implement for the planned flight scenarios. Even adding gliding to scenarios no.1 and no.2 will not exceed the flight time to full one day. Perhaps the optimization of the flight path planning will allow for a 24-hour flight, however, if the location of Gliwice is used for the flight, the mission date will most likely have to oscillate around the summer solstice.

A 24-hour flight is no obstacle for the TS12. Its much larger wing area allows for almost 9 times more solar cells to be placed. The battery capacity is 4.5 times greater. In turn, the energy demand in the case of TS12 is 3-4 times higher. This results in a non-linear relationship between energy demand, energy production, and energy storage. Thanks to this, it can be concluded that the larger the scale, the easier it is to achieve energy autonomy when using UAV capabilities allowing for high-altitude flight.

The highest altitude of 20 km is not able to be reached by TS12 at the vernal equinox. The large amount of energy needed to perform this maneuver means that the PV energy must also be high. For this reason, the ability to fly at 20,000 meters is possible on the summer solstice.

On the other hand, flights at an altitude of 10 km and 15 km, whether in accordance with the scenario that includes gliding and successively climbing or performing a cruise

flight at a given altitude, require much less energy input in the initial phase of reaching the given altitude. On the summer solstice, there is not the slightest problem to obtain full energy autonomy. A well-designed flight path planning should allow for flights of more than 48 hours at the spring equinox.

The initially adopted scenario developed for TS12 with climbing and gliding seemed to be the most economical. However, as it turned out after the simulation results, sometimes maintaining the flight at a given altitude is more economical. Energy demand during gliding and climbing is sometimes higher than during an overnight flight at a set one altitude. It is then necessary to obtain favorable conditions for the PV system. As in the scenario, the summer solstice allows to obtain a high energy value, a positive energy balance, and a very short night during which the energy surplus accumulated in the batteries is used.

In the case of VTOL, its completely different characteristics and purpose based on the impact of the PV on UAV flight time. Surprisingly, the planned flight scenarios for the TS17 achieved worse flight endurance than the VTOL, which is not intended for such missions. The reason for this result is twice the number of solar cells and a 50% larger battery. Greater ability to produce and store energy means that the VTOL losses compared to the TS17 resulting from the greater energy demand were leveled. The difference may also lie in the less thoroughly tested VTOL model. While aviation engineers worked on the TS17 and TS12 models for a very long time due to its implementation stages, the tail-sitter model is a conceptual model at an early stage of idea development.

For TS17 and TS12, each scenario was considered within 48 hours. It can be seen in some graphs that on the second day there is a situation when the SOC rises from 0% after the previous discharge. This is due to the positive energy balance. The simulation was carried out in such a way that it does not turn off when the SOC reaches a certain preset level. In addition, due to the undefined UAV in space, the simulation additionally does not know where the UAV is located. For a more accurate flight path planning, constraints and inputs should be added, which have been omitted at this stage due to their minor importance.

### *7.3.1 Cloudiness*

On the example of the TS17 flight, according to scenario no. 1 (flight to the altitude of 5 km) and scenario no. 1 for VTOL (flight to the altitude of 1 km), it was decided to check how cloud cover will affect the flight time. In the case of TS12 and flights at higher altitudes, cloud cover will not play such a big role. June 21 was selected as the time.

Figure 7.24 shows the characteristics of the TS17 SOC depending on the cloud cover. The solar limiting values are taken from subchapter 3.2.1.

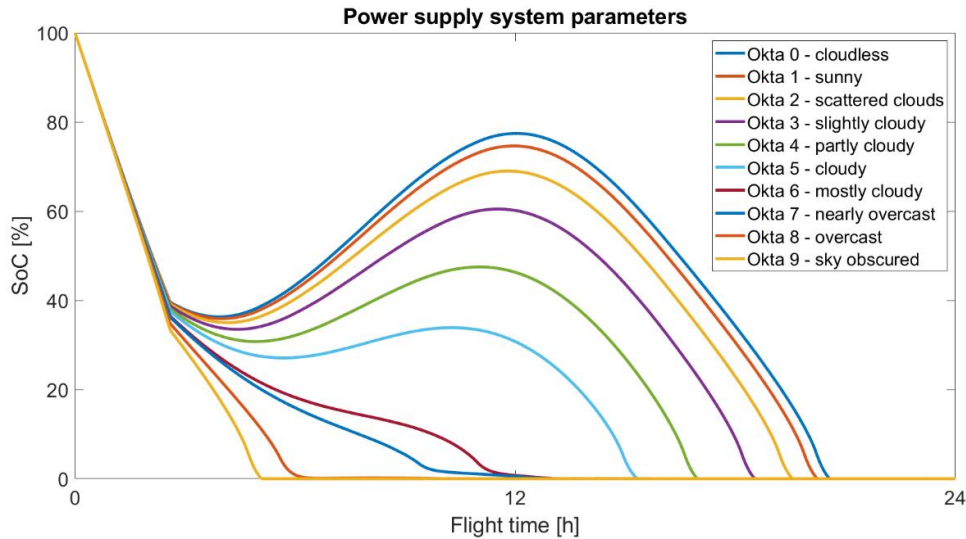


**Figure 7.24.** Twin Stratos 17.5 km scenario in the summer solstice with cloudiness level included.

By analyzing the graph, it can be observed that in the case of a flight on the summer solstice, the PV system is able to obtain a positive energy balance even in a cloudy sky (up to okta 5) — visible increase in SOC level. With the occurrence of greater cloudiness, the energy balance deteriorates significantly. This results in a lack of positive energy balance and faster discharge of the battery.

Regardless of the scenario developed for TS17, taking cloud cover into account for the entire duration of the mission, the results will be comparable. In order to understand the effect of cloud cover on the VTOL, a similar simulation was developed for the tail-sitter (Figure 7.25).

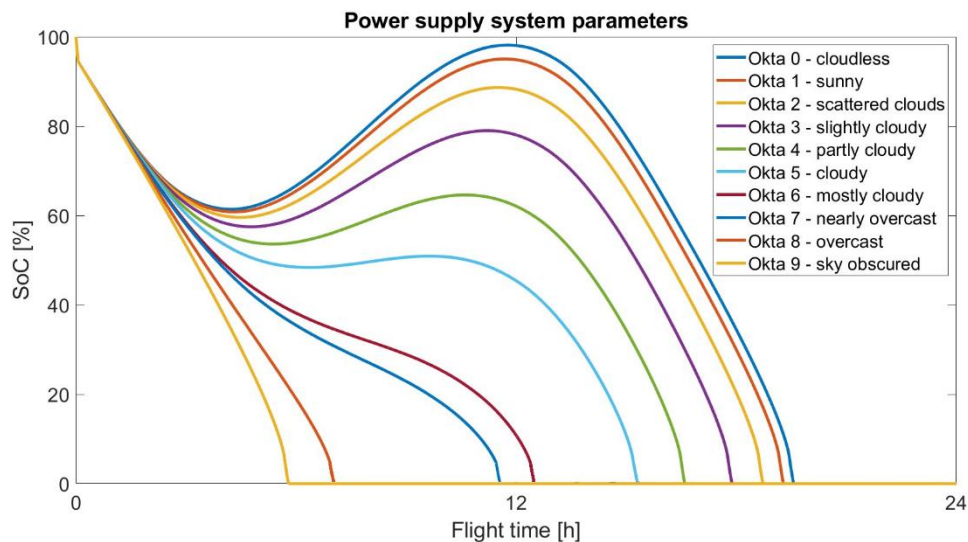


**Figure 7.25.** VTOL 1 km scenario in the summer solstice with cloudiness level included.

By analyzing the characteristics of the SOC for VTOL, it can be seen that the range from okta 0 to okta 5 allows to obtain a periodically positive energy balance similarly to TS17. Other characteristics are not able to achieve a positive energy balance that can be noticed by continuous SOC drop.

Comparing graphs 7.24 and 7.25, there is a similarity in flight endurance capabilities and the ability to recharge the battery. Both UAVs can recharge batteries up to 5 okta cloudiness. VTOL, despite its greater battery capacity than TS17, it is able to

charge the batteries to a greater extent than TS17. The reason is twice the number of solar cells on the drone surface.

VTOL, due to the large area of the wings and the constant cooperation between the people responsible for the construction and the power supply system, allowed to develop a certain consensus. In the case of TS17, where the structure was rigidly defined and changes could not be made, the only option was to use what the UAV offers. However, the maximum occupancy with PV panels did not allow for energy autonomy. It can be said that the error in the case of TS17 was created at the very beginning of the design process. The wing chord allowed for the placement of 2.5 pcs of photovoltaic cells. Changing the wing profile could allow for placing, e.g., 3 pcs. Similarly in the case of winglets, whose shape does not match the number and shape of solar cells at all.

The simulations were carried out and the obtained results allow to conclude that the 24-hour flight, which was included as one of the milestones, is impossible to achieve in the TS17 configuration that was presented. An alternative to the TS17 achieving a 24 hour flight milestone is an optimized flight planning path and maximizing battery capacity and thus weight (there will be no additional payload) for the milestone flight. The second guideline is to obtain the best possible flight conditions regarding weather conditions, the length of the day, and thus the flight around the summer solstice.

Table 7.6 presents the results concerning the ratio of the energy produced by the PV system of each UAV to the capacity of the battery.

**Table 7.6.** Relation between solar power and battery capacity.

	<b>TS17</b>	<b>TS12</b>	<b>VTOL</b>
Solar cells (pcs.)	40	350	80
Battery cells (pcs.)	48	216	72
Solar cells energy produced — March 21 (kWh)	0.59	5.13	1.17
Solar cells energy produced — June 21 (kWh)	1.12	9.8	2.24
Battery capacity (kWh)	0.605	2.722	0.907
Ratio — March 2	0.98	1.88	1.29
Ratio — June 21	1.85	3.6	2.47

In addition to determining the battery capacity and the power of the PV panels, it is also important to ensure the right proportion between the two systems. A different proportion may occur between different vehicle designs and between different classes of objects, e.g., HALE, LALE.

It can be seen that for the LALE UAV, the proportion between the energy from PV to battery capacity at the summer solstice is comparable to the HALE UAV ratio at the vernal equinox. The differences resulting from the difference in ceilings, vehicle scale, and energy demand, cause that the TS17 is not able to fly more than 24 hours even on June 21, while TS12 is able to fly more than 24 hours even in March.

In addition, in the LALE UAV, weather conditions have a much greater impact, which ultimately should also be taken into account. They limit the energy that can be produced by the PV system.

The LALE scale, i.e., TS17, can be compared with VTOL. A comparable maximum flight ceiling and similar restrictions on weather conditions allow to observe some kind of similarity, e.g., in the ratio of power from the PV system to the capacity of the batteries. In this case, a ratio of about 2.5:1 should allow LALE class objects to fly for more than 24 hours.

The greater the ratio between the energy produced and the capacity of energy storage, the greater the probability of obtaining a long-endurance flight and energy autonomy for some good weather conditions. This is also directly related to the correct selection of the battery, which takes into account not only the weight, but also the ability to use the charging capacity to the maximum SOC level.

# 8. Verification

## 8.1 Twin Stratos 17 Prototype

The developed simulations and their results made it possible to initially determine in what conditions and with what parameters UAVs are able to extend the flight time and even achieve full energy autonomy. The simulation idealizes the results, so it was necessary to perform measurements on real systems.

To check how the designed power supply system will work in the target environment, a verification was carried out gradually. During the entire work of this doctoral dissertation, the TS17 was partially designed and manufactured as a prototype for verification tests of some systems, including the power supply system and the photovoltaic system (Figure 8.1 and Figure 8.2).



**Figure 8.1.** TS17 front view.



**Figure 8.2.** TS17 rear view.

Due to the early stage of work, it was impossible to perform the first flight of TS17. The entire verification process had to be stationary on the test stands and the assembled UAV.

The verification stage was divided into 4 parts:

- BMS verification;
- Battery verification;
- MPPT system verification;
- Verification of solar cells.

### 8.1.1 Batteries and Battery Management System

Work related to the BMS was also directly coupled to the operation of the batteries. The works included:

- Recognizing and checking the physical connections of BMS with the battery pack (Figure 8.3a);
- Connecting BMS to a PC using the UART-USB adapter and checking the configuration in the BMS programming application;
- Activating the "Ignition" input, enabling hardware wake-up of the BMS from the sleep state (low power consumption); BMS reset;
- Connecting UART-CAN adapters and checking CAN communication in "Idle" state;
- Loading the battery with a 6.3 ohm resistor and checking CAN communication in the active state during discharging (current approx. 2A);
- Connecting the CV/CC (Constant Voltage/Constant Current) power supply and checking CAN communication in the active state during charging (3A current). Communication tests were carried out for both BMSs using the PCAN-USB adapter and the PCAN-View program. The work consisted in reading the basic values, showing the condition of the battery modules and BMSs: voltage, current, temperature, status.

Figure 8.3a presents a BMS (Enepaq TinyBMS v2.1) when Figure 8.3b shows a flexible battery module placed in styrodur foam. Next to the module, there is a heating foil, which, if necessary, will heat the chamber in which the batteries will be located.

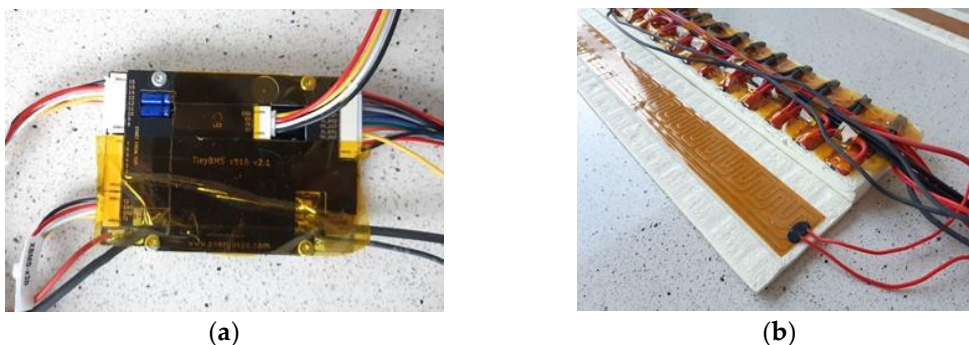


**Figure 8.3.** Power supply system elements: (a) BMS; (b) Battery cells in the thermal insulation cover.

The works with the BMS and batteries were carried out correctly, thanks to which it was possible to continue the work related to the study of the next system — MPPT.

### 8.1.2 MPPT

Obtaining a constant irradiation value of sunlight was impossible in the real environment. For this purpose, to verify the correct operation of the MPPT converter, its inputs were connected to the Itech IT6522C — photovoltaic system simulator. The only difference was

the use of 4 pcs. of LFP battery cells (4S connection) with a capacity of 40 Ah (Figure 8.4). The large capacity of the battery cells allowed for longer work and extended the time needed to charge the battery. It also allowed to check the MPPT system for a longer time.



**Figure 8.4.** MPPT on the test stand.

The input data to the simulator came from the current-voltage characteristics shown in Figure 6.11. Additionally, they covered the range of  $250 \text{ W/m}^2$ ,  $500 \text{ W/m}^2$ , and  $750 \text{ W/m}^2$ . In order to present the whole system, these values have been multiplied by the number of solar cells in the power chain.

Initially, it was assumed that two power chains would be on board the TS17 to ensure the redundancy of the power supply system. After connecting the system, the tested MPPT Genasun GV-5 did not work in the full range of voltage and power. The obtained results were unsatisfactory. Sometimes the MPPT wouldn't even start because the voltage was too low. A possible solution to resolve the problem was a decision to combine two power chains into one power chain. The downside of this solution is the lack of system redundancy and power losses resulting from the blockade, which turned out to be the maximum MPPT output power. Another disadvantage of this solution was exceeding the maximum voltage value in the case of well-lit PV panels. The maximum input voltage of the Genasun GV-5 is 27V, while 40 solar cells connected in series can generate up to 29 V of voltage. Well-lit panels generating higher voltage can damage the MPPT system.

For the Genasun GV-5, the maximum output power is approx. 70 watts, while under STC conditions, the laminated PV panels are able to generate 143.56 watts of power. The tests carried out for 4 values of irradiation showed the following results. (Table 8.1).

**Table 8.1.** MPPT output parameters depending on the irradiation value.

<b>Irradiation</b>	<b>Remarks</b>
<b>1000 W/m<sup>2</sup></b>	System did not work at the maximum power point due to excess power (maximum charging current was reached)
<b>750 W/m<sup>2</sup></b>	System did not work at the maximum power point due to excess power (maximum charging current was reached)
<b>500 W/m<sup>2</sup></b>	The inverter did not find the maximum power point exactly, but the charging was carried out with a current close to the maximum
<b>250 W/m<sup>2</sup></b>	The inverter has found the maximum power point

The high value of irradiation occurring in the case of well-lit photovoltaic panels causes that the output current from the PV will be higher than the maximum current that can flow through the MPPT. For the Genasun GV-5, it is 5 amps.

When the MPPT was able to reach the maximum power point, the charging efficiency was 92%. The Genasun MPPT works fine and is sufficient for a SPMS prototype. For commercial use, however, it should be changed due to the non-optimal use of available PV energy. In order to reduce the weight, the MPPT was pulled out of the housing and placed inside the TS17.

### 8.1.3 Photovoltaic Cells

The last verification stage were photovoltaic cells. The connection of adjacent solar cells is done not only by connecting opposite poles, but also using bypass diodes (Figure 8.5).

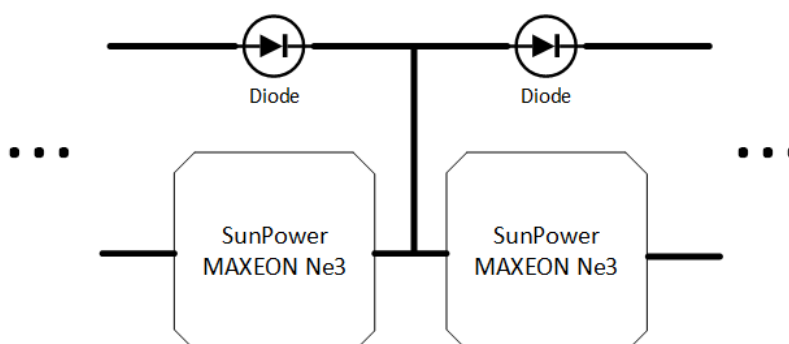


**Figure 8.5.** Connection diagram of solar cells.

Diodes allow to "bypass" solar cells that are, e.g., shaded or damaged. Reversed polarity can occur in shaded solar cells. This can cause that the temperature will be too high due to drawing energy from neighboring solar cells.

In order to check the correct operation of the system, the center wing, wings, and winglets were placed outside for measurements (Figure 8.6).

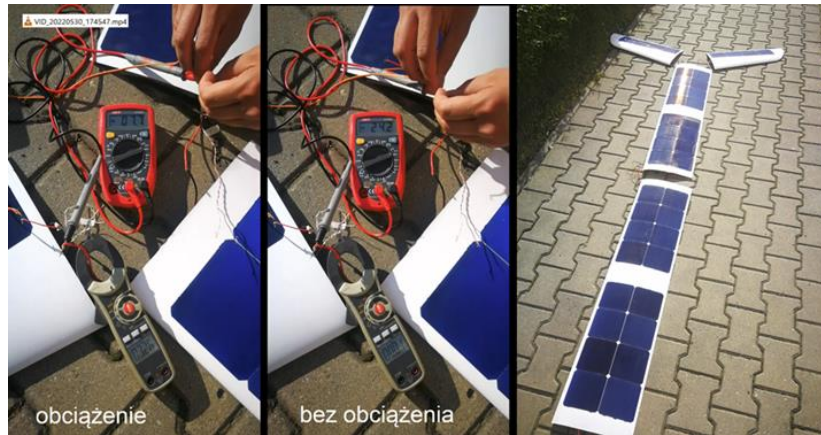


**Figure 8.6.** Solar cells tested outside.

By making a quick short-circuit of the system (apart from the MPPT system), the information was received that the power obtained by the PV panels was 24.2 watts. The obtained power value was compared to the simulation model (Table 8.2).

**Table 8.2.** Parameters of the performed test.

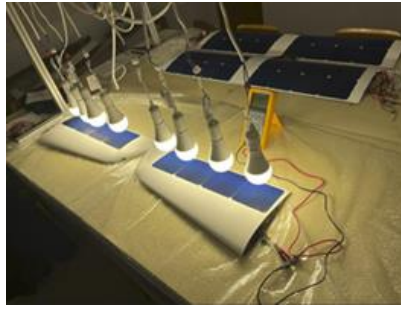
Parameter	Date and Time	Solar cells	Obtained power	Irradiation value
<b>Power test stand</b>	30 May 2022 17.45	40 pcs.	24.2 W	—
<b>Power simulation</b>	30 May 2022 17.45	40 pcs.	32.7 W	225 W/m <sup>2</sup>
<i>Accuracy of simulation results and real system — 74%</i>				

In order to clarify the results, cloudiness had to be taken into account as well. The weather was not sunny, but slightly cloudy. Using data on weather conditions at that time [150], the decrease in the irradiation value under the influence of cloudiness was also taken into account. The decrease in irradiation was set at 12% [118]. Updated results are shown in Table 8.3.

**Table 8.3.** Parameters of the performed test.

Parameter	Date and Time	Solar cells	Obtained power	Irradiation value
<b>Power test stand</b>	30 May 2022 17.45	40 pcs.	24.2 W	—
<b>Power simulation</b>	30 May 2022 17.45	40 pcs.	28.8 W	198 W/m <sup>2</sup>
<i>Accuracy of simulation results and real system — 84%</i>				

The accuracy of the results at the level of 84% was not the highest. It was decided to test each solar cell separately (Figure 8.7b) in order to verify that all solar cells have the correct electrical parameters. Artificial LED lighting was used for this purpose (Figure 8.7a).



(a)



(b)

**Figure 8.7.** Verification tests on the test stands: (a) Irradiation of the solar cells placed in the winglets with 200 watts led bulbs; (b) Single solar cell test.

The aim of the research was to check whether a single solar cell was not damaged during installation on the surface of the wings. The voltage of a well-lit solar cell should be around 0.5-0.6 volts. It was noticed that 3 out of 40 photovoltaic cells have worse parameters. The voltage of these solar cells oscillated around 0.2 volts.

After a more thorough verification, small cracks were noticed on the surface of the solar cells, which could have been caused by stresses (Figure 8.8).



**Figure 8.8.** Damaged solar cell on the wing surface.

After noticing irregularities in the operation of the photovoltaic system, a new simulation was carried out, which included not 40, but 37 solar cells. Damaged solar cells caused deterioration of the parameters of the solar chain, and also falsified the result of the correctness of calculations from the simulation with real results. Further results are presented in Table 8.4.

**Table 8.4.** Parameters of the performed test.

Parameter	Date and Time	Solar cells	Obtained power	Irradiation value
<b>Power test stand</b>	30 May 2022 17.45	40 pcs.	24.2 W	—
<b>Power simulation</b>	30 May 2022 17.45	37 pcs.	26.6 W	198 W/m <sup>2</sup>
<i>Accuracy of simulation results and real system — 91%</i>				

Three defective solar cells were replaced. After another check of the operation of the TS17 system and correct results for each of the 40 pcs. of photovoltaic cells, the UAV was glued. At this stage of work it was not clear what was the real value of the irradiation. The last tests were planned before the first test flight of the TS17. In this tests, it was also planned to verify the real irradiation value by a solar light meter.

## 8.2 System Check Before First Flight

Based on previous experience, UAV was prepared for the first flight. Taking into account the limitations of the MPPT system, it was decided to abandon the connection of solar cells located on the winglets. Too high voltage resulting from the serial connection of photovoltaic cells could damage the MPPT system, especially during the summer period.

TS17 will be able to use 32 solar cells out of 40 located on the drone's surface. This way, the MPPT input voltage value will not exceed the maximum voltage.

The system was prepared and checked on June 2, 2023 (Figure 8.9) between 10.00 - 12.00 astronomical time (summer time in Poland is then 11.00 - 13.00).



**Figure 8.9.** Tests before the first flight.

The previous part of the chapter focused on verifying the operation of individual subsystems. The installation of the entire system on board the UAV allowed for further tests to be carried out to verify the correct operation of the entire system.

Using an solar light meter (Votcraft PL-110SM), a multimeter, a clamp meter, and BMS software, the electrical values of the system were checked. During the research, there were unstable weather conditions with numerous clouds. This made it possible to observe the first change, i.e., fluctuations in the power values of the MPPT system.

Another test verified the correct operation of the system consisted in setting the angle of wings surface to the sun rays by tilting the UAV. The range was  $-30^{\circ}$  to  $30^{\circ}$ , which is much higher than during a standard flight. The difference in the results oscillated around 25% between the value of the horizontally located wing and the angled wing. The wings were located perpendicular to the south direction — the plane of symmetry of the wings was in a straight line to the south direction.

The data collected during the tests are presented in Table 8.5. They take into account both the values from the real system and the simulation system. The table includes the results of measurements during a cloudless sky.

**Table 8.5.** Final compare in sunny weather.

<b>Parameter</b>	<b>Date and Time</b>	<b>Solar cells</b>	<b>Irradiation value</b>	<b>Obtained power</b>
<b>TS17</b>	2 June 2023 10:30	32 pcs.	918 W/m <sup>2</sup>	71.5 W
<b>Simulation</b>	2 June 2023 10:30	32 pcs.	775 W/m <sup>2</sup>	89.3 W
<b>TS17</b>	2 June 2023 11:00	32 pcs.	945 W/m <sup>2</sup>	70.4 W
<b>Simulation</b>	2 June 2023 11:00	32 pcs.	809 W/m <sup>2</sup>	93 W
<b>TS17</b>	2 June 2023 11:30	32 pcs.	1045 W/m <sup>2</sup>	70.5 W
<b>Simulation</b>	2 June 2023 11:30	32 pcs.	820 W/m <sup>2</sup>	93.7 W

By analyzing the results from Table 8.5, it can be noticed a significant discrepancies in the comparison of the irradiation value for the real system and the simulation system. In the case of a cloudless sky, these values were even 200 W/m<sup>2</sup> higher than those obtained from analytical calculations. It may be necessary to calibrate the solar light meter.

The obtained energy values are correct. The output power from the MPPT system was equal to the maximum power that can be output from the system. The maximum charging current was also achieved by the system during irradiation in good conditions, i.e., in the case of a cloudless sky.

It was decided to wait for worse weather conditions, when the clouds will cause deterioration of the irradiation value. Table 8.6 presents the results during a cloudy sky and compare them with the results of the simulation system.

**Table 8.6.** Final compare during cloudy sky.

<b>Parameter</b>	<b>Date and Time</b>	<b>Solar cells</b>	<b>Irradiation value</b>	<b>Obtained power</b>
<b>TS17</b>	2 June 2023 11:10	32 pcs.	227 W/m <sup>2</sup>	11.6 W
<b>Simulation</b>	2 June 2023 11:10	32 pcs.	227 W/m <sup>2</sup>	24.6 W
<b>TS17</b>	2 June 2023 11:10	32 pcs.	457 W/m <sup>2</sup>	31.6 W
<b>Simulation</b>	2 June 2023 11:10	32 pcs.	457 W/m <sup>2</sup>	51 W
<b>TS17</b>	2 June 2023 11:08	32 pcs.	649 W/m <sup>2</sup>	45 W
<b>Simulation</b>	2 June 2023 11:08	32 pcs.	649 W/m <sup>2</sup>	74 W

Changes both in the sky and in the measurement systems occurred dynamically. The irradiation values that were included in the simulation came from the solar light meter. In this case, the value of the obtained power was significantly different between

simulation and real results. The value of the output power in the simulation was even twice as high as in the case of the real system. The lower the irradiation value, the greater the difference between the simulation result and the real system.

After this test, it was decided that the solar light meter should be calibrated on the test stand as shown in Figure 6.4a. When the irradiation values exceeded  $1000 \text{ W/m}^2$ , it already seemed that the meter showed imprecise measurements. Such a value is very rare in Poland, especially in the Upper Silesian agglomeration and almost 3 weeks before the summer solstice. Another argument showing false measurement results is obtaining such a value with a slightly cloudy sky. During the period of a cloudless sky between successive clouds, such a value was obtained. In addition, such a result was obtained about 30 minutes before noon, when the value of irradiation will increase even more.

Therefore, it is impossible to say with certainty what the exact irradiation was. Before further measurements, the solar light meter should be carefully verified to determine if the values it shows are accurate to the real one.

It can be assumed that the obtained results allow to present similar conclusions for different ranges of irradiation as in Table 8.1. For high irradiation values, which cause the MPPT input power to exceed its range, the MPPT works with the maximum output current, guaranteeing a maximum output power of approx. 70 watts. Then, the system does not find the maximum power point. This point is achievable in poor sunlight, which does not exceed the maximum output power of the MPPT.

The test also made it possible to check the operation of the batteries, which were charged with the current depending on the irradiation of the PV panels during the tests. It ranged from 1 amp to 5 amps. SOC level increased from 50% to 70%. Verification of the operation of the thermistors and master systems allowed to confirm the correct operation of the entire power supply system.

## 9. Summary

The doctoral dissertation concerns the development of a method of increasing the flight endurance of VTOL. The limited energy resources of drones related to the minimization of weight and space meant that a solution had to be sought in an external energy source. Photovoltaic cells were chosen as the energy source. The developed method took into account both energy production, energy storage, and UAV energy demand.

Parallel to the activities related to the work on the doctoral dissertation, the LEADER project was carried out. The purpose and subject of the LEADER were consistent with the issues of this doctoral thesis. Thanks to the possibility of verifying the developed method on a real object, the doctoral dissertation included not only VTOL, but also two other fixed-wing UAVs — Twin Stratos.

At the stage of writing this doctoral dissertation, the first test flights of the TS17 were not performed. For this reason, only the statically tested system allowed to obtain verification data. Only the TS17 flight with the planned flight path will allow for a more accurate verification of the systems on board the prototype, including the propulsion system and the operation of the batteries during flight.

### 9.1 Conclusions

The research results presented in this doctoral dissertation confirm the validity of the thesis adopted in the work. It has been confirmed that the method based on Model-Based Design (MBD) modeling allows to design a VTOL UAV with a significantly increased flight endurance.

During the work on the doctoral dissertation, conclusions were drawn gradually and concerned the simulation, laboratory, and workshop environment. Table 9.1 lists the most important elements of the SPMS with their parameters.

**Table 9.1.** Summary of the most important power supply system parameters.

	<b>TS17</b>	<b>TS12</b>	<b>VTOL</b>
Solar cells model		SunPower Maxeon Ne3	
Solar cells (pcs.)	40	350	80
Battery cells model		Samsung INR18650-35E	
Battery cells (pcs.)	48	216	72
Battery configuration	4S12P	12S18P	12S6P
Solar cells connection	20S2P (changed to 40S1P)	70S5P	40S2P
Film lamination		PVC 100 $\mu$ m	
MPPT converter	Genasun GV-5 (changed to Genasun GV-10)	Genasun GVB-8	Genasun GVB-8

Research conducted during the doctoral thesis led to numerous conclusions. It was decided to group them in order to improve their clarity.

**General conclusions regarding UAVs:**

- The larger scale of UAV, the easier possibility to achieve a positive energy balance and full energy autonomy;
- For the tested UAVs, the proportion of energy consumption and its production by PV panels located on the wings is not proportional — as the scale increases, the ratio is in favor of energy production;
- The analysis of graphs for TS17, TS12, and VTOL allows to observe how much is the impact of the energy possible to produce on SOC. It is important to ensure the largest possible surface of the wings, while minimizing the weight by using modern, ultra-light composite materials, using energy-efficient drives and high-performance batteries;
- The impact of weather conditions is much more significant in the case of LALE UAVs and VTOLs than in the case of HALE class UAVs. An accurate forecast of weather is necessary to know the exact value of energy produced by PV panels, calculate the energy balance and SOC level;
- Flying at high altitudes allows to minimize the energy consumption of the propulsion system. Cruise flight should be performed at the highest altitudes due to the lower energy demand of UAV propulsion systems, however, it should be verified in terms of electric motors' power and efficiency. On the example of the TS12 analysis, it can be observed that not always a flight at a higher altitude will turn out to be more energy-efficient. The efficiency of the electric motors should also be taken into account. It can increase the energy consumption when the load on the drive system is lower;
- When the objective of a flight mission is to fly continuously for 24 hours a day, it is important to carefully develop the flight scenario. It is a waste to fly at low altitudes with a fully charged battery on a sunny summer day. The high positive energy balance should be used, e.g., to climb UAV to a higher altitude;
- On 24-hour flights, it is best to take-off at sunrise. Take-off and climb are the stages that consume the most energy, so it is good to compensate high energy consumption with energy produced from the photovoltaic system;
- One way to achieve the 24 hours flight is a continuous, gradual increase in altitude during the day and keeping the altitude as high as possible until sunset or even more depending on the type of mission. Commencement of the UAV gliding stage at sunset or supporting a specific altitude in such a way as to complete the stage of gliding to a given altitude at sunrise or later depending on the type of mission;
- Depending on the capabilities of the UAV, the duration of the flight and favorable weather conditions, a continuous flight at night at one constant altitude may be a better solution. Continuous discharge of the batteries may prove to be energy-efficient than no energy consumption by electric motors during gliding and increased energy value during climbing;
- In the case of UAVs, energy can be stored in two ways: batteries and/or altitude. The potential energy accumulated in the form of height should be used as a time buffer, which is best used at night when the photovoltaic system does not produce energy and the drive system does not consume energy from the power supply system;

- Reaching the milestone of the highest flight altitude may not always be achieved. The best way seems to be calculate the time needed to reach the maximum altitude and then define the start time in such a way that at noon the UAV is halfway the mission to reach a given altitude (not flight altitude but flight time). The flight time defined in this way will allow the PV system to produce more energy than when UAV is taking-off at sunrise;
- When it is not possible to obtain long-endurance flight for the UAV, it may be necessary to change the flight duration, location, time of flight, or flight path;
- If it is not possible to obtain flight long-endurance for key set parameters, it may be necessary to change the design of the UAV, the number of solar cells, the capacity of the battery, or the weight of the payload;
- Additionally, it should be noted that the mission type can change the power consumption, especially at unexpected moments, which will cause the need to climb;
- To accurately plan UAV flight scenario, it should be used an optimization tool that will be able to constantly compare the values of PV energy, battery energy, and energy demand along with the predicted changes in weather conditions (wind, cloudiness).

#### **Solar cells:**

- Parameters of the SunPower Maxeon Ne3 solar cell covered with 100 $\mu$ m thick PVC film showed a decrease in efficiency of approx. 4% compared to the non-laminated solar cell;
- The efficiency reported by the manufacturer is >24.34%. During the tests, an average efficiency value of 24.29% was obtained for the non-laminated photovoltaic cells and 23.33% for the laminated solar cells;
- The 100 micron thick PVC film used in the lamination process showed high transmission and reflection properties as well as a low absorption value;
- The constant value of the above properties in the entire range of visible light allows to conclude that regardless of the lighting conditions, the ratio of efficiency of the non-laminated and laminated photovoltaic cells will be constant;
- Lamination of solar cells with a thin film provide not only protection from dirt, dust, and moisture but also enhancement the PV cells what allow for a greater extent to bending and forces acting;
- No microcracks were observed in the laminated photovoltaic cell, therefore the loss in efficiency is related only with the laminating foil and the thickness of this material;
- The cracks in the photovoltaic cell noticed on the surface of the UAV wings during the verification phase most likely result from poor preparation of the substrate for glued PV panels. Stresses and surface unevenness resulted in cracking of the solar cells and deterioration of the energy parameters of the PV power chain.

#### **Batteries:**

- The correctness of the research on Samsung INR 18650-35E battery cells has been verified, among others, by comparing the obtained characteristics with the pre-used characteristics of the reviewed batteries to which the reference was made;
- Tuned characteristics were introduced into the simulation model in order to reflect the response of the power supply system as realistically as possible;

- Tuning the simulation model to one specific characteristic allowed for a significant simplification of the model. The verification of this simplification will be tested during the first flight of TS17;
- The exact operating conditions, energy demand, possibility of the battery charging, and the frequency of switching on the battery heater will be known only after the start of test flights. Depending on the ambient temperature, the flight scenario, and the given stage of the mission, the value of energy consumed from the batteries will change.

#### **MPPT:**

- Following an MPPT mismatch, due to an incorrect input voltage range, it was necessary to reconfigure the PV power chain. The two chains which were envisaged had to be integrated into one system. The used MPPT had numerous limitations related to the power of the used PV panels. Due to the fact that this error was detected during the tests preceding the assembly of the UAV wings, it was impossible to use a different MPPT system due to its too large size. The larger MPPT could not fit inside the UAV wings. It caused that TS17 was able to use not 40 pcs. but only 32 pcs. of solar cells. An alternative is making a pocket in the lower part of the wing, enabling the use of MPPT with larger dimensions;
- It can be assumed that the MPPT dedicated to a specific application will achieve higher efficiency and better output power results. In the case of the prototype, the commercial solution verified the correct operation of the system, but it is not an optimal solution. Perhaps, the use of Genasun GV-10 will allow for better performance.

#### **Irradiation:**

- The solar light meter most likely showed false irradiation values. These values not only did not agree with the numerical calculations, but also exceeded the maximum irradiation values found in the studied location. In order to obtain precise results, the meter should be calibrated under a Standard Test Conditions just like the solar cells were tested;
- The use of a solar light meter made it possible to observe dynamic changes in the intensity of sunlight. On the day the research was conducted, there was a wide range of several types of cloud cover. The meter showed values from about 200 W/m<sup>2</sup> to 1050 W/m<sup>2</sup>. Even assuming the imprecision of the meter, it could be observed the frequency and range of changes in the irradiation value, which entails the value of the energy produced by the PV system.

The developed conclusions allow to conclude that during the work related to the development of the methodology aimed at extending the UAV flight, not only the concept and simulation model are important, but also the measuring equipment, used materials, hardware capabilities, and manufacturing technology.

The conclusions that resulted from the conducted work allowed to notice important issues that can or even should be applied in other versions of the UAVs. The research allowed to notice the similarity between fixed-wing UAVs of different classes, such as LALE, HALE, VTOL tail-sitter. Despite the differences in the method of achieving the intended ceiling, maximum flight altitude, cruising and climbing speeds, and differences in the flight path angle, the same methodology and method of operation to achieve a positive energy balance remains the same for each tested drone.

## 9.2 Future Works

Most of the information will be available during the first TS17 flight. Only a flight in real conditions, implementing a specific scenario, will be able to know the values of energy demand, the value of energy produced by the photovoltaic system, and verify these data with the simulation results.

In future works directly related to the simulation model and the UAV TS17, the following issues are planned to be addressed:

- Does the curvature of the wings matter? What is the difference in simplifying the model to a flat and not a curved surface?
- Does the angle of the winglets significantly affect the value of the energy produced? Is it better to connect it as a separate PV power chain?
- Should solar cells be considered on the empennage?
- Should MPPT be a dedicated solution? Will the change of the Genasun model or other commercial solution will be fine?
- Will it be necessary to change the way the solar cells are laminated? Should EVA film instead of PVC film be considered? How the PVC film will cope with the UAV flights?

Due to the ongoing work in the LEADER project, further work on the UAV model is planned, which will take into account the conclusions, among others, from this doctoral dissertation. The developed simulations, tests, and verification of the systems on board the UAV allowed the development of a new LALE class UAV model. It has been developed to maximize flight endurance towards greater energy autonomy than the TS17. The know-how obtained during this doctoral dissertation allowed for the creation of a new UAV concept, which is based to a greater extent on the number of solar cells and maximizing the use of the wing area.

Obtained, very promising data from the simulation of the VTOL power supply system made it possible to see how important it is to increase the number of photovoltaic cells to the maximum. Therefore, it should be striven to maximize the coverage of the drone with PV panels. The chord and the wingspan should additionally allow for the arrangement of the photovoltaic cells in such a way that it is an integer and not a floating point number. Floating point number is a waste from the energy point of view. At the current stage of the work, the same batteries were used as in all previously tested cases. Possible changes will be introduced after the first TS17 flight. The new UAV model was named Twin Stratos NXG (Figure 9.1).

One of the results of the work of this doctoral dissertation is, among others, registration and full publication of the Registered Community Design (RCD) for both Twin Stratos UAV [151] and Twin Stratos NXG UAV [152]. The technical solutions of presented demonstrator are also protected by two patents (pending). The first application number is P.444450 and is called "Nowa konstrukcja energooszczędnego statku powietrznego zwłaszcza drona wraz z energooszczędnym sterowaniem". The second application number is P.445855 and is called "Nowa konstrukcja wzmocnionego termicznie zasilania zwłaszcza dla bezzałogowych statków powietrznych".

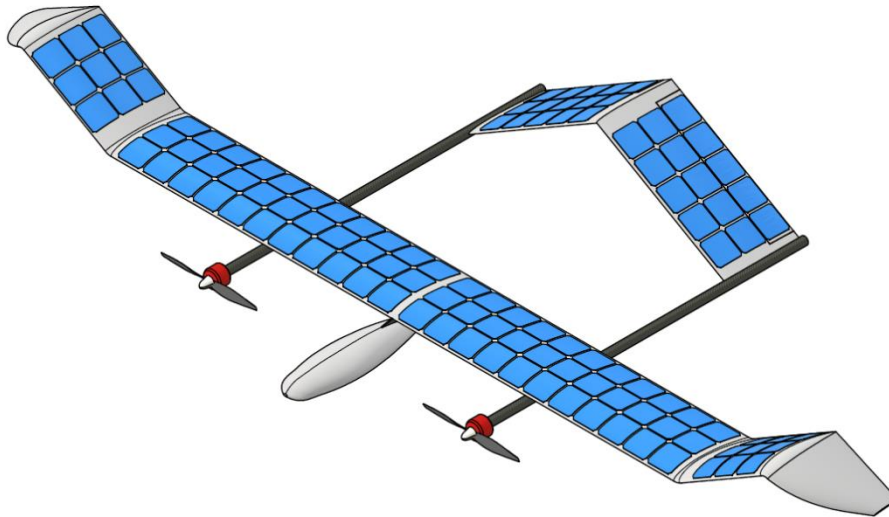


**Figure 9.1.** Twin Stratos NXG [152].

## References

1. East, O.G. *Wright Brothers*, National Park Service Historical Handbook series No. 34, Washington, D.C., 1961.
2. Storm, R.; Benson, T.; Galica, C.; McCredie, P. *Learning to Fly: The Wright Brothers' Adventure*, National Aeronautics and Space Administration, Glenn Research Center, Cleveland, Ohio, 2003.
3. Nex, F.; Armenakis, C.; Cramer, M.; Cucci, D.A.; Gerke, M.; Honkavaara, E.; Kukko, A.; Persello, C.; Skaloud, J. UAV in the advent of the twenties: Where we stand and what is next. *ISPRS J. Photogramm. Remote Sens.* **2022**, *184*, 215–242.
4. 7 Pros and Cons of Drones and Unmanned Aerial Vehicles. Available online: <https://onlinemasters.ohio.edu/blog/the-pros-and-cons-of-unmanned-aerial-vehicles-uavs> (accessed on 15 May 2023).
5. Mohd Noor, N.; Abdullah, A.; Hashim, M. Remote sensing UAV/drones and its applications for urban areas: A review. *IOP Conf. Ser. Earth Environ. Sci.* **2018**, *169*, 012003.
6. Goraj, Z.; Frydrychewicz, A.; Świtkiewicz, R.; Hernik, B.; Gadomski, J.; Goetzendorf, T.; Figat, M.; Suchodolski, St.; Chajec, W. High altitude long endurance unmanned aerial vehicle of a new generation – a design challenge for a low cost, reliable and high performance aircraft, *Bulletin of the Polish Academy of Sciences. Technical Sciences* **2004**, *52*, 3, 173-194.
7. Orgeira-Crespo, P.; Ulloa, C.; Rey-Gonzalez, G.; Pérez García, J.A. Methodology for Indoor Positioning and Landing of an Unmanned Aerial Vehicle in a Smart Manufacturing Plant for Light Part Delivery. *Electronics* **2020**, *9*, 1680.
8. Kosior, M. Model-Based Adaptive Path Planning Algorithm for Unmanned Aerial Vehicles, Ph.D. Thesis, Silesian University of Technology, Faculty of Mechanical Engineering, Department of Fundamentals of Machinery Design, Gliwice, 2022.
9. Li, X.; Yang, L. Design and Implementation of UAV Intelligent Aerial Photography System. In *Proceedings of the 2012 4th International Conference on Intelligent Human-Machine Systems and Cybernetics*, Nanchang, China, 26–27 August 2012; pp. 200–203.
10. Chadwick, S.; Miller, C.R. Military Unmanned Aerial Vehicles and Diversification Opportunities. Mississippi Defense Diversification Initiative. 2018, pp. 1–70. Available online: [https://aquila.usm.edu/fac\\_pubs/16830](https://aquila.usm.edu/fac_pubs/16830) (accessed on 2 November 2022).
11. Doskocz, J.; Kardasz, P.; Hejduk, M.; Wiejcut, P. The possibilities of using drones in the courier services. *World Sci. News* **2016**, *48*, 119–132.
12. Papež, N.; Dallaev, R.; Țălu, Ș.; Kaštyl, J. Overview of the Current State of Gallium Arsenide-Based Solar Cells. *Materials* **2021**, *14*, 3075.

13. Colella, N.; Wenneker, G. Pathfinder: Developing a solar rechargeable aircraft. *IEEE Potentials* **1996**, *15*, 18–23.
14. Oettershagen, P.; Melzer, A.; Mantel, T.; Rudin, K.; Lotz, R.; Siebenmann, D. A Solar-Powered Hand-Launchable UAV for Low-Altitude Multi-Day Continuous Flight. In *Proceedings of the IEEE International Conference on Robotics and Automation (ICRA)*, Seattle, DC, USA, 26–30 May 2015; pp. 3986–3993.
15. Mateja, K.; Skarka, W.; Peciak, M.; Niestrój, R.; Gude, M. Energy Autonomy Simulation Model of Solar Powered UAV. *Energies* **2023**, *16*, 479.
16. Available online: <https://science.howstuffworks.com/satellite10.htm> (accessed on 15 May 2023).
17. Oettershagen, P.; Melzer, A.; Mantel, T.; Rudin, K.; Stastny, T.; Wawrzacz, B.; Hinzmann, T.; Leutenegger, S.; Alexis, K.; Siegwart, R. Design of small hand-launched solar-powered UAVs: From concept study to a multi-day world endurance record flight. *J. Field Robot.* **2017**, *34*, 1352–1377.
18. Solar Impulse. Available online: <https://aroundtheworld.solarimpulse.com/> (accessed on 1 November 2022).
19. Zephyr-UAV-Airbus. Available online: <https://www.airbus.com/defence/uav/zephyr.html> (accessed on 1 November 2022).
20. PHASA-35 First Flight|Newsroom|BAE Systems|International. 2020. Available online: <https://www.baesystems.com/en/article/ground-breaking-solar-powered-unmanned-aircraft-makes-first-flight> (accessed on 1 November 2022).
21. High Altitude, Ultra-Long Endurance, Pseudo-Satellite—HAPS—Odysseus—Aurora Flight Sciences. Available online: <https://www.aurora.aero/odysseus-high-altitude-pseudo-satellite-haps/> (accessed on 1 November 2022).
22. Hale UAV. Available online: <https://www.avinc.com/innovative-solutions/hale-uas> (accessed on 15 May 2023).
23. Cocconi, A. Solong UAV: First solar-powered perpetual flight in history. *AC Propulsion*, 2005. Available online: <https://archive.org/details/ACPropulsionSolongUAV2005> (accessed on 15 May 2023).
24. Drones and HAPS bringing new opportunities closer to the Earth. Available online: <https://parsec-accelerator.eu/insight/drones-and-haps-bringing-new-opportunities-closer-to-the-earth> (accessed on 15 May 2023).
25. Yang, X.; Pei, X. 15—Hybrid system for powering unmanned aerial vehicles: Demonstration and study cases. In *Hybrid Energy Systems Hybrid Technologies for Power Generation*; Elsevier: Amsterdam, The Netherlands, 2022; pp. 439–473.
26. Rahman, Y.A.; Hajibeigy, M.T.; Al-Obaidi, A.S.; Cheah, K.H. Design and Fabrication of Small Vertical-Take-Off-Landing Unmanned Aerial Vehicle. *MATEC Web Conf.* **2018**, *152*, 02023.
27. Peciak, M.; Skarka, W.; Mateja, K.; Gude, M. Impact Analysis of Solar Cells on Vertical Take-Off and Landing (VTOL) Fixed-Wing UAV. *Aerospace* **2023**, *10*, 247.
28. Misra, A.; Jayachandran, S.; Kenche, S.; Katoch, A.; Suresh, A.; Gundabattini, E.; Selvaraj, S.K.; Legesse, A.A. A Review on Vertical Take-Off and Landing (VTOL) Tilt-Rotor and Tilt Wing Unmanned Aerial Vehicles (UAVs). *J. Eng.* **2022**, *2022*, 1803638.

29. SKYX. Available online: <https://skyx.com> (accessed on 18 January 2023).
30. E-flite Convergence. Available online: <https://www.horizonhobby.com/product/convergence-vtol-bnf-basic-650mm/EFL11050.html> (accessed on 18 January 2023).
31. VALAQ Patrol. Available online: <https://www.valaqqpatrol.com> (accessed on 18 January 2023).
32. WingtraOne. Available online: <https://wingtra.com> (accessed on 18 January 2023).
33. ElevationX. Available online: <https://www.elevationx.com> (accessed on 18 January 2023).
34. Types Of Hybrid Fixed-Wing/VTOL UAVs Explained. Available online: <https://www.thecoronawire.com/types-hybrid-fixed-wing-vtol-uavs-explained/> (accessed on 18 January 2023).
35. Mateja, K.; Skarka, W.; Drygała, A. Efficiency Decreases in a Laminated Solar Cell Developed for a UAV. *Materials* **2022**, *15*, 8774.
36. Ali, S.; Tuhin, R.A.; Khan, S.H. Advances in Clean Energy Technologies. Chapter 1 - Sun: The main source of ground energy and power. Elsevier: Amsterdam, The Netherlands, 2021; pp.3-18.
37. Chu, Y.; Ho, C.; Lee, Y.; Li, B. Development of a Solar-Powered Unmanned Aerial Vehicle for Extended Flight Endurance. *Drones* **2021**, *5*, 44.
38. Aktaş A.; Kirçiçek Y. Solar Hybrid Systems: Chapter 13—Examples of Solar Hybrid System Layouts, Design Guidelines, Energy Performance, Economic Concern, and Life Cycle Analyses; Elsevier: San Diego, CA, USA, 2021; pp. 331–349.
39. Kalogirou, S. Solar Energy Engineering: Processes and Systems; Elsevier: Amsterdam, The Netherlands; Academic Press: Burlington, MA, USA, 2009.
40. Qazi, S. Standalone Photovoltaic (PV) Systems for Disaster Relief and Remote Areas: Chapter 7—Solar Thermal Electricity and Solar Insolation; Elsevier: Amsterdam, The Netherlands, 2017; pp. 203–237.
41. Li, K.; Wu, Y.; Bakar, A.; Wang, S.; Li, Y.; Wen, D. Energy System Optimization and Simulation for Low-Altitude Solar-Powered Unmanned Aerial Vehicles. *Aerospace* **2022**, *9*, 331.
42. Zhang, L.; Li, J.; Wu, Y.; Lv, M. Analysis of attitude planning and energy balance of stratospheric airship. *Energy* **2019**, *183*, 1089–1103.
43. Benveniste, G.; Rallo, H.; Canals Casals, L.; Merino, A.; Amante, B. Comparison of the state of Lithium-Sulphur and lithium-ion batteries applied to electromobility. *J. Environ. Manag.* **2018**, *226*, 1–12.
44. Xu, C.; Dai, Q.; Gaines, L.; Hu, M.; Tukker, A.; Steubing B. Future material demand for automotive lithium-based batteries. *Commun Mater* **2020**, *1*, 99.
45. Keshan, H.; Thornburg, J.; Ustun, T.S. Comparison of lead-acid and lithium ion batteries for stationary storage in off-grid energy systems. In Proceedings of the 4th IET Clean Energy and Technology Conference (CEAT 2016), Kuala Lumpur, Malaysia, 14–15 November 2016; Institution of Engineering and Technology (IET): Kuala Lumpur, Malaysia, 2016; pp. 1–7.
46. Miao, Y.; Hynan, P.; von Jouanne, A.; Yokochi, A. Current Li-Ion Battery Technologies in Electric Vehicles and Opportunities for Advancements. *Energies* **2019**, *12*, 1074.
47. Tarascon, J.-M.; Armand, M. Issues and challenges facing rechargeable lithium batteries. *Nature* **2001**, *414*, 359–367.
48. Is Lithium-ion the Ideal Battery? Available online: <https://batteryuniversity.com/article/is-lithium-ion-the-ideal-battery> (accessed on 15 May 2023).

49. Is Li-ion the Solution for the Electric Vehicle? Available online: <https://batteryuniversity.com/article/is-li-ion-the-solution-for-the-electric-vehicle> (accessed on 15 May 2023).
50. Datasheet KOKAM Li-ion/Polymer Cell. Available online: [https://moodle.utc.fr/pluginfile.php/202328/mod\\_resource/content/1/2019\\_Kokam\\_Cell\\_ver\\_4.1-compressed.pdf](https://moodle.utc.fr/pluginfile.php/202328/mod_resource/content/1/2019_Kokam_Cell_ver_4.1-compressed.pdf) (accessed on 15 May 2023).
51. Choi, J.W.; Aurbach, D. Promise and reality of post-Li-ion batteries with high energy densities. *Nat. Rev. Mater.* **2016**, *1*, 16013.
52. Battery cell shapes. Available online: [https://media.springernature.com/full/springer-static/image/art%3A10.1038%2Fnatrevmats.2016.13/MediaObjects/41578\\_2016\\_Article\\_BFnatrevmats201613\\_Fig1\\_HTML.jpg](https://media.springernature.com/full/springer-static/image/art%3A10.1038%2Fnatrevmats.2016.13/MediaObjects/41578_2016_Article_BFnatrevmats201613_Fig1_HTML.jpg) (accessed on 15 May 2023).
53. Soga, T. Nanostructured Materials for Solar Energy Conversion: Chapter 1 - Fundamentals of Solar Cell; Elsevier: Amsterdam, The Netherlands, 2006; pp. 3-43.
54. Solar Photovoltaic Cell Basics. Available online: <https://www.energy.gov/eere/solar/solar-photovoltaic-cell-basics> (accessed on 15 May 2023).
55. Patil, P.; Sangale, S.S.; Kwon, S.-N.; Na, S.-I. Innovative Approaches to Semi-Transparent Perovskite Solar Cells. *Nanomaterials* **2023**, *13*, 1084.
56. Zhao, F.; Lin, J.; Lei, Z.; Yi, Z.; Qin, F.; Zhang, J.; Wu, P. Realization of 18.97% theoretical efficiency of 0.9  $\mu\text{m}$  thick c-Si/ZnO heterojunction ultrathin-film solar cells via surface plasmon resonance enhancement. *Phys. Chem. Chem. Phys.* **2022**, *24*, 4871–4880.
57. Khokhar, M.Q.; Hussain, S.Q.; Chowdhury, S.; Zahid, M.A. High-efficiency hybrid solar cell with a nano-crystalline silicon oxide layer as an electron-selective contact. *Energy Convers. Manag.* **2022**, *252*, 115033.
58. Omazic, A.; Oreski, G.; Halwachs, M.; Eder, G.C.; Hirschl, C.; Neumaier, L.; Pinter, G.; Erceg, M. Relation between degradation of polymeric components in crystalline silicon PV module and climatic conditions: A literature review. *Sol. Energy Mater. Sol. Cells* **2019**, *192*, 123–133.
59. Xue, B.; Li, F.; Song, M.; Shang, X.; Cui, D.; Chu, J.; Dai, S. Crack Extraction for Polycrystalline Solar Panels. *Energies* **2021**, *14*, 374.
60. Kokkos, S.; Morfidis, E. Aerodynamic Design and Analysis of Solar Powered UAV (Unmanned Aerial Vehicle); University of Thessaly: Volos, Greece, 2020.
61. Solar Technology for Drones. Available online: <https://www.unmannedsystemstechnology.com/expo/solar-technology-for-drones/> (accessed on 15 May 2023).
62. Soonmin, H.; Hardani; Nandi, P.; Mwankemwa, B.S.; Malevu, T.D.; Malik, M.I. Overview on Different Types of Solar Cells: An Update. *Appl. Sci.* **2023**, *13*, 2051.
63. Al-Ezzi, A.S.; Ansari, M.N.M. Photovoltaic Solar Cells: A Review. *Appl. Syst. Innov.* **2022**, *5*, 67.
64. Gnida, P.; Amin, M.F.; Pająk, A.K.; Jarzabek, B. Polymers in High-Efficiency Solar Cells: The Latest Reports. *Polymers* **2022**, *14*, 1946.
65. Kayes, B.M.; Zhang, L.; Twist, R.; Ding, I.K.; Higashi, G.S. Flexible thin-film tandem solar cells with >30% efficiency. *IEEE J. Photovolt.* **2014**, *4*, 729–733.
66. GaAs or Si solar cells of the highest efficiency, from leading cell manufacturers. Available online: <https://www.gochermann.com/gaas-or-si-solar-cells/> (accessed on 15 May 2023).
67. Park, S.; Simon, J.; Schulte, K.L.; Ptak, A.J.; Wi, J.S.; Young, D.L.; Oh, J. Germanium-on-Nothing for Epitaxial Liftoff of GaAs Solar Cells. *Joule* **2019**, *3*, 1782–1793.
68. Rahamanab, M.S.; Rahman, M.; Mise, N.; Sikderd, T.; Ichihara, G.; Uddin, K.; Kurasaki, M.; Ichihara, S. Environmental arsenic exposure and its contribution to

- human diseases, toxicity mechanism and management. *Environ. Pollut.* **2021**, 289, 117940.
69. Papež, N.; Škvarenina, L.; Tofel, P.; Sobola, D. Thermal stability of gallium arsenide solar cells. In Proceedings of the SPIE, San Diego, CA, USA, 6–10 August 2017; p. 10603.
  70. Ren, Y.; Zhang, D.; Suo, J.; Cao, Y.; Eickemeyer, F.T.; Vlachopoulos, N.; Zakeeruddin, S.M.; Hagfeldt, A.; Grätzel, M. Hydroxamic Acid PreadSORption Raises Efficiency of Cosensitized Solar Cells. *Nature* **2023**, 613, 60–65.
  71. Siuzdak, K.; Klein, M.; Łapiński, K.; Cenian, A. Barwnikowe ogniwa słoneczne, *Rynek Energii* **2015**, 5, 75-83.
  72. Perovskite solar modules. Available online: <https://sauletech.com/blinds/> (accessed on 15 May 2023).
  73. Patil, P.; Sangale, S.S.; Kwon, S.-N.; Na, S.-I. Innovative Approaches to Semi-Transparent Perovskite Solar Cells. *Nanomaterials* **2023**, 13, 1084.
  74. Learn about a Perovskite: Function, Advantages, Disadvantages, and More. Available online: <https://www.solarsquare.in/blog/perovskite-function> (accessed on 15 May 2023).
  75. Moot, T.; Patel, J. B.; McAndrews, G.; Wolf, E. J.; Morales, D.; Gould, I. E.; Rosales, B. A.; Boyd, C. C.; Wheeler, L. M.; Parilla, P. A.; Johnston, S. W.; Schelhas, L. T.; McGehee, M. D.; Luther, J. M. Temperature Coefficients of Perovskite Photovoltaics for Energy Yield Calculations. *ACS energy letters* **2021**, 6, 5, 2038–2047.
  76. Amorphous silicon. Available online: [https://en.wikipedia.org/wiki/Amorphous\\_silicon](https://en.wikipedia.org/wiki/Amorphous_silicon) (accessed on 15 May 2023).
  77. Thin-film solar panels: what you need to know. Available online: <https://news.energysage.com/types-of-thin-film-solar-panels/> (accessed on 15 May 2023).
  78. Um, H. D.; Hwang, I.; Choi, D.; Seo, K. Flexible crystalline-silicon photovoltaics: light management with surface structures, *Acc. Mater. Res.* **2021**, 2, 9, 701–713.
  79. Kim, S.; Hoang, V.Q.; Bark, C.W. Silicon-Based Technologies for Flexible Photovoltaic (PV) Devices: From Basic Mechanism to Manufacturing Technologies. *Nanomaterials* **2021**, 11, 2944.
  80. Asim, M.; Milano, J.; Khan, H.I.; Hanzla Tahir, M.; Mujtaba, M.A.; Shamsuddin, A.H.; Abdullah, M.; Kalam, M.A. Investigation of Mono-Crystalline Photovoltaic Active Cooling Thermal System for Hot Climate of Pakistan. *Sustainability* **2022**, 14, 10228.
  81. Monocrystalline vs. polycrystalline solar panels: which is the best for you? Available online: <https://news.energysage.com/monocrystalline-vs-polycrystalline-solar/> (accessed on 15 May 2023).
  82. Rokonzaman, M.; Shakeri, M.; Hamid, F.A.; Mishu, M.K.; Pasupuleti, J.; Rahman, K.S.; Tiong, S.K.; Amin, N. IoT-Enabled High Efficiency Smart Solar Charge Controller with Maximum Power Point Tracking—Design, Hardware Implementation and Performance Testing. *Electronics* **2020**, 9, 1267.
  83. Devarakonda, A.K.; Karuppiyah, N.; Selvaraj, T.; Balachandran, P.K.; Shanmugasundaram, R.; Senjyu, T. A Comparative Analysis of Maximum Power Point Techniques for Solar Photovoltaic Systems. *Energies* **2022**, 15, 8776.
  84. García, E.; Quiles, E.; Correcher, A.; Morant, F. Predictive Diagnosis Based on Predictor Symptoms for Isolated Photovoltaic Systems Using MPPT Charge Regulators. *Sensors* **2022**, 22, 7819.
  85. Dittrich, T. Basic characteristics and characterization of solar cells. *Sol. Energy Mater. Sol. Cell* **2018**, 3-43.

86. Introduction of EVA solar cell encapsulation film. Available online: <https://www.osterfilms.com/Introduction-of-EVA-solar-cell-encapsulation-film-n.html> (accessed on 15 May 2023).
87. Liu, Y.; Xu, Z.; Du, H.; Lv, M. Multidisciplinary Optimization of Thermal Insulation Layer for Stratospheric Airship with a Solar Array. *Aerospace* **2022**, *9*, 83.
88. Feister, U.; Cabrol, N.; Häder, D. UV Irradiance Enhancements by Scattering of Solar Radiation from Clouds. *Atmosphere* **2015**, *6*, 1211-1228.
89. Brizon, M. Solar Energy Generation Model for High Altitude Long Endurance Platforms. Master's Thesis, KTH—Royal Institute of Technology, Stockholm, Sweden, 2016.
90. Han, X.T.; Xie, A.Y.; Bi, X.C.; Liu, S.J.; Hu, L.H. Effects of altitude, ambient temperature and solar radiation on fasting heat production in yellow cattle (*Bos taurus*). *Br. J. Nutr.* **2003**, *89*, 399–408.
91. Jiang, S.; Wang, K.; Zhang, H.; Ding, Y.; Yu, Q. Encapsulation of PV Modules Using Ethylene Vinyl Acetate Copolymer as the Encapsulant. *Macromol. React. Eng.* **2015**, *9*, 522–529.
92. Tsach, S.; Ankri, L.; Cohen, M.; Ehrlich, Y.; Goldenberg, T.; Levy, H.; Regev, I.; Vladimirovsky, A.; Weider, A.; Yossef, Z. Sunsailor: Solar Powered UAV. In Proceedings of the 47th Israel Annual Conference on Aerospace Sciences, Tel Aviv, Israel, 21–22 February 2007.
93. AFRL Incorporates Solar Cell Technology into Small Unmanned Aircraft Systems. Available online: <https://www.wpafb.af.mil/News/Article-Display/Article/399512/afri-incorporates-solar-cell-technology-into-small-unmanned-aircraft-systems/> (accessed on 15 June 2022).
94. Oettershagen, P. Solar-Powered Unmanned Aerial Vehicles: Design and Environment-Aware Navigation for Robust Low-Altitude Multi-Day Continuous Flight. Ph.D. Thesis, ETH Zurich, Zurich, Switzerland, 2018.
95. Sousa, J.C. Solar System for a Long Endurance Electric UAV. Master's Thesis, University of Beira Interior, Covilhã, Portuguese, 2015.
96. Energy to Cross Oceans and Continents. Available online: <https://aroundtheworld.solarimpulse.com/adventure> (accessed on 15 June 2022).
97. Polymers Aiding Solar Impulse 2's Round-the-World Adventure. Available online: <https://knowledge.ulprospector.com/4541/polymers-aiding-solar-impulse-2s-round-world-adventure/> (accessed on 15 June 2022).
98. Jacewicz, M.; Żugaj, M.; Głębocki, R.; Bibik, P. Quadrotor Model for Energy Consumption Analysis. *Energies* **2022**, *15*, 7136.
99. Pham, K.L.; Leuchter, J.; Bystricky, R.; Andrie, M.; Pham, N.N.; Pham, V.T. The Study of Electrical Energy Power Supply System for UAVs Based on the Energy Storage Technology. *Aerospace* **2022**, *9*, 500.
100. UML diagrams vs. SysML diagrams. Available online: <https://www.lucidchart.com/blog/uml-diagrams-vs-sysml-diagrams> (accessed on 3 July 2023).
101. Wolny, S., Mazak, A., Carpella, C. et al. Thirteen years of SysML: a systematic mapping study. *Softw Syst Model* **2022**, *19*, 111–169.
102. Herzog, E.; Hallonquist, J.; Naeser, J. 4.5.1 Systems Modeling with SysML - an experience report, INCOSE International Symposium 2012, *22*, 1, 600-611.
103. It's Time to Clean Up Our Model-Based Problem. Available online: <https://www.engineering.com/story/its-time-to-clean-up-our-model-based-problem> (accessed on 3 July 2023).
104. MBSE and SysML. Available online: <https://www.visual-paradigm.com/guide/sysml/mbse-and-sysml/> (accessed on 3 July 2023).

105. Model-Based Design with Simulink. Available online: <https://www.mathworks.com/help/simulink/gs/model-based-design.html> (accessed on 3 July 2023).
106. What is Model-Based Design? Available online: <https://www.synopsys.com/glossary/what-is-model-based-design.html> (accessed on 3 July 2023).
107. Peciak, M.; Skarka, W. Assessment of the Potential of Electric Propulsion for General Aviation Using Model-Based System Engineering (MBSE) Methodology. *Aerospace* **2022**, *9*, 74.
108. Skarka, W. Model-based design and optimization of electric vehicles. In Proceedings of the 25th ISTE International Conference on Transdisciplinary Engineering, Modena, Italy, 3–6 July 2018; pp. 566-575.
109. Skarka, W. Methodology for the optimization of an energy efficient electric vehicle. In Proceedings of the 6th International Conference on Integrity-Reliability-Failure, Lisbon, Portugal, 22–26 July 2018; pp. 415-422.
110. Targosz, M.; Skarka, W.; Przystałka, P. Model-based optimization of velocity strategy for lightweight electric racing cars. *J. Adv. Transp.* **2018**, 2018, 3614025.
111. Mateja, K.; Skarka, W. Towards Energetic Autonomy of UAV. In Proceedings of the 27th ISTE International Conference on Transdisciplinary Engineering, Warsaw, Poland, 1–10 July 2020; pp. 423–432.
112. Góra, K.; Smyczyński, P.; Kujawiński, M.; Granosik, G. Machine Learning in Creating Energy Consumption Model for UAV. *Energies* **2022**, *15*, 6810.
113. Rydh, C.J.; Sandén, B.A. Energy analysis of batteries in photovoltaic systems Part II: Energy return factors and overall battery efficiencies. *Energy Convers. Manag.* **2005**, *46*, 1980–2000.
114. Rydh, C.J.; Sandén, B.A. Energy analysis of batteries in photovoltaic systems. Part I: Performance and energy requirements. *Energy Convers. Manag.* **2005**, *46*, 1957–1979.
115. Duffie, J.A.; Beckman, W.A. *Solar Engineering of Thermal Processes*, 4th ed.; John Wiley & Sons, Inc.: Hoboken, NJ, USA, 2013.
116. Hottel, H.C. A simple model for estimating the transmittance of direct solar radiation through clear atmospheres. *Solar Energy* **1976**, *18*, 129–134.
117. Skala oktantowa. Available online: <https://polarpedia.eu/pl/skala-oktantowa/> (accessed on 15 May 2023).
118. Myers, D.R. *Solar Radiation: Practical Modeling for Renewable Energy Applications*; CRC Press: Boca Raton, FL, USA, 2017.
119. Smith, C.J.; Bright, J.M.; Crook, R. Cloud cover effect of clear-sky index distributions and differences between human and automatic cloud observations. *Sol. Energy* **2017**, *144*, 10–21.
120. Wacker, S.; Gröbner, J.; Zysset, C.; Diener, L.; Tzoumanikas, P.; Kazantzidis, A.; Vuilleumier, L.; Stöckli, R.; Nyeki, S.; Kämpfer, N. Cloud observations in Switzerland using hemispherical sky cameras. *J. Geophys. Res.* **2015**, *120*, 695–707.
121. Most Efficient Solar Panels 2022. Available online: <https://www.cleanenergyreviews.info/blog/most-efficient-solar-panels> (accessed on 1 November 2022).
122. Sarniak, M.T. The Efficiency of Obtaining Electricity and Heat from the Photovoltaic Module under Different Irradiance Conditions. *Energies* **2021**, *14*, 8271.
123. Amelia, A.R.; Irwan, Y.M.; Leow, W.Z.; Irwanto, M.; Safwati, I.; Zhafarina, M. Investigation of the effect temperature on photovoltaic (PV) panel output performance. *Int. J. Adv. Sci. Eng. Inf. Technol.* **2016**, *6*, 682–688.

124. The atmosphere. Available online: [https://www.centennialofflight.net/essay/Theories\\_of\\_Flight/atmosphere/TH1.htm](https://www.centennialofflight.net/essay/Theories_of_Flight/atmosphere/TH1.htm) (accessed on 15 May 2023).
125. Lapse rate. Available online: [https://en.wikipedia.org/wiki/Lapse\\_rate](https://en.wikipedia.org/wiki/Lapse_rate) (accessed on 15 May 2023).
126. PV Array. Available online: <https://www.mathworks.com/help/sps/powersys/ref/pvarray.html> (accessed on 15 May 2023).
127. Datasheet SunPower Maxeon Ne3. Available online: <https://www.makeyoursolar.com/> (accessed on 29 September 2022).
128. Datasheet SunPower Maxeon. Available online: <https://us.sunpower.com/solar-resources/sunpower-maxeon-gen-iii-solar-cells> (accessed on 15 May 2023).
129. MPPT Solar Charge Controller Model. Available online: [https://www.mathworks.com/matlabcentral/fileexchange/73115-mppt-solar-charge-controller-model?s\\_tid=srchtitle\\_mppt\\_1](https://www.mathworks.com/matlabcentral/fileexchange/73115-mppt-solar-charge-controller-model?s_tid=srchtitle_mppt_1) (accessed on 15 May 2023).
130. Tan, R.H.; Er, C.K.; Solanki, S.G. Modeling of Photovoltaic MPPT Lead Acid Battery Charge Controller for Standalone System Applications. *E3S Web Conf.* **2020**, *182*, 03005.
131. Katche, M.L.; Makokha, A.B.; Zachary, S.O.; Adaramola, M.S. A Comprehensive Review of Maximum Power Point Tracking (MPPT) Techniques Used in Solar PV Systems. *Energies* **2023**, *16*, 2206.
132. Genasun. Available online: <https://genasun.eu/> (accessed on 15 May 2023).
133. Bollipo, R.B.; Mikkili, S.; Bonthagorla, P.K. Hybrid, optimal, intelligent and classical PV MPPT techniques: A review. *CSEE J. Power Energy Syst.* **2021**, *7*, 9–33.
134. Generic battery model. Available online: [https://www.mathworks.com/help/sps/powersys/ref/battery.html?searchHighlight=battery&s\\_tid=srchtitle\\_battery\\_2](https://www.mathworks.com/help/sps/powersys/ref/battery.html?searchHighlight=battery&s_tid=srchtitle_battery_2) (accessed on 15 May 2023).
135. Specification of product; for Lithium-ion rechargeable cell; Model name : INR18650-35E Available online: <https://www.orbtronic.com/content/samsung-35e-datasheet-inr18650-35e.pdf> (accessed on 15 May 2023).
136. Genasun GV-5 Manual. Available online: [https://cdn.shopify.com/s/files/1/0062/2959/0114/files/GV-5\\_Manual.pdf?v=1680700429](https://cdn.shopify.com/s/files/1/0062/2959/0114/files/GV-5_Manual.pdf?v=1680700429) (accessed on 15 May 2023).
137. GeoHack. Available online: <https://geohack.toolforge.org/> (accessed on 15 May 2023).
138. POLNOR LEADER. Available online: <https://polnor-leader.eu/> (accessed on 15 May 2023).
139. Skarka, W.; Jałowicki, A. Automation of a Thin-Layer Load-Bearing Structure Design on the Example of High Altitude Long Endurance Unmanned Aerial Vehicle (HALE UAV). *Appl. Sci.* **2021**, *11*, 2645.
140. Frankrig rundt med "Himlens knallert" Available online: <https://nordicgliding.com/frankrig-rundt-med-himlens-knallert/> (accessed on 15 May 2023).
141. Determining Electric Motor Load and Efficiency. Available online: <https://www.energy.gov/sites/prod/files/2014/04/f15/10097517.pdf> (accessed on 30 January 2023).
142. How to read DC motor & gear motor performance curves. Available online: <https://islproducts.com/design-note/how-to-read-dc-motor-gear-motor-performance-curves> (accessed on 15 May 2023).
143. Kleniewska, M.; Mitrowska, D.; Wasilewicz, M. Estimating Daily Global Solar Radiation with No Meteorological Data in Poland. *Appl. Sci.* **2020**, *10*, 778.

144. Laboratorium fotowoltaiczne. Available online: <http://www.imim.pl/laboratoria-akredytowane/594> (accessed on 15 May 2023).
145. Kim, S.; Hoang, V.Q.; Bark, C.W. Silicon-Based Technologies for Flexible Photovoltaic (PV) Devices: From Basic Mechanism to Manufacturing Technologies. *Nanomaterials* **2021**, *11*, 2944.
146. IEC 60904-3; Photovoltaic Devices—Part 3: Measurement Principles for Terrestrial Photovoltaic (PV) Solar Devices with Reference Spectral Irradiance Data. IEC: Geneva, Switzerland, 2019.
147. IEC 60904-1; Photovoltaic Devices—Part 1: Measurement of PV Current-Voltage Characteristics. IEC: Geneva, Switzerland, 2019.
148. Leitão, D.; Torres, J.P.N.; Fernandes, J.F.P. Spectral Irradiance Influence on Solar Cells Efficiency. *Energies* **2020**, *13*, 5017.
149. Samsung INR18650-35E 3500mAh Available online: <http://lygte-info.dk/review/batteries2012/Samsung%20INR18650-35E%203500mAh%20%28Pink%29%20UK.html> (accessed on 15 May 2023).
150. Gliwice prognoza na maj 2022 - śląskie, Polska Available online: <https://www.ekologia.pl/pogoda/polska/slaskie/gliwice/archiwum,maj,2022,22> (accessed on 15 May 2023).
151. Registered Community Design 015024728-0001. Available online: <https://euipo.europa.eu/eSearch/#details/designs/015024728-0001> (accessed on 25 September 2023).
152. Registered Community Design 015024780-0001. Available online: <https://euipo.europa.eu/eSearch/#details/designs/015024780-0001> (accessed on 25 September 2023).

# Abstract

Unmanned Aerial Vehicles (UAVs) have become increasingly popular in recent years, both in the commercial industry and in hobby applications. The applications of UAVs are very wide. These include taking videos and photos from a bird's eye view, monitoring threats such as fires, mapping areas, crop inspection, search and rescue works. Depending on the structure, geometry, power transmission method, and flight duration, the target purpose of the UAV may change.

One type of Unmanned Aerial Vehicles are Vertical Take-Off and Landing (VTOL). The ability to take-off vertically allows to start flight anywhere without the use of runway. The advantage of VTOL is also access to highly urbanized areas, remote areas, and observations in difficult weather conditions.

The issue that most limits UAVs and other flying vehicles is the flight time and range. The limited flight time of the UAV causes the need to land and the resulting loss of time in terms of interrupting the mission, charging or replacing batteries. In order to extend the mission, designers are looking for opportunities to obtain external energy. The goal is to achieve full energy autonomy enabling continuous flight without the need for unnecessary landings. Energy autonomy of UAVs is an important direction in the field of aerospace because, in addition to the possibility of continuous operation, an additional advantage is the lower cost of this type of application than using a satellite.

The aim of the doctoral dissertation was to develop a method to extend the flight time of an Vertical Take-Off and Landing Unmanned Aerial Vehicle. Due to its universality, the method was also supposed to be applicable to various types of UAVs, including: VTOL, HALE (High-Altitude Long-Endurance) UAV, LALE (Low-Altitude Long-Endurance) UAV, and other types of UAVs.

The doctoral thesis focused on developing a general model of the solar-powered UAV power supply system. It included, among others: a solar irradiation model depending on the date, location and weather conditions, a photovoltaic system model, an energy storage model, and an energy demand model.

The result of the author's work is a simulation model that has been appropriately tuned with data obtained during numerous laboratory tests — among others, photovoltaic cells, battery cells, and other systems on board the UAV.

The doctoral dissertation includes three case studies: two fixed-wing UAVs - one LALE and HALE class object - as well as a tail-sitter VTOL. A different power supply configuration was developed for each case study. The analyzes carried out allowed obtaining data of the energy balance, battery state of charge, and the degree of possibility of extending the UAV flight depending on the type of class of the flying vehicle.

During work related to the doctoral thesis, a LALE UAV prototype was built, which was included in this doctoral dissertation as one of the case studies. Verification of the systems and individual elements allowed for comparison of the results of the simulation model with the real system.

# Streszczenie

Bezzałogowe Statki Powietrzne (BSP) zyskują w ostatnich latach coraz większą popularność zarówno w przemyśle komercyjnym jak i w zastosowaniach hobbystycznych. Zastosowania BSP są bardzo szerokie. Można do nich zaliczyć robienie filmów i zdjęć z lotu ptaka, monitorowanie zagrożeń np. pożarów, mapowanie terenów, kontrolę upraw, prace poszukiwawcze oraz ratunkowe. W zależności od konstrukcji, geometrii, sposobu przenoszenia napędu, długości lotu docelowe przeznaczenie BSP może ulegać zmianie.

Jednym z rodzajów Bezzałogowych Statków Powietrznych są pionowzloty (z ang. Vertical Take-off and Landing, VTOL). Możliwość pionowego startu pozwala na rozpoczęcie lotu w dowolnym miejscu bez konieczności korzystania z pasa startowego. Zaletą VTOL-i jest również dostęp do mocno zurbanizowanych terenów, odległych obszarów oraz obserwacji w trudnych warunkach pogodowych.

Kwestią, która najbardziej ogranicza BSP oraz inne pojazdy latające jest czas oraz zasięg lotu. Ograniczony czas lotu BSP powoduje konieczność lądowania i związaną z tym stratę czasu w zakresie przerwania misji, lądowania czy wymiany akumulatorów. W celu wydłużenia misji konstruktorzy szukają możliwości na pozyskanie energii z zewnątrz. Celem jest osiągnięcie pełnej autonomii energetycznej umożliwiającej ciągły lot bez konieczności zbędnych lądowań. Autonomia energetyczna UAV jest ważnym kierunkiem w dziedzinie kosmonautyki, ponieważ oprócz możliwości ciągłej pracy dodatkową zaletą jest niższy koszt tego rodzaju aplikacji niż przy użyciu satelity.

Celem rozprawy doktorskiej było opracowanie metody pozwalającej na wydłużenie czasu lotu Bezzałogowego Statku Powietrznego Pionowego Startu i Lądowania. Metoda ze względu na swoją uniwersalność miała również być możliwa do zastosowania w różnych typach BSP wliczając w to m.in. VTOL, BSP klasy HALE (High-Altitude Long-Endurance), LALE (Low-Altitude Long-Endurance) oraz w innych rodzajach BSP.

W pracy doktorskiej skupiono się na opracowaniu ogólnego modelu układu zasilania solarnego BSP. Uwzględniał on m.in. model nasłonecznienia zależny od daty, lokalizacji i warunków atmosferycznych, model układu fotowoltaicznego, model magazynu energii oraz model zapotrzebowania energetycznego.

Owocem pracy autora jest model symulacyjny, który został odpowiednio dostrojony danymi uzyskanymi podczas licznych badań laboratoryjnych. Badano m.in. ogniwa fotowoltaiczne, ogniwa bateryjne oraz inne układy znajdujące się pokładzie BSP.

W rozprawie doktorskiej uwzględniono trzy studia przypadków: dwa fixed-wing UAV – po jednym obiekcie klasy LALE oraz HALE — a także pionowzlot typu tail-sitter. Dla każdego studium przypadku opracowano inną konfigurację układu zasilania. Przeprowadzone analizy pozwoliły na uzyskanie danych dotyczących bilansu energetycznego, stanu naładowania baterii, stopnia możliwości wydłużenia lotu BSP w zależności od rodzaju klasy obiektu latającego.

Podczas prac związanych z pracą doktorską zbudowano prototyp BSP klasy LALE, który był uwzględniony w niniejszej rozprawie doktorskiej jako jedno ze studiów

przypadku. Weryfikacja układów oraz poszczególnych elementów pozwoliła na porównanie wyników modelu symulacyjnego z układem rzeczywistym.